WAVEFORM DESIGN FOR PULSE DOPPLER RADAR

A THESIS SUBMITTED TO
THE GRADUATE SCHOOL OF NATURAL AND APPLIED SCIENCES
OF
MIDDLE EAST TECHNICAL UNIVERSITY

BY

HANDAN AĞIRMAN

IN PARTIAL FULFILLMENT OF THE REQUIREMENTS
FOR
THE DEGREE OF MASTER OF SCIENCE
IN
ELECTRICAL AND ELECTRONICS ENGINEERING

DECEMBER 2005

Approval of the Graduate School of Natural and Applied Sciences

Prof. Dr. Canan Özgen
Director

I certify that this thesis satisfies all the requirements as a thesis for the degree of Master of Science.

Prof. Dr. İsmet Erkmen
Head of Department

This is to certify that we have read this thesis and that in our opinion it is fully adequate, in scope and quality, as a thesis for the degree of Master of Science.

Prof. Dr. Mete Severcan
Supervisor

Examining Committee Members

Prof. Dr. Yalçın Tanık (METU, EE) _____
Prof. Dr. Mete Severcan (METU, EE) _____
Assoc. Prof. Dr. Sencer Koç (METU, EE) _____
Assist. Prof. Dr. Ali Özgür Yılmaz (METU, EE) _____
Dr. Alpay Erdoğan (ASELSAN) _____

I hereby declare that all information in this document has been obtained and presented in accordance with academic rules and ethical conduct. I also declare that, as required by these rules and conduct, I have fully cited and referenced all material and results that are not original to this work.

Name, Last name: Handan AĞIRMAN

Signature :

ABSTRACT

WAVEFORM DESIGN FOR PULSE DOPPLER RADAR

AĞIRMAN, Handan

M.S., Department of Electrical and Electronics Engineering
Supervisor: Prof. Dr. Mete Severcan

December 2005, 100 pages

This study is committed to the investigation of optimum waveforms for a pulse doppler radar which uses a non linear high power amplifier in the transmitter. The optimum waveform is defined as the waveform with the lowest peak and integrated side lobe level, the narrowest main lobe in its autocorrelation and the narrowest bandwidth in its spectrum.

The Pulse Compression method is used in radar systems since it is more advantageous in terms of the resolution. Among all pulse compression methods, the main focus of this study is on Phase Coding. Two types of radar waveforms assessed throughout this study are Discrete Phase Modulated Waveforms and Continuous Phase Modulated Waveforms. The continuous phase modulated waveforms are arranged under two titles: the memoryless phase modulated waveform and the waveform modulated with memory.

In order to form memoryless continuous phase waveforms, initially, discrete phase codes are obtained by using Genetic Algorithm. Following this process, a new phase shaping pulse is defined and applied on the discrete phase waveforms.

Among the applicable modulation with memory techniques, Continuous Phase Modulation maintains to be the most appropriate. The genetic algorithm is used to find different lengths of optimum data sequences which form the continuous phase scheme.

Keywords: Pulse compression, Genetic Algorithm, Continuous Phase Modulation.

ÖZ

DARBE DOPPLER RADAR İÇİN DALGA BİÇİMİ TASARIMI

AĞIRMAN, Handan

Yüksek Lisans, Elektrik ve Elektronik Mühendisliği Bölümü
Tez Yöneticisi: Prof. Dr. Mete Severcan

Aralık 2005, 100 sayfa

Bu çalışma göndermecinde doğrusal olmayan yüksek güçlü bir yükselteç kullanan bir darbe doppler radar için en iyi dalga biçimleri araştırmasını işlemektedir. En iyi dalga biçimi, özilinti işlevinde en alçak tepe ve tümleşik yanlob seviyesi ve en dar analob, frekans etki alanında en dar bant genişliği olan dalga biçimidir.

Çözünürlük açısından üstünlüğü olduğu için radarlarda darbe sıkıştırma metodu kullanılır. Bu çalışmanın ana ilgi odağı, darbe sıkıştırma metotları arasından faz kodlamasıdır. Bu çalışma boyunca değerlendirilen iki radar dalga biçimi ayrık fazlı kiplenmiş dalga biçimleri ve devamlı fazlı kiplenmiş dalga biçimleridir. Devamlı fazlı dalga biçimleri belleksiz kiplenmiş dalga biçimleri ve bellekli kiplenmiş dalga biçimleri olarak iki başlık altında toplanmıştır.

Bellekli kiplenmiş dalga biçimlerini oluşturmak için, ilk olarak, artık fazlı kodlar Genetik Algoritma kullanılarak bulunmuştur. Bu işlemi takiben, yeni bir faz şekilleyici darbe tanımlanmış ve ayrık fazlı dalga biçimleri üzerinde uygulanmıştır. Uygulanabilir bellekli kiplenim teknikleri arasında, devamlı fazlı kiplenim en uygun

görünmektedir. Genetik algoritması, devamlı fazlı tasarıların oluşturulması için kullanılacak farklı uzunluklu en iyi veri sırasının oluşturmak için kullanılır.

Anahtar kelimeler: Darbe Sıkıştırma, Genetik Algoritma, Sürekli Fazlı Kiplenim.

To my family

ACKNOWLEDGEMENTS

I wish to express my sincere gratitude to my advisor Prof. Dr. Mete Severcan for his supervision, valuable guidance and helpful suggestions. I would like to thank Prof. Dr. Yalçın Tanık for suggesting the phase shaping pulses for MLESSM waveforms and his valuable comments. I would also like to thank Assist. Prof. Dr. Ali Özgür Yılmaz for his suggestions and comments.

I am also grateful to ASELSAN Inc. for facilities for the completion of this thesis and it is my obligation to thank Kenan Çağlar for his understanding during my thesis. I would like to thank Taylan Eker and Ulaş Karaca for their helps about writing this thesis.

Special appreciation and gratitude are also due to my family and D.Çağrı Tosun for their encouragement, reassurance, endless love and understanding of spending lots of time on this thesis.

TABLE OF CONTENTS

PLAGIARISM……...iii

ABSTRACT iv

ÖZ vi

ACKNOWLEDGEMENTS ix

TABLE OF CONTENTS x

LIST OF TABLES xiii

LIST OF FIGURES xv

LIST OF ABBREVIATIONS xviii

CHAPTER

1. INTRODUCTION 1

2. FUNDAMENTAL CONCEPTS OF RADAR WAVEFORM DESIGN 4

2.1. COMMON BASIC PROPERTIES OF RADARS 4

2.2. MODULATION THEORY 5

2.2.1. INTRODUCTION 5

2.2.2. MEMORYLESS METHODS (MLESSM) 8

2.2.2.1. INTRODUCTION 8

2.2.2.2. PHASE MODULATED SIGNALS 8

2.2.3. MODULATIONS WITH MEMORY (MWM) 9
2.2.3.1. CONTINUOUS PHASE MODULATION (CPM) 9
2.2.3.2. CONTINUOUS PHASE FSK (CPFSK) 13
2.2.3.3. MINIMUM SHIFT KEYING (MSK) 14
2.3. MATCHED FILTER THEORY 16
2.4. PULSE COMPRESSION 18
2.4.1. DEFINITION 18
2.4.2. PULSE COMPRESSION TECHNIQUES 20
2.4.2.1. INTRODUCTION 20
2.4.2.2. PHASE MODULATION TECHNIQUES 20
2.5. BANDWIDTH CONSIDERATION IN PHASE CODED-SIGNALS 23
3. PHASE CODED PULSE IN PULSE DOPPLER RADAR 25
3.1. INTRODUCTION 25
3.2. GENETIC ALGORITHM 26
3.3. OPTIMUM CPM CODES 27
3.4. OPTIMUM MEMORYLESS PULSE 29
3.4.1. OPTIMUM BPSK CODES 29
3.4.2. OPTIMUM QPSK CODES 33
3.4.3. SIDELOBE SUPPRESSION TECHNIQUES 40
3.4.3.1. INTRODUCTION 40
3.4.3.2. INVERSE FILTERING 41
3.4.3.3. INVERSE FILTERING ON DISCRETE PHASE QPSK CODES 43
3.5. OPTIMUM CONTINUOUS PHASE MEMORYLESS WAVEFORMS 49
3.5.1. PHASE SHAPING PULSE 49
3.6. CONTINUOUS PHASE WAVEFORMS 50
3.6.1. CONTINUOUS PHASE BPSK WAVEFORMS 50
3.6.2. CONTINUOUS PHASE QPSK WAVEFORMS 55
3.6.3. SPECTRAL IMPROVEMENT OF CONTINUOUS PHASE MODULATION 64
3.6.4. CONTINUOUS PHASE MODULATIONS AND SYSTEM IMPERFECTIONS 69

4. SAMPLING MISMATCH IN RADAR WAVEFORMS..... 73

4.1. INTRODUCTION..... 73

4.2. HALF NYQUIST RATE SAMPLING..... 73
4.2.1. SAMPLING MISMATCH ON QPSK CODES..... 73

4.3. NYQUIST RATE SAMPLING..... 80
4.3.1. SAMPLING MISMATCH ON QPSK CODES..... 80
4.3.2. SAMPLING MISMATCH ON BPSK CODES..... 87
4.3.3. SAMPLING MISMATCH ON CPM CODES 89

4.4. HIGHER RATE SAMPLING..... 93

5. SUMMARY AND CONCLUSIONS 95

REFERENCES..... 97

APPENDICES

APPENDIX A MODULATING PULSE SHAPES FOR CPM..... 100

LIST OF TABLES

TABLES

2.1 Known Barker Codes 22
3.1 Optimum CPM Codes, h = 0.5, 1REC 28
3.2 Optimum biphase codes 30
3.3 Optimum quadriphase codes 34
3.4 Optimum LPT-QPSK codes 37
3.5 PSL and ISL of the continuous phase BPSK pulse, N = 20, τ = T/5 52
3.6 PSL and ISL of the BPSK pulse with N = 32, 45, 64 54
3.7 Effect of Duration on PSL and ISL 57
3.8 Effect of Duration on PSL and ISL 59
3.9 Effect of Duration on PSL and ISL 61
3.10 Effect of Duration on PSL and ISL 63
3.11 $B_{90\%}$ and $B_{99\%}$ of the QPSK waveform, N=20 65
3.12 $B_{90\%}$ and $B_{99\%}$ of BPSK waveform, N = 20 66
3.13 $B_{90\%}$ and $B_{99\%}$ of the LPT-QPSK waveform, N = 20 67
3.14 $B_{90\%}$ and $B_{99\%}$ of MLESSM waveforms, N = 20 68
4.1 Max and Min values of PSL and ISL under sampling mismatch, S = 1 80
4.2 Max and Min values of SNR Loss and MLW under sampling mismatch, S=1 .. 80
4.3 Max and Min PSL and ISL values for QPSK waveforms under sampling mismatch, S = 2 83
4.4 Max and Min MLW and Loss values for QPSK waveforms under sampling mismatch, S = 2 84
4.5 Min and Max values of PSL and ISL for LPT-QPSK waveforms under sampling mismatch, S = 2, τ = T/5 86
4.6 Min and Max of MLW and Loss values for LPT-QPSK waveforms under sampling mismatch, S = 2, τ = T/5 86
4.7 Min and Max values of PSL and ISL under sampling mismatch, S = 2, ... 87

4.8 Min and Max values of MLW and SNR Loss under sampling mismatch, ... 88
4.9 Min and Max values of PSL and ISL under sampling mismatch, M = 2,..... 89
4.10 Max MLW and SNR Loss values of CPM waveforms, M = 2, h = 0.5, 1REC 90
4.11 Min and Max values of PSL and ISL under sampling mismatch, M = 4,..... 91
4.12 Max and Min values of MLW and Loss under sampling mismatch, M=4 h = 0.5, 1REC 91
4.13 Min and Max values of PSL and ISL under sampling mismatch, M = 8..... 92
4.14 Max and Min values of MLW and SNR Loss under sampling mismatch, M = 8 h = 0.5, 1REC..... 92
4.15 Effect of Number of Samples on CPM waveform with N = 64, M = 8 93
4.16 Effect of Number of Samples on CPM waveform, N = 64 M = 4 94

LIST OF FIGURES

FIGURES

2.1 Principles of Pulse Doppler Radar 5
2.2 Digital Modulation Tree 6
2.3 Phase trajectory of binary CPM 11
2.4 Phase trajectories of Continuous Phase FSK 14
2.5 Matched Filter System 16
2.6 Binary phase coding of a transmitted pulse, [+ + -] 21
2.7 Ambiguity Function of 13-length Barker Codes 22
2.8 ACFs of Discrete and Continuous Phase Barker Code 24
3.1 Phase variation of the CPM pulse N = 20, M = 2, h = 0.5 29
3.2 ACFs of optimum BPSK codes of lengths of 20(a), 32(b), 45(c) and 64(d) 31
3.3 Phase variation of the biphase code of length 20 32
3.4 Commonly used signal constellations for QPSK 33
3.5 ACFs of QPSK codes of lengths 20(a), 32(b), 45(c), 64(d) 35
3.6 Phase variation of QPSK code of length 20 36
3.7 Signal constellation of LPT-QPSK 37
3.8 ACFs of LPT-QPSK code of lengths 20(a), 32(b), 45(c), 64(d). 38
3.9 Phase variation of LPT-QPSK code of length 20 39
3.10 PSL versus ISL 40
3.11 QPSK code of length 20 filtered with IF of length 20 43
3.12 QPSK code of length 20 filtered with the IF of length 60 44
3.13 PSL versus IF filter length 45
3.14 ISL versus IF length 46
3.15 MLW versus IF length 47
3.16 SNR loss versus IF length 48
3.17 Phase Shaping Pulse for $\tau = T/5$, T=100 49
3.18 Phase variation of the continuous phase 20-length BPSK signal, $\tau = T/5$ 50

3.19 Aperiodic ACF of BPSK pulse, N = 20, τ = T/5 51
3.20 Aperiodic ACF of the BPSK pulse, N = 32, τ = T/5 52
3.21 Aperiodic ACF of the BPSK pulse, N = 45, τ = T/5 53
3.22 Aperiodic ACF of the BPSK pulse, N = 64, τ = T/5 53
3.23 Phase variation of the continuous phase QPSK pulse, N=20, τ = T/5 55
3.24 Aperiodic ACF of the QPSK pulse, N = 20, τ = T/5 56
3.25 Aperiodic ACFs of the QPSK pulse, N=20 57
3.26 Aperiodic ACFs of QPSK pulses, N=20(a), 32(b), 45(c), 64(d) 58
3.27 Phase variation of the LPT-QPSK pulse with N = 20, τ = T/5. 60
3.28 Aperiodic ACF of the LPT-QPSK pulse, N = 20, τ = T/5. 60
3.29 Aperiodic ACFs of LPT-QPSK pulses, N = 20(a), 32(b) 61
3.31 Simple Radar Transmitter 69
3.32 Bandpass filter 70
3.33 Discrete Phase QPSK Waveform before Filtering 71
3.34 Discrete Phase QPSK Waveform after Filtering 71
3.35 Continuous Phase QPSK Waveform after Filtering, τ = T/4 72
3.36 CPM Waveform after Filtering, M = 4, h = 0.5, 1REC 72
4.1 PSL versus sampling time shift for discrete and continuous phase QPSK waveforms, τ = T/5, S = 1, ... 74
4.2 ISL versus sampling point shift for discrete and continuous phase QPSK waveforms, τ = T/5, S=1 75
4.3 Main lobe width versus sampling point shift for discrete and continuous phase QPSK waveforms, τ = T/5, S = 1. 76
4.4 SNR loss versus sampling point shift for discrete and continuous phase QPSK waveforms, τ = T/5, S=1. 76
4.5 PSL versus sampling point shift for QPSK waveforms with N = 20, 32, 45 and 64, S = 1, τ = T/5. 77
4.6 ISL versus sampling point shift for QPSK waveforms with N = 20, 32, 45 and 64, S = 1, τ = T/5. 78
4.7 MLW versus sampling point shift for QPSK waveforms with N = 20, 32, 45, 64, S = 1, τ = T/5. 78
4.8 SNR loss versus sampling point shift for QPSK waveforms with N = 20, 32, 45

and 64, S = 1, τ = T/5. 79
4.9 PSL versus sampling point shift for QPSK waveforms with N = 20, 32, 45, and 64, S = 2, τ = T/5 81
4.10 ISL versus sampling point shift for QPSK waveforms with N=20, 32, 45, 64, S = 2, τ = T/5 82
4.11 MLW versus sampling point mismatch for QPSK waveforms with..... 82
4.12 SNR Loss versus sampling point mismatch for QPSK waveforms with 83
4.13 PSL versus sampling point mismatch for LPT-QPSK waveform with 85
4.14 Maximum ISL versus maximum PSL under sampling mismatch 89

LIST OF ABBREVIATIONS

ACF	Autocorrelation Function
A/D	Analog to Digital
ISL	Integrated Sidelobe Level
PSL	Peak Sidelobe Level
MF	Matched Filter
MLW	Main Lobe Width
SNR	Signal to Noise Ratio
MLESSM	Memoryless Modulation
MWM	Modulation with Memory
LPT-QPSK	Limited Phase Transition Quadriphase Keying
GA	Genetic Algorithm

CHAPTER 1

INTRODUCTION

Radar is an electromagnetic system for the detection and ranging of objects. The term radar is a contraction of the words ***ra***dio ***d***etection ***a***nd ***r***anging. Its operation is as follows: radar transmits an rf pulse, a portion of which is intercepted by a reflecting object (target) and is reradiated in all directions and for the detection by the same radar. The distance of the target is measured by observing the time delay between the transmitted and the received signal and the velocity of the target can be measured by the shift in carrier frequency of the received signal [1].

The term ***doppler radar*** refers to any radar that is capable of measuring the frequency shift between the frequencies of the transmitted and received signals [2].

In a radar system, range resolution is proportional to pulse width. High range resolution can be achieved by using short pulses but the pulse energy is directly proportional to pulse width. This difficulty can be overcome by pulse compression, which is a useful technique to send long pulses while retaining high resolution in range. Pulse compression is achieved by phase or frequency coding the transmitted signal and filtering the received signal through a matched filter, which is implemented in the receiver part. The output of the matched filter is the compressed pulse with short duration. The return signal coming from the reflecting object is filtered in the radar receiver –mostly by using a Matched Filter (MF) to detect if a target is present. The output of the filter reaches a peak at the target range bin and

has range sidelobes around the target due to the autocorrelation of the coded pulse. However, these range sidelobes should be reduced since they can mask other targets present nearby the detected target.

This thesis mainly focuses on phase coded pulse compression which is a special type of pulse compression. Although, academic researches have mostly dealt with the discrete phase coded pulse, in this thesis a new approach is embodied. The aim of this approach is to alter the sharp phase transitions in discrete phase coded waveforms and render these transitions continuous and smooth, and consequently to decrease the levels of sidelobes in the spectrum.

In this thesis, optimum phase modulated waveforms are analyzed by using two types of phase modulation techniques, which are Modulation with Memory (MWM) and Memoryless Modulation (MLESSM). While the specific Continuous Phase Modulation (CPM) is chosen as an MWM technique, biphase modulation (BPSK) and Quadrature Modulation (QPSK) are used as MLESSM techniques.

In order to implement continuous phase modulation in MLESSM, discrete phase codes are searched firstly calculating discrete autocorrelations. Searching MWM data sequences is performed on continuous autocorrelations. Throughout the searching processes, Genetic Algorithm is used.

The continuous waveforms are investigated in terms of the variations of peak sidelobe level, integrated sidelobe level, resolution and signal-to-noise ratio at the matched filter output under sampling mismatch.

In Chapter 2, the fundamental concepts of a radar system such as doppler frequency and resolution stated, basic radar parameters, pulse compression theory, matched filter and Ambiguity Function are also mentioned in detail.

Chapter 3 is devoted to the implementation of discrete phase and continuous phase modulated waveforms. Optimum MWM and MLESSM waveforms are searched; different lengths of discrete phase codes are investigated. Subsequently, the PSL and the ISL values of MWM and MLESSM MF outputs are compared. Inverse Filtering, a sidelobe reduction technique, is first analyzed in detail then applied on the extracted codes. At the end of the chapter, bandwidths are calculated for all waveforms formed by using optimum codes and these values are compared.

In Chapter 4, the sampling time jitter effect is analyzed. In addition, the mismatch effects on peak sidelobe level and integrated sidelobe level, resolution and peak signal-to-noise ratio values are demonstrated.

Finally, Chapter 5 contains a conclusion within which possible future studies are discussed.

CHAPTER 2

FUNDAMENTAL CONCEPTS OF RADAR WAVEFORM DESIGN

2.1. Common Basic Properties of Radars

Radars transmit electromagnetic waves and receive echoes from a reflector, target or clutter. The elapsed time between the transmitted and reflected radar signals are utilized to measure the distance of the target. The range R is

$$R = \frac{cT}{2} \tag{2.1}$$

where T is the time taken by the rf pulse to travel to the target and to return back to the radar, while c is the speed of light $c = 3 \times 10^8 \ m/s$. The velocity of the target can be measured by the frequency shift occurring in the carrier frequency [1].

$$f_d = \frac{2\upsilon_R f_0}{c} \tag{2.2}$$

In this equation, f_d is the doppler frequency shift, υ_R is the target velocity and f_0 is the carrier frequency.

The term ***doppler radar*** refers to any radar capable of measuring the Doppler frequency, f_d [2].

A doppler radar using a pulsed signal with a constant or variable Pulse Repetition Interval (PRI) or Pulse Repetition Frequency (PRF) is named as a *Pulse Doppler Radar*. A general block diagram of a Pulse Doppler Radar is given in Figure 2.1.

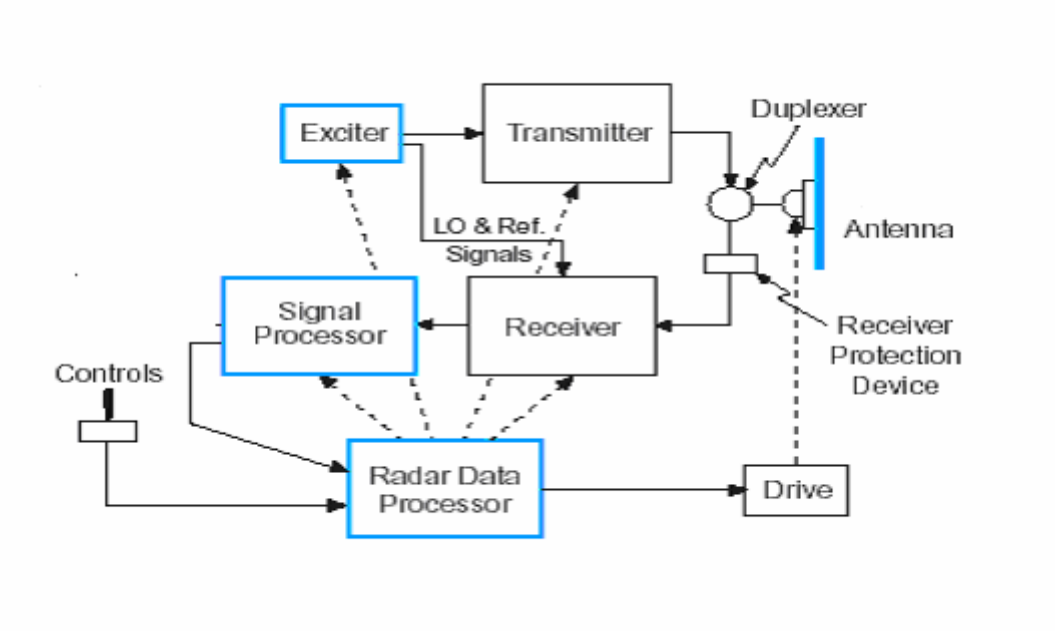

Figure 2.1 Principles of Pulse Doppler Radar

2.2. Modulation Theory

2.2.1. Introduction

In this section, modulation techniques used in digital communication are discussed. Figure 2.2 demonstrates all digital modulation schemes arranged in a tree diagram [9]. The letter ‘D’ labels the differentially encoded schemes and the schemes that can be noncoherently demodulated are labeled by letter ’N’.

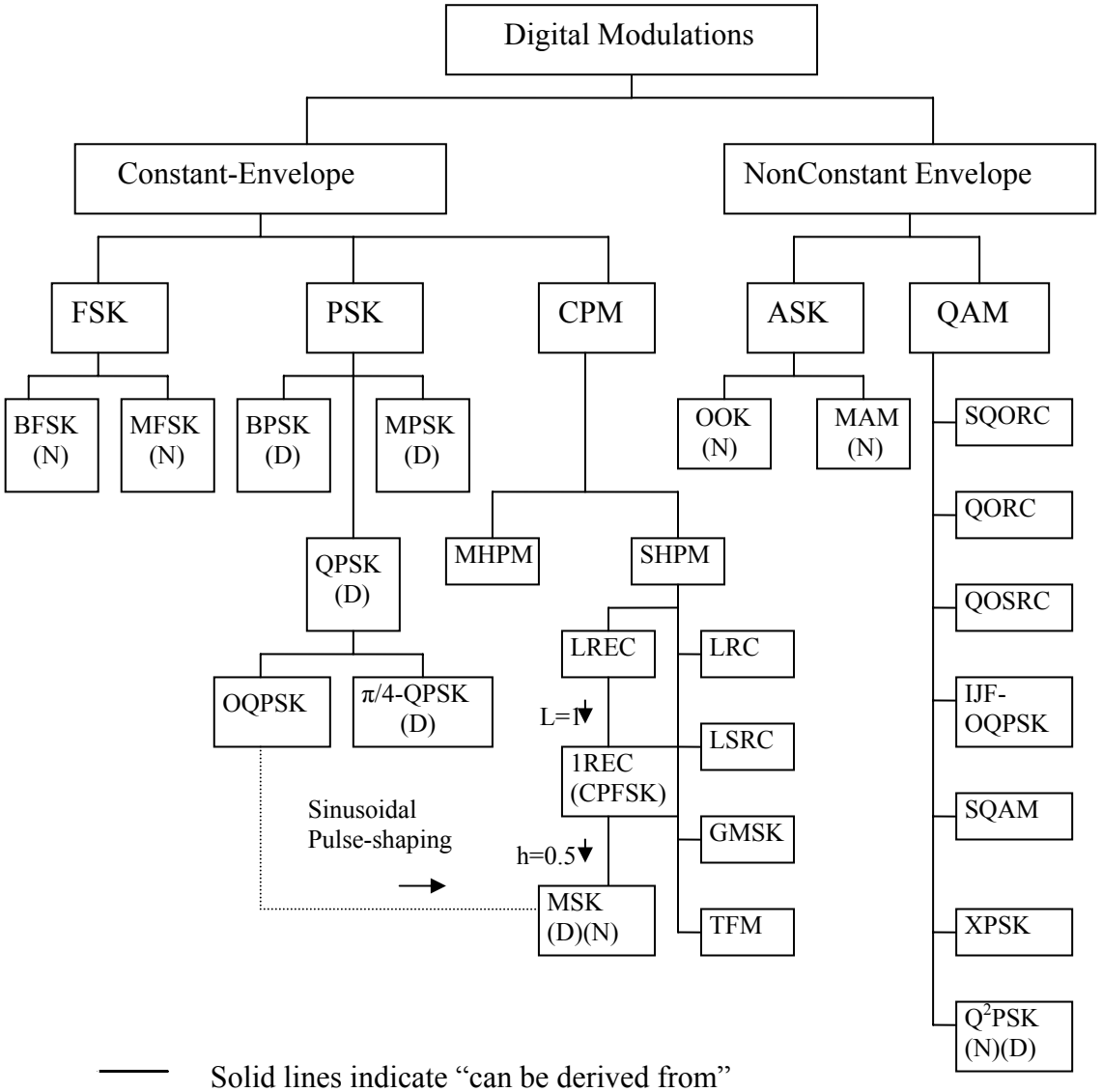

Figure 2.2 Digital Modulation Tree

Modulation schemes can be grouped into two large categories: constant envelope and non-constant envelope. The constant envelope class is generally suitable for communication systems in which the power amplifiers are to operate in the non-linear region of the input-output characteristic. By means, maximum amplifier

efficiency is achieved. Such an amplifier, Traveling Wave Tube Amplifier (TWTA), is commonly used in satellite communications. Due to the low bandwidth consideration, Frequency Shift Keying (FSK) as a constant envelope modulation is not used in satellite communication. On the other hand, the Phase Shift Keying (PSK) schemes contain discontinuous phase transitions between symbol phases. In the contrary, the Continuous Phase Modulation (CPM) another constant envelope scheme has continuous phase transitions. Therefore, they have less side lobe energy in their spectra in comparison with PSK schemes. The CPM class includes raised cosine response with pulse length L (LRC), spectral raised cosine with length L (LSRC), rectangular frequency response with length L (LREC), Gaussian-shaped MSK (GMSK), and TFM (tamed FM) whose definitions are included in Appendix A. h stands for the modulation index in CPM schemes. SHPM in the modulation tree refers to the single-h CPM and MHPM represents the multiple-h CPM scheme [9].

Since dealing with a pulse doppler radar with a non-linear amplifier, only constant envelope modulations will be taken into consideration. In fact, FSK does not provide good bandwidth efficiency compared to other constant envelope modulations schemes, for that reason, it is out of context. Although it is not showed in the modulation tree, the constant envelope schemes can be grouped in two categories: Modulation with Memory (MWM) and Memoryless Modulation (MLESSM). The modulation is said to have memory when a waveform transmitted in a symbol interval bound to previously transmitted waveforms. Otherwise, the modulation is considered to be Memoryless [5].

2.2.2. Memoryless Methods (MLESSM)

2.2.2.1. INTRODUCTION

MLESSM waveforms may differ in amplitude, phase and/or frequency; however, our main concern in this study is the phase modulation with a specific focus on phase modulated memoryless waveforms.

2.2.2.2. PHASE MODULATED SIGNALS

The carrier amplitude is constant in this type of modulation. Therefore, this modulation method is an example of constant envelope modulation. A constant envelope and phase varying signal is of the form

$$(2E/T)^{1/2}\cos(\omega_c t + \phi(t))$$

where ω_c is the carrier frequency in radians, T is the length of the signaling interval and E is the energy expanded during the interval. In each interval, an M-ary data symbol appears and the phase $\phi(t)$ follows a pattern in response to these symbols.

In PSK, the signal is in the form of

$$\begin{aligned} s_k(t) &= \mathrm{Re}\left[Ae^{j2\pi(k-1)/K}e^{j2\pi f_c t}\right] \\ &= A\cos\left[2\pi f_c t + \frac{2\pi}{K}(k-1)\right] \quad k = 1,2,\ldots,K \quad 0 \le t \le T \end{aligned} \tag{2.3}$$

where A is the signal amplitude and $\theta_m = 2\pi(k-1)/K, \quad k = 1, 2, \ldots, K,$ are the M possible phases of the carrier [5]. In binary PSK, two phases, for instance 0 and π, are available during each symbol interval, whereas in quaternary PSK, the signal can take on four phases, be it 0, $\pi/2$, π, $3\pi/2$, during an interval.

2.2.3. Modulations with Memory (MWM)

2.2.3.1. CONTINUOUS PHASE MODULATION (CPM)

Continuous Phase Modulation is a spectrally efficient method with memory. The memory results from the continuity of the carrier phase from one signal interval to the next.

The general CPM signal is represented as

$$s(t) = \sqrt{2E/T}\,\cos(\omega t + \phi(t) + \phi_0) \qquad nT \le t \le (n+1)T \tag{2.4}$$

$\omega = 2\pi f_0$, f_0 = carrier frequency

T = symbol duration

The phase $\phi(t)$ in the equation is,

$$\phi(t) = 2\pi \int_{-\infty}^{t} \sum_{0}^{k} I_k h_k g(\tau - kT) d\tau \tag{2.5}$$

$$I_k = \pm 1, \pm 3 \ldots \pm (\text{M-1}) \tag{2.6}$$

$$q(t) = \int_{-\infty}^{t} g(\tau) d\tau \tag{2.7}$$

The data I_k are M-ary data symbols, taken from the alphabet $\pm 1, \pm 3 \ldots \pm$ (M-1), M is even. The sequences of real constants …, h_{-2}, $h_{-1,}$ $h_{-0,}$ $h_{1,}$ h_2 … are the modulation indices, and the underlined subscripts mean that they appear modulo H. This means that only H different constants are used in a cyclical fashion, i.e. …, h_0, h_1, $h_{2,}$ …, h_{H-1}, h_0, h_1, h_2 **[7].** This system is called multi-h CPM. When H = 1, there is only one modulation index $h_{0,}$ which can be denoted as h. This type of CPM modulation is called fixed-h (single-h) modulation. q(t) is the phase response function. CPM schemes are denoted by their phase responses, LRC, LSRC, LREC, TFM, and GMSK. The detailed definitions are included in Appendix A. The prefix "L" denotes the length of the response.

If L = 1 the modulation is called full-response CPM; since each data symbol effects the signal for only one symbol interval. Otherwise, the scheme is partial-response.

The plot, in Figure 2.3, is called the phase tree and it demonstrates an entire set of phase trajectories, the transitions of phase across interval boundaries, and it makes easier to see the effect of interval-to-interval memory in $\phi(t)$.

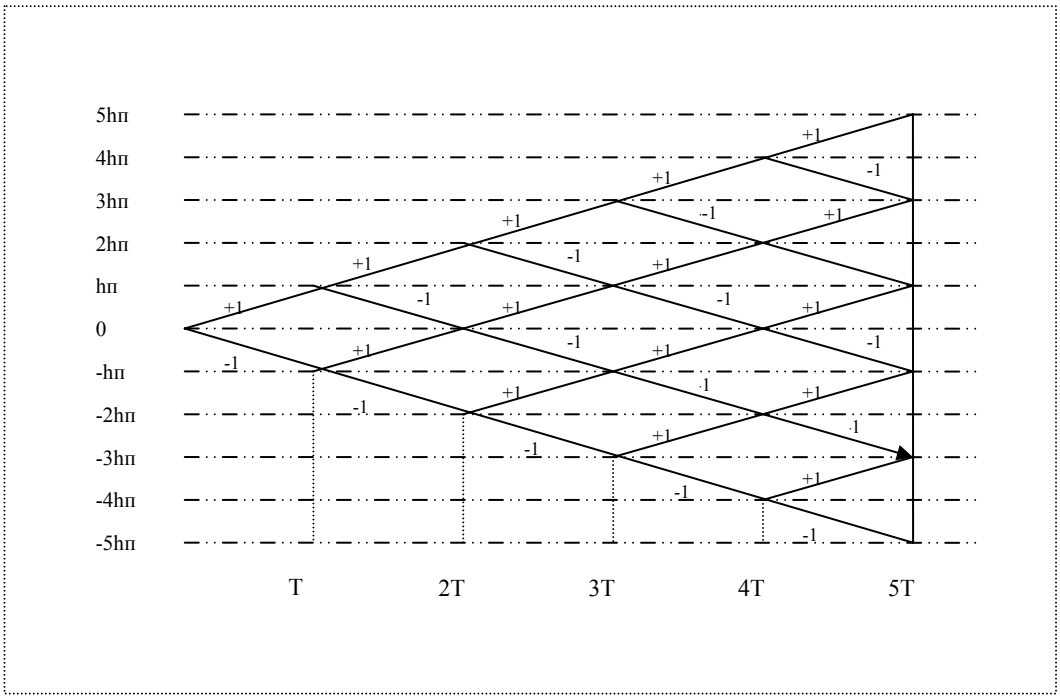

Figure 2.3 Phase trajectory of binary CPM

When modulation index h is rational, h = m/p, where m and p are prime integers, there are p phase states if m is even, 2p states otherwise. These phase states are **[5]**

$$\Theta_s = \left\{0, \frac{m\pi}{p}, \frac{2m\pi}{p}, \ldots, \frac{(p-1)m\pi}{p}\right\} \qquad m \text{ is even} \tag{2.8}$$

$$\Theta_s = \left\{0, \frac{m\pi}{p}, \frac{2m\pi}{p}, \ldots, \frac{(2p-1)m\pi}{p}\right\} \qquad m \text{ is odd} \tag{2.9}$$

If L = 1, these are the only states. Otherwise there are additional phase states due to partial characteristic of g (t), which are

$$\theta(t;I) = 2\pi h \sum_{k=nL+1}^{n-1} I_k q(t-kT) + 2\pi h I_n q(t-nT) \tag{2.10}$$

The summation in this formula represents the data symbols that could not reach their final values. These symbols combine and form the ***correlative state vector*** shows an entire set of phase trajectories The phase of the CPM signal at t = nT is denoted as,

$$S_n = \{\theta_n, I_{n-1}, I_{n-2}, \ldots, I_{n-L+1}\} \tag{2.11}$$

IF the signal is to be a partial response signal with a pulse length LT, the number of states equates to ,

$$N_s = \begin{cases} pM^{L-1} & even\ m \\ 2pM^{L-1} & odd\ m \end{cases} \tag{2.12}$$

when h = m/p.

If the final state of the modulator at t = nT is S_n, then the effect of the new symbol in the time interval $nT \le t \le (n+1)T$ is to alter the state from S_n to S_{n+1} **[5].**

As a result the incoming state turns out to be

$$S_{n+1} = \{\theta_{n+1}, I_n, I_{n+1}, \ldots, I_{n-L+2}\} \tag{2.13}$$

where

$$\theta_{n+1} = \theta_n + \pi h\, I_{n-L+1} \tag{2.14}$$

2.2.3.2. CONTINUOUS PHASE FSK (CPFSK)

The most important type of CPM, used in digital communication today, is CPFSK. In this modulation scheme, the phase shaping pulse is 0 outside the interval [0, T] which means that L is 1. The CPFSK signal is generated by shifting the frequency by an amount f_d, the peak frequency deviation. The general CPFSK representation is then

$$s(t) = \sqrt{2E/T}\,\cos(\omega t + \phi(t) + \phi_0) \quad kT \langle\, t \,\langle (k+1)T \tag{2.15}$$

where $\phi(t)$ is

$$\phi(t) = 4\pi T f_d \int_{-\infty}^{t} \left[\sum_{0}^{k} \alpha_n g(\tau - kT) \right] d\tau$$

It can also be written as:

$$\phi(t) = 2\pi T f_d \sum_{m=-\infty}^{k-1} I_m + 2\pi f_d (t - kT) I_n \tag{2.16}$$

$$= \theta_k + 2\pi h I_k q(t - kT)$$

and

$$h = 2 f_d T,\ \theta_k = \pi h \sum_{m=-\infty}^{k-1} I_m,\ q(t) = \begin{cases} 0 & (t < 0) \\ t/2T & (0 \le t \le T) \\ \frac{1}{2} & (t \rangle T) \end{cases}$$

In Figure 2.4, all of the possible trajectories starting from reference time (zero) for continuous phase FSK, in which phase transitions across the boundaries are constrained to be continuous, are shown. Within any interval, the phase slope is

either $+h\pi/T$ or $-h\pi/T$, and the modulation can be viewed as transmitting one of these two frequencies in each interval in response to a (binary) data sequence.

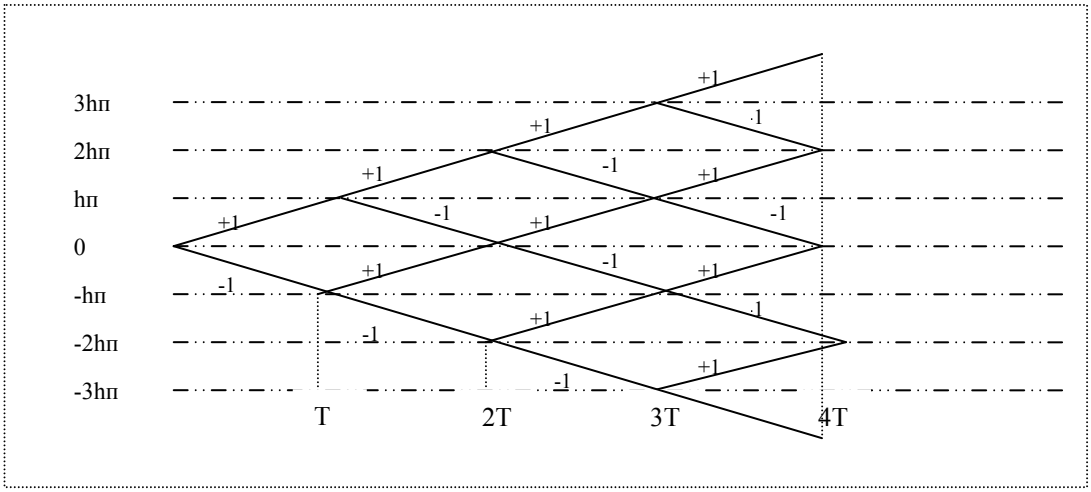

Figure 2.4 Phase trajectories of Continuous Phase FSK

2.2.3.3. MINIMUM SHIFT KEYING (MSK)

MSK is a special form of binary CPFSK with h = 1/2. The phase of the carrier in the interval $kT\langle t\langle(k+1)T$ is

$$\begin{aligned}\phi(t) &= \frac{1}{2}\pi\sum_{m=-\infty}^{k-1} I_m + \pi I_k q(t-kT) \\ &= \theta_k + \frac{1}{2}\pi I_k\left(\frac{t-kT}{T}\right), \quad kT \le t \le (k+1)T\end{aligned} \tag{2.17}$$

and the modulated carrier is

$$\begin{aligned}s(t) &= A\cos\left[2\pi f_c t + \theta_n + \frac{1}{2}\pi I_n\left(\frac{t-nT}{T}\right)\right] \\ &= A\cos\left[2\pi\left(f_c + \frac{1}{4T}I_n\right)t - \frac{1}{2}n\pi I_n + \theta_n\right], \quad nT \le t \le (n+1)T\end{aligned} \tag{2.18}$$

From this expression, it is clear that MSK signal can be expressed as a sinusoid having one of two possible frequencies in the interval $kT \le t \le (k+1)T$.

If these two frequencies are defined as

$$f_1 = f - \frac{1}{4T} \tag{2.19}$$

$$f_2 = f_c + \frac{1}{4T} \tag{2.20}$$

then the MSK signal can be written in the form

$$s_m(t) = \sqrt{2E/T}\cos\left[\ 2\pi f_m t + \theta_k + \frac{1}{2}k\pi(-1)^{i-1}\ \right] \quad m = 1,2 \tag{2.21}$$

The frequency separation between the different symbols is $\Delta f = 1/2T$. It means that $s_1(t)$ and $s_2(t)$ have the required minimum frequency separation for orthogonality. For that reason, this modulation is called Minimum Shift Keying (MSK). In MSK, M = 2 (± 1) and S = 4 (0 RAD, $\pi/2$ RAD, π RAD, $3\pi/2$ RAD).

Another common used type of CPM is GMSK (Gaussian –Shaped MSK). It is a derivative of MSK with the difference that phase shaping pulse is Gaussian filtered. And Gaussian Pulse Shape is almost 0 for $|t| \le 1.5T$

General Gaussian filtered pulse is defined as:

$$g(t) = \left\{ Q\left(\frac{2\pi B}{\sqrt{\ln 2}}(t - \frac{T}{2}) \right) - Q\left(\frac{2\pi B}{\sqrt{\ln 2}}(t + \frac{T}{2}) \right) \right\} \tag{2.22}$$

where the Q function is defined as:

$$Q(t) = \int_{t}^{\infty} \frac{1}{\sqrt{2\pi}} e^{\frac{x^2}{2}} dx. \tag{2.23}$$

2.3. Matched Filter Theory

In radar applications, generally known signals are utilized to detect the existence of target. Since the probability of detection is closely related to signal to noise ratio, the main concern in radar systems is to maximize SNR. A matched filter is a linear filter, whose impulse response is determined by a specific signal in a way that will result in the maximum attainable SNR at the output of the filter, when that particular signal and white noise are passed through the filter [3]. A basic matched filter system is given in Figure 2.5.

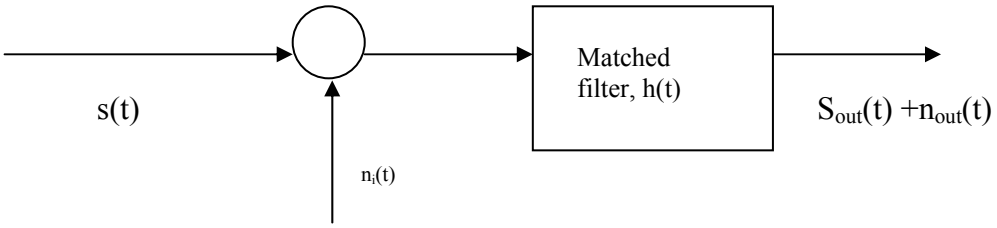

Figure 2.5 Matched Filter System

The input to the matched filter is s(t) plus additive white noise $n_i(t)$. h(t) is searched to have maximum SNR at a delay T (needed to make filter realizable) at the output. It means that the ratio

$$\left(\frac{S}{N}\right)_{out} = \frac{\left|s_{out}(T)\right|^2}{n_{out}{}^2(t)} \tag{2.24}$$

is maximized. This ratio is maximized when the frequency response of the matched filter, H (w) is in the form of Equation 2.25.

$$H(w) = KS^{*}(w)\exp(-jwtT) \tag{2.25}$$

and in time domain, impulse response of the matched filter is given as

$$h(t) = Ks^{*}(T-t) \tag{2.26}$$

Therefore, the output of matched filter is given as

$$\begin{aligned} s_{out} &= s(t) \otimes h(t) = \int_{-\infty}^{\infty} s(\tau)h(t-\tau)d\tau = \int_{-\infty}^{\infty} s(\tau)Ks^{*}\left[T-(t-\tau)\right] \\ s_{out} &\underset{K=IT=0}{=} \int_{-\infty}^{\infty} s(\tau)s^{*}(\tau-t)d\tau \end{aligned} \tag{2.27}$$

The last equation is called autocorrelation function (ACF) of *s (t).*

In this equation, s (t) is the received signal from a target. If target is moving, the received signal will be doppler-shifted and represented as

$$s_D(t) = s(t)\exp(j2\pi\upsilon t) \tag{2.28}$$

where υ is the velocity of the target. Here, matched filter output changes and becomes as follows:

$$s_{out}(t,\upsilon) = \int_{-\infty}^{\infty} s(\tau)\exp(j2\pi\upsilon t)s^{*}(\tau-t)d\tau \tag{2.29}$$

reversing t and τ we have,

$$\chi(\tau,\upsilon) = \int_{-\infty}^{\infty} s(t)s^{*}(\tau-t)\exp(j2\pi\upsilon t)dt \tag{2.30}$$

This equation is a very special kind of ambiguity function (AF). AF describes the output of the matched filter when the input signal is delayed by τ and doppler shifted by υ. In literature, AF itself is given as follows:

$$\left|\chi(\tau,\upsilon)\right| = \left|\int_{-\infty}^{\infty} s(t)s^{*}(\tau - t)\exp(j2\pi\upsilon t)dt\right| \tag{2.31}$$

AF is a very useful property in choosing optimum waveforms in radar applications.

2.4. Pulse Compression

2.4.1. Definition

Pulse compression allows the transmission of long pulses while retaining the advantages in high-resolution waveforms. Range resolution that is achievable in a radar system is

$$dR = cT/2 \tag{2.32}$$

where T is the pulse duration and c is the speed of light $(3\times10^{8} m/s)$. The bandwidth of the signal is $B = 1/T$.

In a pulse compression system, the transmitted signal is modulated in phase or frequency so that $B \rangle\rangle 1/T$. If $\tau = 1/B$ is chosen then the new range resolution becomes

$$dR = c\tau/2 \tag{2.33}$$

τ is the effective pulse duration in the radar after pulse compression. The ratio between the pulse duration and the effective pulse duration is called “compression

ratio" and it is equal to the time-bandwidth product of the system.

The compressed pulse in a radar system can be obtained by passing the pulse with the duration of T, through its matched filter, but the output signal length is 2T, not τ, then the response outside the interval $|t| < \tau$ is called range side lobes. For a given range bin, the sidelobes of the MF responses appear as signals in adjacent range bins, therefore they must be reduced or controlled.

There are 3 measures, PSL, ISL and LPG, to characterize the output compressed signal which are defined as

$$\text{Peak Sidelobe Level(PSL)} = 10\log(\text{max imum sidelobe power / peak power})$$

$$\text{Integrated Sidelobe Level(ISL)} = 10\log(\text{total power in the sidelobes / peak power}$$

$$\text{Loss in Pr ogressive Gain(LPG)} = 20\log(\text{Compression Ratio / peak voltage})$$

Another common parameter to characterize the compressed pulse is the main lobe width or time resolution defined by the Formula 2.34.

$$T_{res} = \frac{\int_{-\infty}^{\infty} \left| R(\tau) \right|^2 d\tau}{\left[R(0) \right]^2} \tag{2.34}$$

where $R(\tau)$ is the ACF of the radar signal (zero doppler).

In designing a radar system which utilizes the advantages of pulse compression, the choice of the waveform is one of the most important issues. In order to compare the possible waveforms, Ambiguity Function (AF) is used. The AF represents the time response of a filter matched to a given finite energy signal when the signal is

received with a delay τ and a Doppler shift υ relative to the nominal values (zeros) expected by the filter. Therefore, the AF definition followed in this thesis is

$$\left|\chi(\tau,\upsilon)\right| = \left|\int_{-\infty}^{\infty} u(t)u^{*}(t+\tau)\exp(j2\pi\upsilon t)dt\right| \tag{2.35}$$

where u represents the complex envelope of the signal. A positive υ means a target moving toward the radar and a positive τ means a target farther from the radar reference position ($\tau = 0$) **[3].**

2.4.2. Pulse Compression Techniques

2.4.2.1. INTRODUCTION

Although the widespread applications of pulse compression in pulse-doppler radar systems are frequency modulation and phase modulation, only phase modulation will be dealt with in this thesis.

2.4.2.2. PHASE MODULATION TECHNIQUES

Pulse compression by using phase modulation is realized simply by dividing the pulse length T into N subpulses, each of duration τ , and coding these subpulses with different phases. The complex envelope is given as

$$s(t) = \frac{1}{\sqrt{T}}\sum_{n=1}^{N} s_n \, rect\left[\frac{t-(n-1)\tau}{\tau}\right] \qquad s_n = \exp(j\phi_{n)} \quad \tau = T/N \tag{2.36}$$

Binary (biphase) codes can be represented by pluses and minuses, where a plus means 0º phase shift and a minus means 180º phase changes. The biphase coding of a

pulse is shown in Figure 2.9 **[4].**

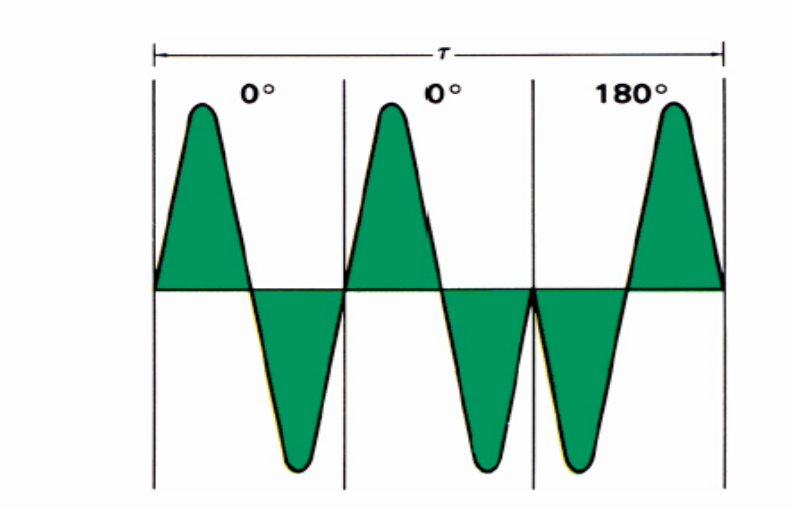

Figure 2.6 Binary phase coding of a transmitted pulse, [+ + -]

In polyphase codes, there are M different phases possible where M is the order of the code and possible phases can be written as

$$\phi_i = (2\pi / M)i, \ for \quad i = 1, \ldots, M \tag{2.37}$$

The most famous biphase codes with low PSL values are Barker Codes. They have the property that peak side lobes of the all types are equal to 1/N in magnitude, N is the code length. Barker Codes are the most important codes of biphase codes, because they have the minimum sidelobe power values that are possible theoretically. Because of this property, Barker Codes are called perfect codes. Some known barker codes and their PSL and ISL values are given in Table 2.1.

Table 2.1 Known Barker Codes

Code Length	Code	PSL(dB)	ISL(dB)
2	+ -, + +	-6.0	-3.0
3	+ + -, + - +	-9,5	-6.5
4	+ + - + ,+ + + -	-12.0	-6.0
5	+ + + - +	-14.0	-8.0
7	+ + + - - + -	-16.9	-9.1
11	+ + + - - - + - - + -	-20.8	-10.8
13	+ + + + + - - + + - + - +	-22.3	-11.5

The ambiguity function of 13-length Barker Code is shown in Figure 2.9 [3]

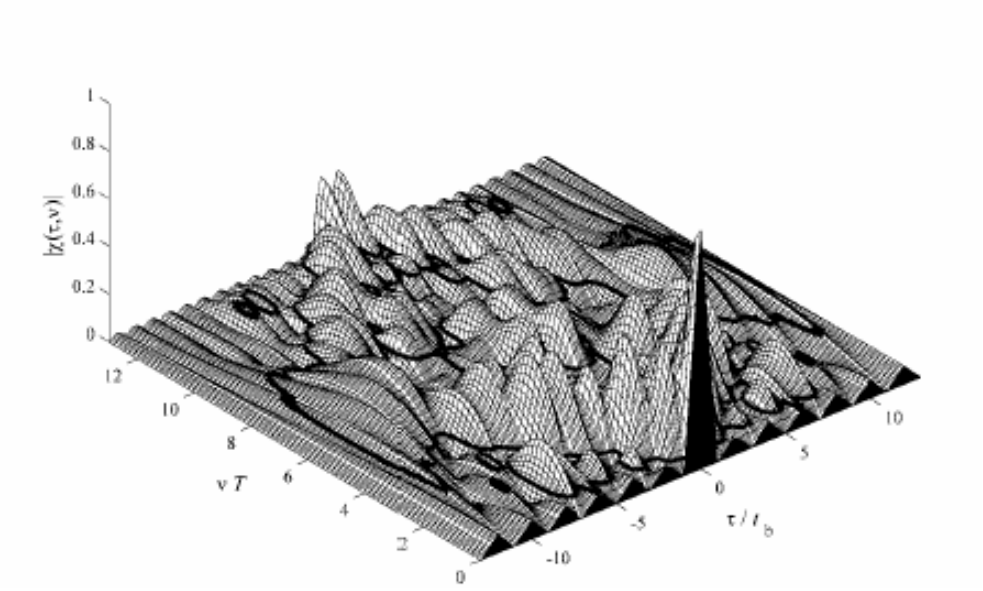

Figure 2.7 Ambiguity Function of 13-length Barker Codes

Generating optimum codes longer than 13 in length can be achieved by combining shorter Barker Codes. These codes are called Combined Barker Codes or Nested Codes. For example if a system with 35:1 pulse compression ratio is needed, 7x5 or 5x7 Barker codes can be used. 7x5 Barker code consists of the 7-bit Barker code and

5 bit Barker code. And for $13 \langle N \langle 45$ there are polyphase codes that are carried out by optimization methods. Other important derivatives of Barker Codes are Pseudorandom Codes and Golay Side-lobe Canceling Codes.

Other phase modulation codes are chirp like Phase Codes. Special forms of these modulation techniques are Frank Codes, P1, P2 and Px Codes, Zadoff-Chu Codes, P3, P4 and Golomb Polyphase Codes, the codes based on a Nonlinear FM Pulse.

2.5. Bandwidth Consideration in Phase Coded-Signals

The sharp phase transition and amplitude rise time in phase coded signals causes high spectral side lobes. In a practical receiver, the matched filter is implemented digitally in a correlator, that follows an analog-digital (A/D) converter. To limit the noise power reaching the A/D converter, an analog narrowband filter is likely to precede it. This filter will cut off the spectrum tail. Rather than allow the band pass filter to influence the delay response, the spectrum tail can be narrowed in the transmitter [3]. This can be achieved by smoothing the phase transitions in the transmitted pulse. Figure 2.11 shows the ACFs of sharp transition and smooth transition 13-length Barker waveforms. In the continuous phase version, the phase of a chip is shaped by a shaping pulse with the transition duration of T/5 which will be defined in the next chapter.

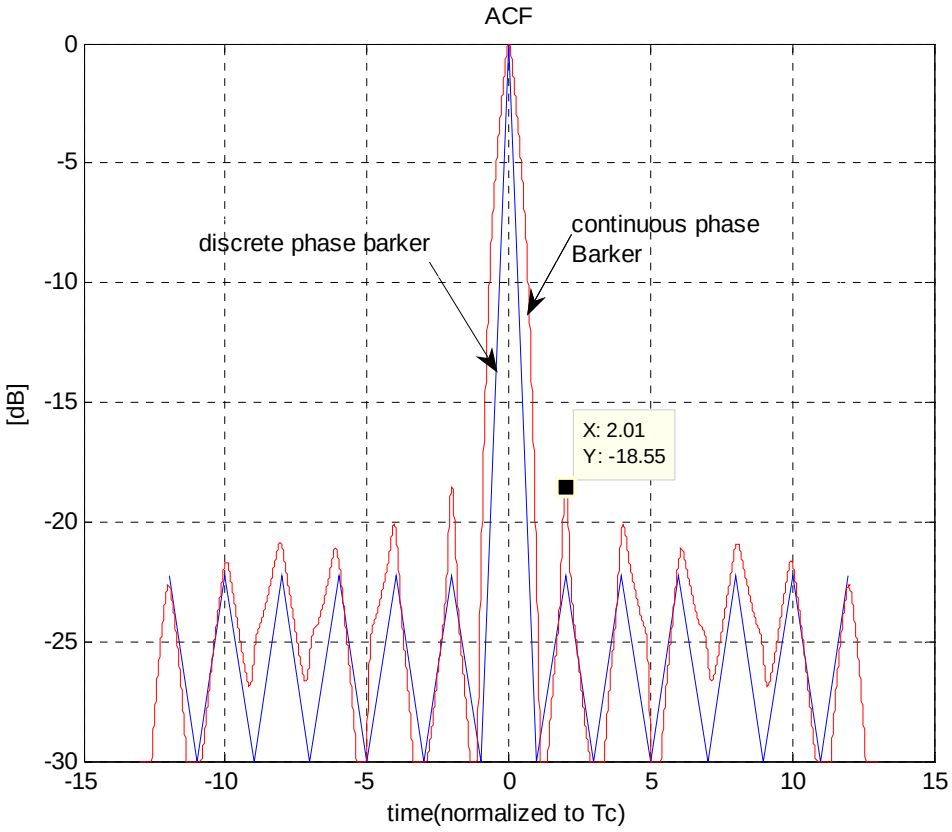

Figure 2.8 ACFs of Discrete and Continuous Phase Barker Code

CHAPTER 3

PHASE CODED PULSE IN PULSE DOPPLER RADAR

3.1. Introduction

Radar can be thought as a digital communication system with a completely known signal in the receiver just as the pulse compression technique can be considered as a digital modulation technique. In digital communication, the data are transmitted in terms of bit or symbol whereas in radar applications with pulse compression, the medium for transmission is the chip.

The reason of the usage of pulse compression in radar was stated in the previous sections. The next step is to search several phase coded pulses having optimum aperiodic autocorrelation functions for a pulse doppler radar with the operating frequency of 9.5 GHz, a chip width of 100ns (T_c), and an Intermediate Frequency of 70 MHz. The digital receiver implemented in this radar maximizes the advantages of using matched filters. The modulated or coded pulse is generated initially at 70 MHz, up converted to 9500 MHz and later amplified in a traveling wave tube amplifier (TWTA) before transmission. TWTA determines the type of the modulation because of its destructive effect on the radar amplitude or phase; therefore, it is an integral element of radar. This effect should be taken into consideration if one tries to find the optimum waveform.

Throughout the general searching process, initially the theory of Genetic Algorithm (GA) is provided, and later applied. It is not only the MLESSM modulations, BPSK

and QPSK optimum codes that are searched, but also a spectrally efficient MWM modulation, full-response CPM is investigated. At the end of this chapter, the spectrums of MLESSM and MWM waveforms are compared briefly.

3.2. Genetic Algorithm

Genetic algorithms are inspired by Darwin's theory of evolution since a process very similar to the process of evolution is used in problem solving via genetic algorithms. The genetic algorithm starts with a **set of solutions** (**chromosomes**) called **population**. Chromosomes are typically represented as simple strings of data and instructions. Initially several individuals are randomly generated to form the first population. During the evaluation of each individual, a value of fitness is returned by a fitness function. Fitness function is a type of objective function that quantifies the optimality of individuals or solutions. The individuals are later kept in a pool in which they are ranked from top to bottom according to their fitness values. The next step is to create a second generation of population based on the selection processes and reproduction of solutions through mutation and crossover. There are several selection algorithms to be used in selection process. An example is the roulette wheel selection. In this algorithm, normalized fitness value of each individual is computed, a random number that must be between 0 and 1 is defined, and the individuals with the fitness values greater than the defined random number are selected. Following this procedure, a crossover is performed with the selected individuals. Every genetic algorithm has a crossover probability typically between 0.6 and 1. In accordance with this probability, individuals are recombined. This process is repeated until the sufficient number of individuals for the next generation is reached. Subsequently, a new generation is mutated. The probability of mutation in genetic algorithms is 0.01 or less. Based on this probability, chromosomes of new individuals are mutated. Compared to the previous generation, the next generation, in general has a better average fitness value. The creation of generations is repeated until a termination condition is reached. The termination conditions reached are specific to each and

every particular application. In example, reaching a minimum fitness value can be the termination condition of one application whereas, reaching a maximum value can be the termination condition of another.

In the searching processes, different numbers of population are used according to the code length. 10000 and 50000 are used for the minimum number and maximum number of populations respectively. For the selection method, a constant number of top ranked solutions (10% in our algorithm) are chosen. Probabilities of crossover and mutation are defined as 0.9 and 0.01.

3.3. Optimum CPM Codes

In order to find the optimum CPM data sequences, a program should be coded in MATLAB. In this program each chip is designed by 100 samples, rendering the sampling period of the searching system 1ns. The CPM modulation has such a flexible structure that by changing any of the parameters forming the waveform, one can produce many CPM schemes. However, the particular focus of this study is on single-h and full response CPM schemes. In order to shape the phase of each chip implemented in CPM pulse, 1REC scheme given in Appendix A, is used. The single modulation index is considered to be 0.5 which is the most widely used value. From this point and on, the CPM code is referred to M-ary data sequence, I_k, which is used to generate CPM waveforms. Instead of "data sequence for CPM scheme", simply "CPM code" is used.

Regarding a genetic algorithm with a population number of 10000, the probabilities of crossover and mutation are defined as 0.9 and 0.01 respectively. These values are used to get the optimum I_k data sequences of the lengths 20, 32, 45 and 64 for different values of M (2, 4, and 8). The sequences where the searching process reaches a minimum PSL value are considered to be the optimum sequences. PSL,

ISL and Main Lobe Width (MLW) values of these codes are tabulated in Table 3.1

Table 3.1 Optimum CPM Codes, h = 0.5, 1REC

Code Length	PSL(dB)			ISL(dB)			MLW[chips]		
	M=2	M=4	M=8	M=2	M=4	M=8	M=2	M=4	M=8
20	-18.1	-19.02	-18.56	-5.27	-4.8	-3.89	1.40	0.70	0.40
32	-17.63	-18.95	-20.05	-6.40	-3.98	-2.5	1.34	0.74	0.44
45	-17.13	-20.05	-20.19	-3.50	-3.66	-2.45	1.60	0.75	0.40
64	-17.81	-20.50	-20.62	-3.3	-2.58	-1.56	1.69	0.80	0.45

PSL values improve as the alphabet size increases generally except that of the code of length 20. As an example, the PSL value of the CPM code of length 32 with M = 4 is 1.32 dB lower than the code with M = 2. In addition, ISL values get worse as the size of the alphabet and the length of the code increases. In fact, the main lobe width is very sensitive to the alphabet size, the code of length 64 has 1.69 chips of width for M = 2 and 0.45 chips of width for M = 8.

In order to demonstrate the phase structure in the CPM waveforms, the 20-length data sequence is selected from the other sequences found as and the phase structure for this waveform is given in Figure 3.1.

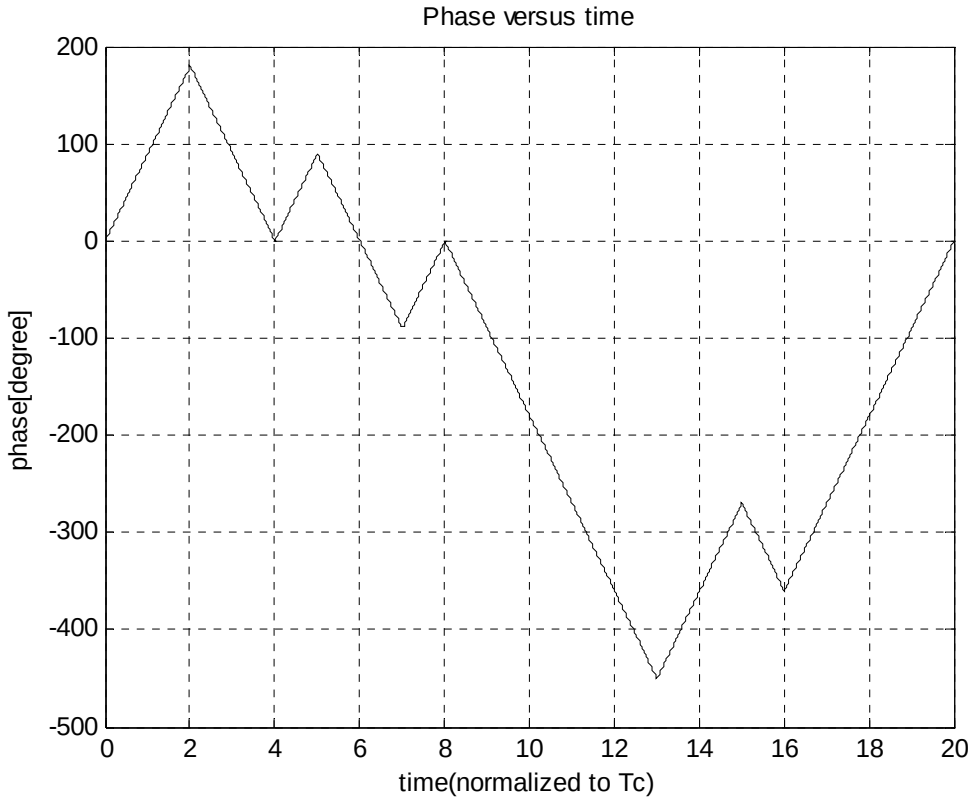

Figure 3.1 Phase variation of the CPM pulse N = 20, M = 2, h = 0.5

3.4. Optimum Memoryless Pulse

3.4.1. Optimum BPSK Codes

In fact, the output of the matched filter is simply the autocorrelation of the transmitted code in noise-free environments. Therefore, the discrete autocorrelation function is used in the optimization process. This optimization process uses the genetic algorithm with the parameters given in Section 3.2. The PSL value of each individual represents the fitness value in the genetic algorithm. The optimization is terminated when the process converges to a minimum PSL value. In Table 3.2, optimum biphase codes of lengths 20, 32, 45 and 64 are provided.

Although there is more than one code for some lengths, all are not given here. These codes can be found in [3].

Table 3.2 Optimum biphase codes

Length	PSL(dB)	ISL(dB)	Binary code
20	-20.00	-7.49	01010001100000011011
32	-20.56	-8.95	00000001111001011010101011001100
45	-23.5	-8.62	000101010111100001100110001101101101111110110
64	-24.08	-7.41	0100000010010000101000101110100111100110001100100011011111000010

It can be inferred from the table that if the length of the code increases, the PSL value of its ACF lowers. The ACF of the BPSK code of length 64 has 4.08 dB lower PSL value than that of the BPSK code of length 20. If PSL value is critical in any radar waveform design, it is recommended to increase the code length to any value which provides the required PSL value. The autocorrelation functions of these codes are computed in MATLAB and shown in the Figure 3.2.

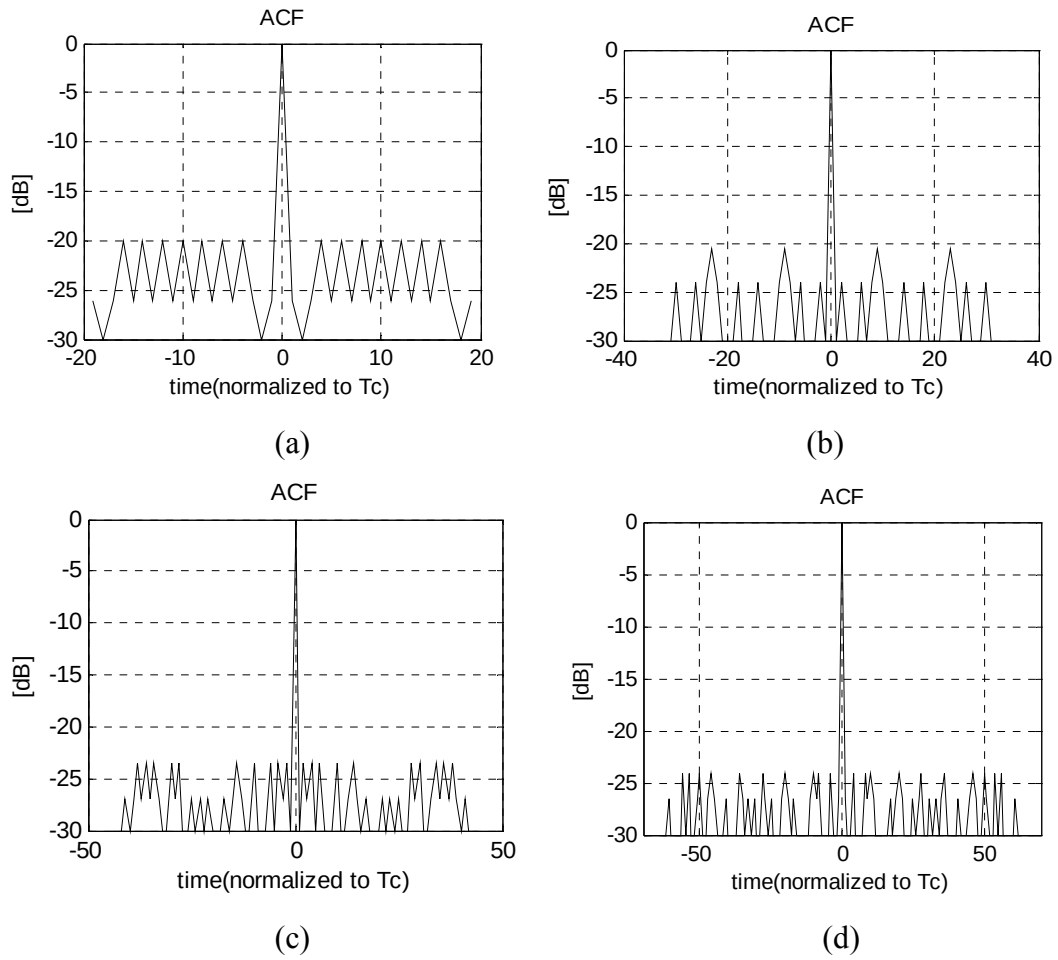

Figure 3.2 ACFs of optimum BPSK codes of lengths of 20(a), 32(b), 45(c) and 64(d)

In a phase coded pulse, the phase has a discrete value in each chip interval and this value sharply changes from one chip to another. These sharp changes are clearly observable in Figure 3.3 which shows the phase variation of the biphase code of length 20 with respect to time.

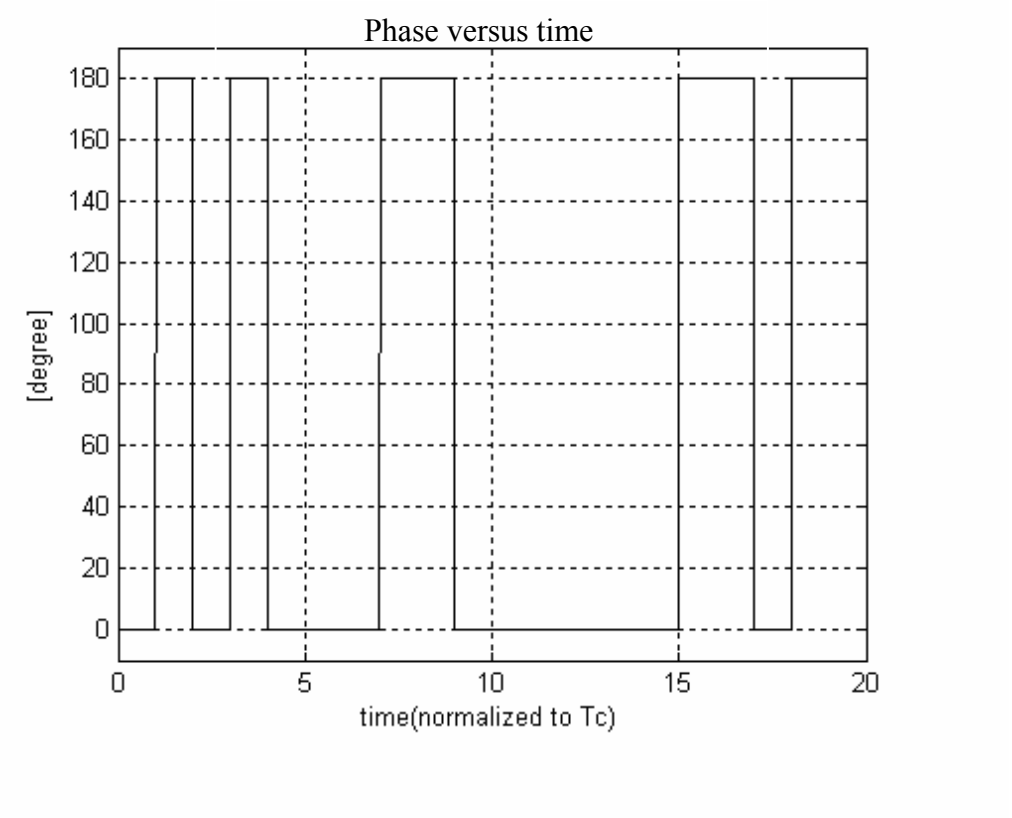

Figure 3.3 Phase variation of the biphase code of length 20

3.4.2. Optimum QPSK Codes

The commonly used QPSK constellations are given in Figure 3.4. In this study, the constellation in Figure 3.4 (a) is employed to represent QPSK chips. The arrows indicate the paths along which the QPSK modulator can change its state.

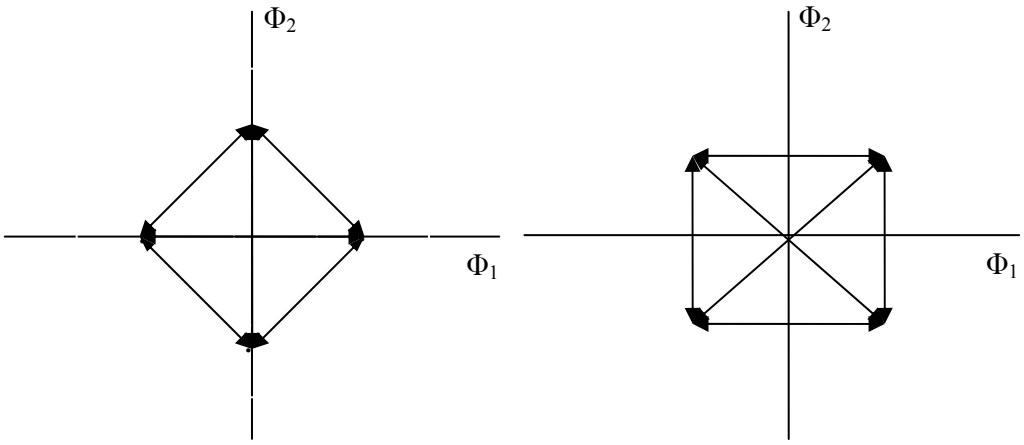

Figure 3.4 Commonly used signal constellations for QPSK

The searching algorithm is processed for the codes of lengths 20, 32, 45 and 64. In GA, the fitness values are the PSL values, therefore minimum ISL codes are not guaranteed to be found. This is the reason why the ISL values given in Table 3.3 get higher when the code length increases. In the contrary, PSL values lower as the length increases.

Table 3.3 Optimum quadriphase codes

Length	PSL(dB)	ISL(dB)	Code
20	-20.00	-7.1181	π/2[2 2 1 0 -1 0 2 1 0 1 1 0 1 2 0 -1 0 1 2 2]
32	-20.10	-7.1213	π/2 [1 2 2 2 2 -1 0 2 1 2 2 -1 2 0 -1 1 2 0 0 1 2 0
45	-20.76	-5.2380	π/2[2 2 2 0 -1 2 0 0 2 2 -1 2 2 2 -1 0 -1 -1 0 2
64	-21.5	-4.2583	π/2[2 2 -1 -1 -1 2 2 0 0 0 0 -1 1 -1 1 0 2 -1 -1

In general, the PSL values of quadriphase codes are higher compared to that of biphase codes.

ACFs of the optimum quadriphase codes are sketched in MATLAB and given in Figure 3.5

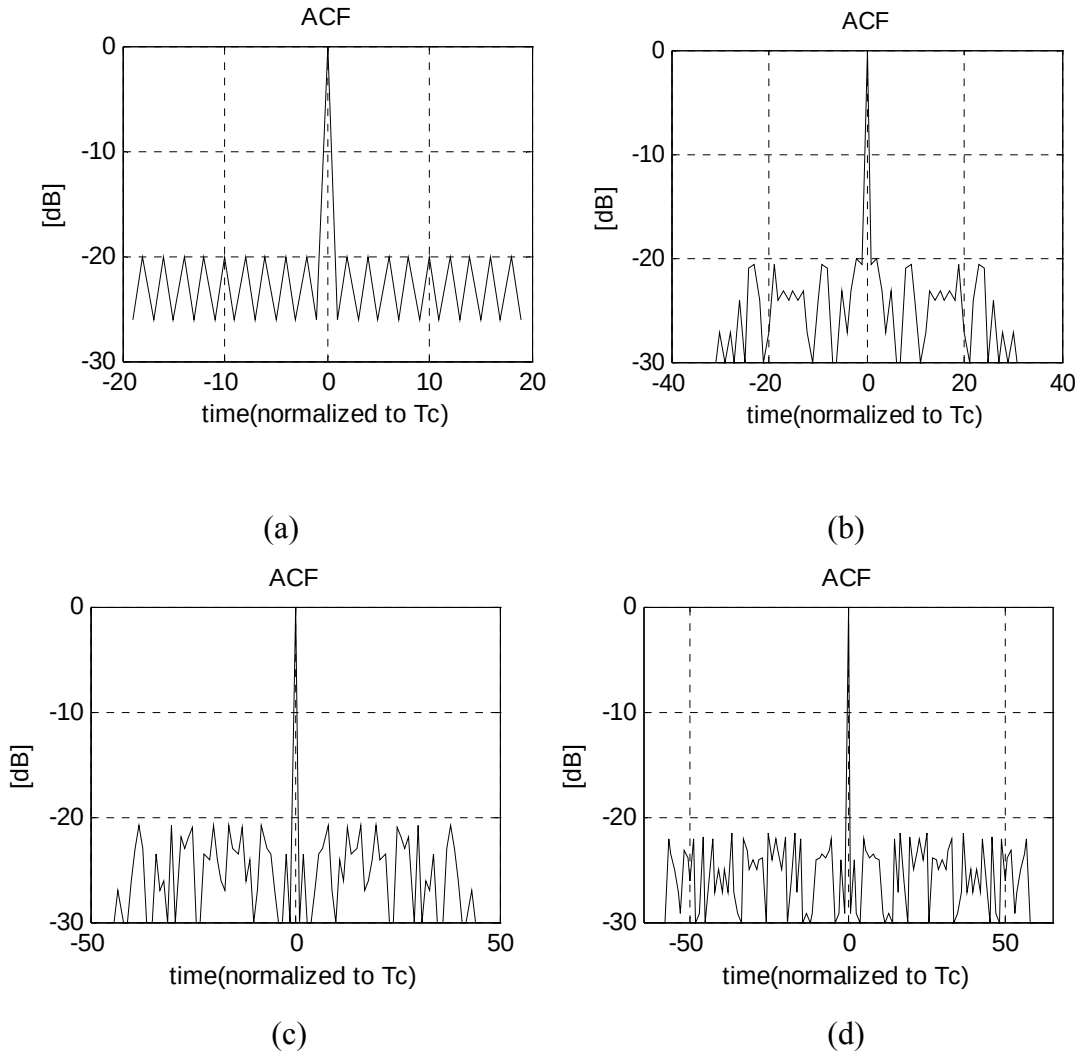

Figure 3.5 ACFs of QPSK codes of lengths 20(a), 32(b), 45(c), 64(d)

The phase variation of the quadriphase code of length 20 with respect to time is shown in Figure 3.6. This phase variation can be compared to that of BPSK (20-length BPSK) in Figure 3.3. The phase jumps sharply from one chip to another.

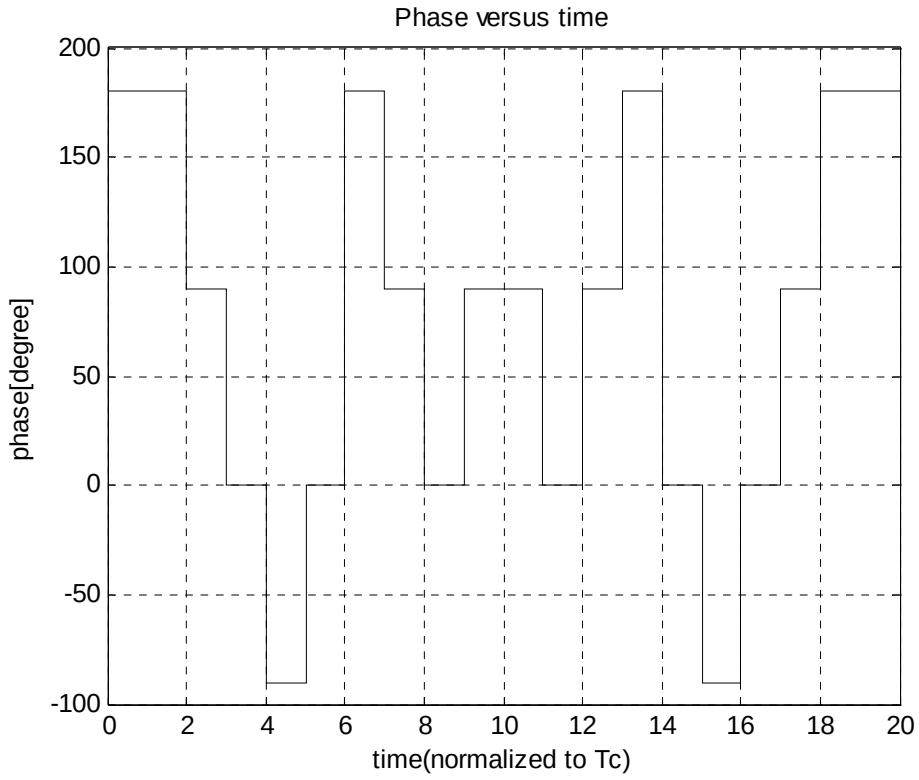

Figure 3.6 Phase variation of QPSK code of length 20

We have extracted the general QPSK codes until now. However, related researches refer to the concept offset QPSK which is used to limit phase changes to 90 degrees. Alternatively, in this study, a modulation similar to Offset-QPSK which is abbreviated as Limited Phase Transition QPSK (LPT-QPSK) is used. The LPT-QPSK can be considered as a version of Offset QPSK which is suitable for radar applications. The constellation diagram shown in Figure 3.7 is utilized for LPT-QPSK codes.

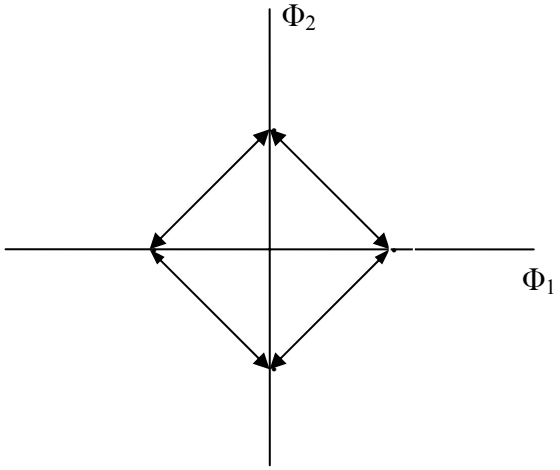

Figure 3.7 Signal constellation of LPT-QPSK

GA results in the optimum LPT-QPSK codes tabulated in Table 3.4. The main advantages of these codes will be well understood when the bandwidth efficiency and the sampling mismatch effect are analyzed throughout this chapter and the next chapter respectively. This modulation has low sidelobes in the spectrum due to the limited transition of the change in phase (90 degrees).

Table 3.4 Optimum LPT-QPSK codes

Length	PSL(dB)	ISL (dB)	LPT-QPSK code
20	-17.00	-5.38	π /2[2 1 0 -1 -1 0 -1 0 1 2 1 2 1 0 0 1 2 1 0 1]
32	-18.96	-5.51	π /2 [-1 0 1 0 -1 0 1 2 1 0 -1 0 1 1 2 1 0 -1 0 1 0 1
45	-19.08	-4.21	π /2 [1 0 1 2 1 0 0 -1 0 1 2 1 0 1 2 1 0 -1 0 -1 0 1
64	-20.10	-3.20	π /2[0 1 0 1 0 0 1 2 1 2 2 1 0 -1 0 1 2 1 0 -1 -1 0 1

The data acquired from Table 3.4 shows that as length increases, PSL values get lower. In general, PSL values of LPT-QPSK codes are higher than those of QPSK codes. The PSL value of the QPSK code of length 20 is 3 dB lower than that of the LPT-QPSK code of the same length. Autocorrelations of these codes are computed in MATLAB,

given in Figure 3.8.

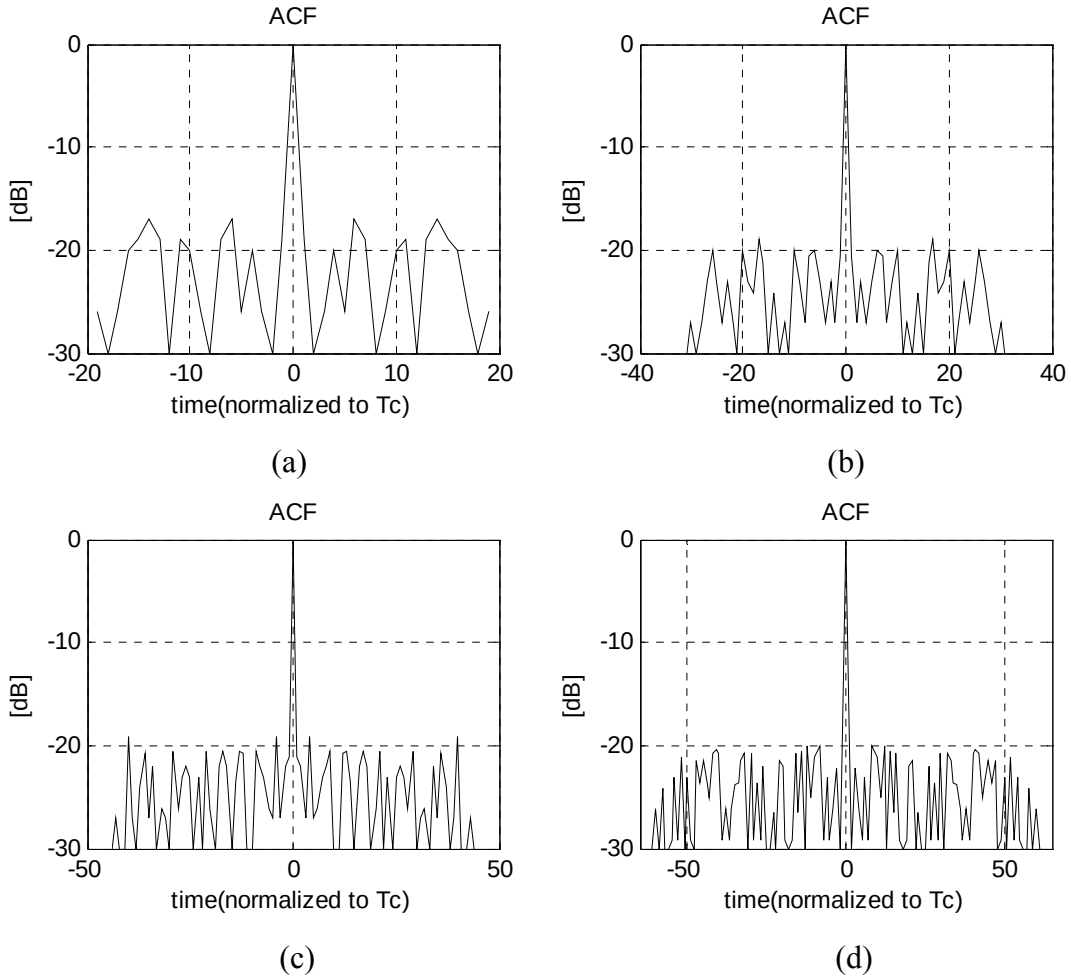

Figure 3.8 ACFs of LPT-QPSK code of lengths 20(a), 32(b), 45(c), 64(d).

In order to see the limited phase transitions, the phase variation of LPT-QPSK code of length 20 with respect to time is drawn in Figure 3.9. The phase transitions are limited to 90 degrees. As a result, the sharpness is reduced and consequently the spectrum is improved.

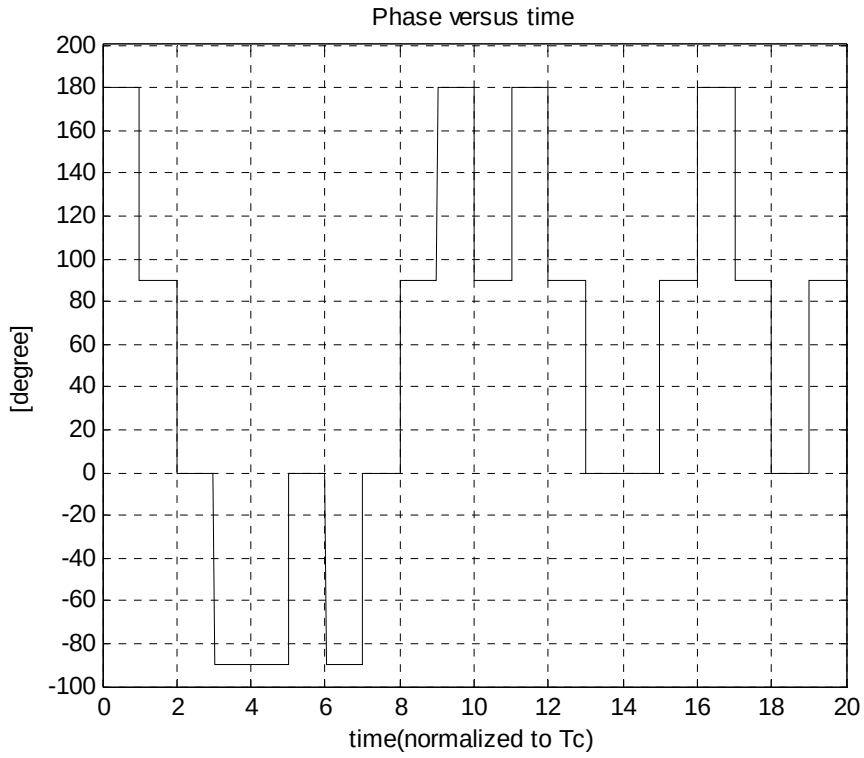

Figure 3.9 Phase variation of LPT-QPSK code of length 20

Up until now, all MLESSM codes have been searched and reported. They are all arranged in a graph seen in Figure 3.10. This graph is useful to decide on optimum discrete phase codes. As the code gets closer to the left-down corner, optimality increases. It is obvious that the BPSK code of length 45 is very close to optimality due to its low PSL and ISL values.

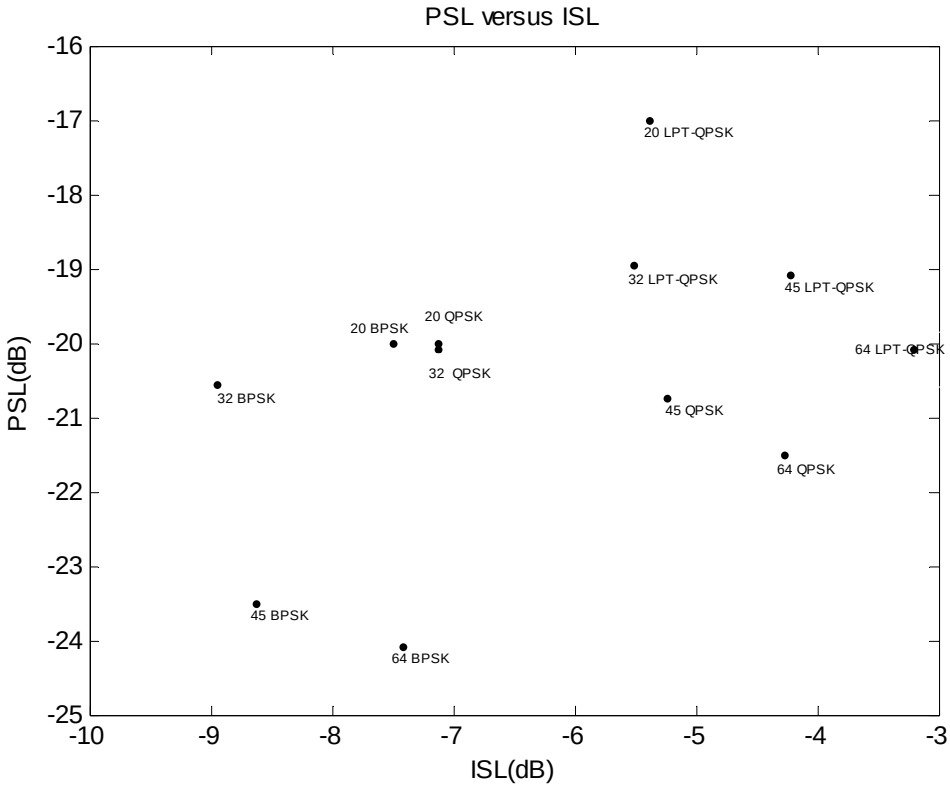

Figure 3.10 PSL versus ISL

3.4.3. Sidelobe Suppression Techniques

3.4.3.1. INTRODUCTION

In multiple-target environments, where there are large point reflectors, it is often desirable that the time sidelobes of ACF of the phase coded pulses be reduced to the lowest level possible. Otherwise, the integrated sidelobes can appear as smaller targets at other ranges or as extended targets [8]. Basically, there are two widely used sidelobe reduction techniques namely Weighting and Inverse Filtering. Weighting is applied to the optimum codes obtained in the previous sections and it is observed that this technique does not work on these codes. The weighting technique instead of reducing the sidelobe levels either increases the sidelobe levels or has no effect on them. For that reason, the inverse filtering technique is currently the only applicable

method. In the next section, the theory of inverse filtering is accessed; and applied to the optimum codes obtained in the previous sections.

3.4.3.2. INVERSE FILTERING

Pulse compression allows a radar system to transmit long duration signal and achieve the range resolution of short duration pulses. The compression is achieved by correlating the receive signal with the code sent. This is called matched filtering. In this system there is not only compressed signal but also range sidelobes, causing false alarms in the receiver. This problem can be overcome by the intelligent choice of the codes. In the previous sections we have tried to obtain these codes with smallest range sidelobes. However, the results are limited by the length of the codes and the number of phases used. Better results can be reached by using mismatch filtering. This method tries to minimize the total energy in sidelobes in other words; it tries to minimize ISL. Due to this property it can be called as optimal ISL filtering.

Assume the output of the correlator is given by y_k , input code sequence of length N by a_k and the filter of length M by h_k . The output sequence can be expressed as

$$y_k = \sum_{j=0}^{P} a_j h_{k-j} \qquad k = -p,..., p \tag{2.39}$$

Here, p is an integer representing the greater of the code and filter lengths, and the code is zero-padded to the same length as filter length.

In calculating total power in side lobes, main peak must be subtracted out. The total power in sidelobes is given by the formula

$$E = \sum_{k=-p}^{p} {y_k}^2 - {y_0}^2 \tag{2.40}$$

In minimizing E, the solution $h_k = 0$ must be disallowed. Then a constraint equation that the peak is a constant must be used.

$$\Phi = \sum_{j=0}^{P} a_j h_j - C \tag{2.41}$$

Lagrange Multiplier method can be used to find coefficients h_n. Now, E(h) is minimized by considering the constraint equation given in Equation 2.41 as $\Phi = 0$.

$$\frac{\partial}{\partial h}(E - \lambda\Phi) = 0 \qquad k = 1,..., p \tag{2.42}$$

λ is the Lagrange Multiplier. Substituting Eq.2.40 and Eq. 2.41 into Eq. 2.42, we get:

$$\frac{\partial}{\partial h_m}\left[(\sum_{k=-p}^{p} y_k{}^2 - y_0{}^2) - \lambda(\sum_{j=0}^{P} a_j h_j - C) \right] = 0 \qquad m = 0,..., p \tag{2.43}$$

By taking the partial derivatives, Eq. 2.43 becomes

$$2\sum_{k=-p}^{p}\left(\sum_{k=0}^{p} a_j h_{j-k}\right) a_{k+m} - 2\sum_{j=0}^{P} a_j a_m h_j - C = \lambda a_m \qquad m = 0,..., p \tag{2.44}$$

There are p+1 linear equation, and they can be written in matrix notation as

$$\mathbf{YH} = \frac{\lambda}{2}\mathbf{A} \tag{2.45}$$

$\mathbf{Y}$ is p+1 by p+1 matrix, H is p+1 by 1 column vector, A is the p+1 by 1 column vector consisting of a_k's. So, Eq.2.45 can be written as

$$\mathbf{H} = \frac{\lambda}{2}\mathbf{Y}^{-1}\mathbf{A} \tag{2.46}$$

$\frac{\lambda}{2}$ is only a scaling factor and it does not change the structure of the filter. But it can be chosen to have the equal amplitude as matched filter peak.

3.4.3.3. INVERSE FILTERING ON DISCRETE PHASE QPSK CODES

Initially, the QPSK code of length 20 is selected to observe the sidelobe reduction when the inverse filtering technique is applied. The ACF of this code was given in Figure 3.5(a). Figure 3.11 depicts the response of the IF filter of length 20 obtained with the solution of Equation 2.46.

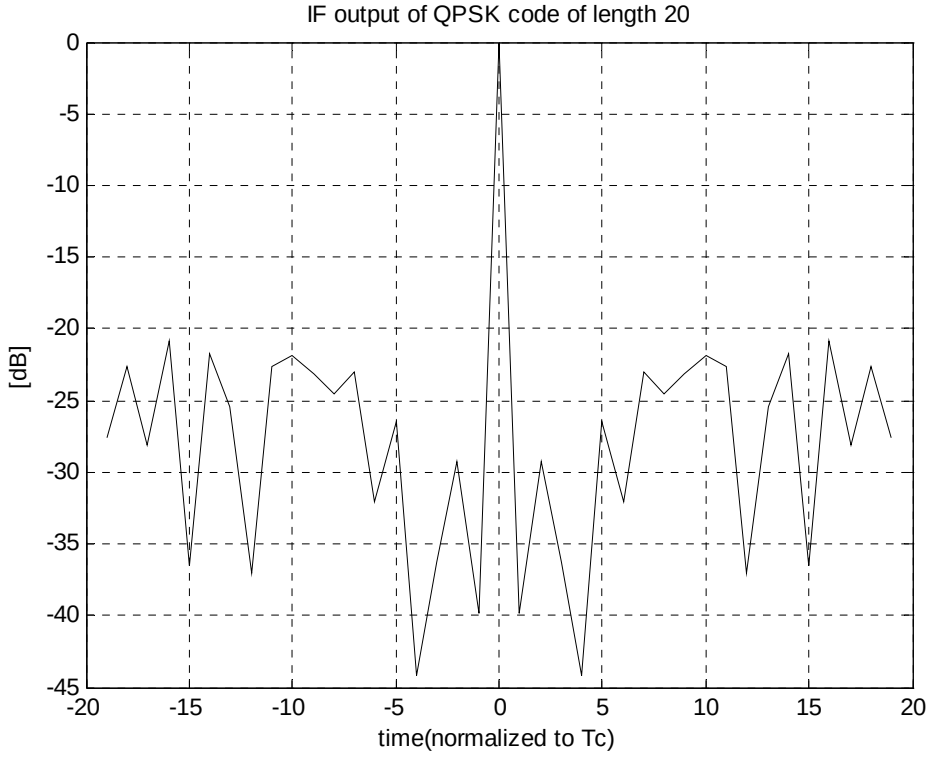

Figure 3.11 QPSK code of length 20 filtered with IF of length 20

When the inverse filter of length 20 is applied to the QPSK code of length 20, the output has an ISL value of -9.68 dB which is 2.58 dB lower than the matched filter output. In ISL minimization process, inverse filtering also lowers the PSL. The inverse filtered QPSK code has a PSL value of -20.84 dB which is 0.84 dB lower than that of the matched filter output. In the inverse filtered output, the sidelobes close to the main peak have lower values in comparison to the side lobes which are distant to the mean peak. If two close targets are tried to be detected, this result turns

out to be an advantage. On the other hand, the drawback of inverse filtering is the necessity of mismatch filtering which results with SNR loss. The related inverse filtered code has a mismatch loss of 0.21 dB for the case considered.

In the previous section, it is stated that IF length can be greater than the code length. Figure 3.12 shows the response of the IF filter of length 60 applied to the QPSK code of length 20. In this case, the ISL value is lowered to -16.95 dB which is 9.85 dB lower than the ISL of the matched filter output while the PSL of the response is -25.67 dB, which is 5.67 dB lower than that of the matched filter output. Finally, the SNR loss amounts approximately to 1.14 dB. In addition, inverse filtering has one more advantage with respect to matched filtering which is the main lobe getting narrower.

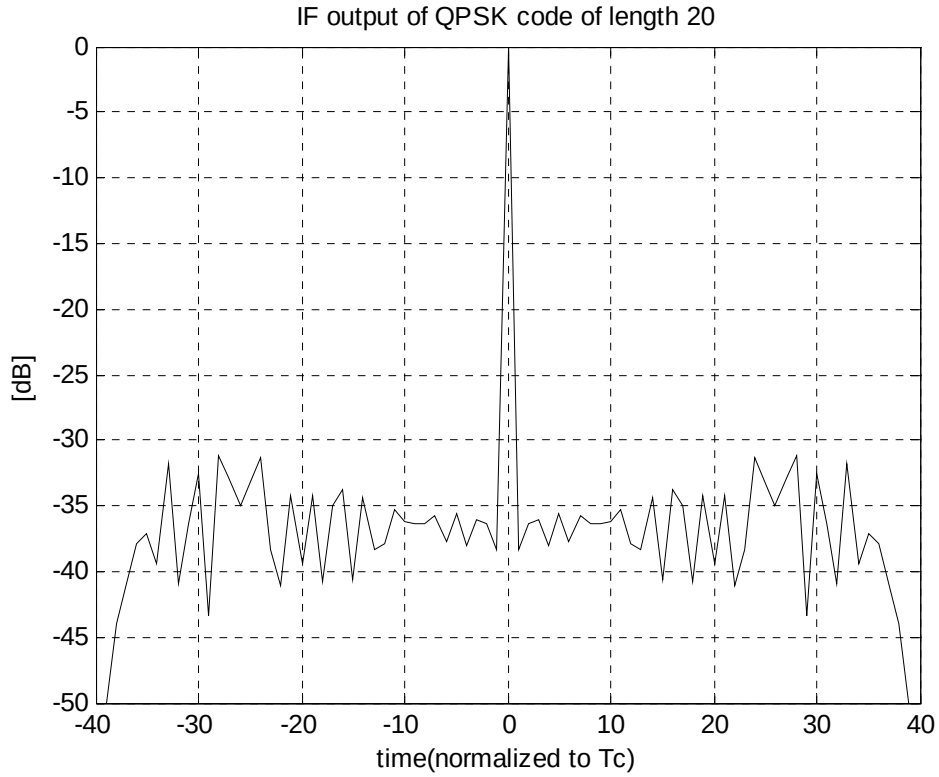

Figure 3.12 QPSK code of length 20 filtered with the IF of length 60

In the Figures 3.13, 3.14, 3.15 and 3.16, the variations of SNR loss, MLW, PSL and ISL are sketched with respect to the IF filter length for the QPSK code of length 20.

The filter length varies between 20 and 100.

In the inverse filtering method, the total power in side lobes is attempted to be minimized, however, PSL values also improve. The 20-length IF output has a PSL value, which is 0.84 dB lower than the PSL of the matched filter output. Besides, the IF output of length 100 has a 20 dB lower PSL value compared to that of the matched filter output. The variation of the PSL with respect to the filter length is given in Figure 3.13.

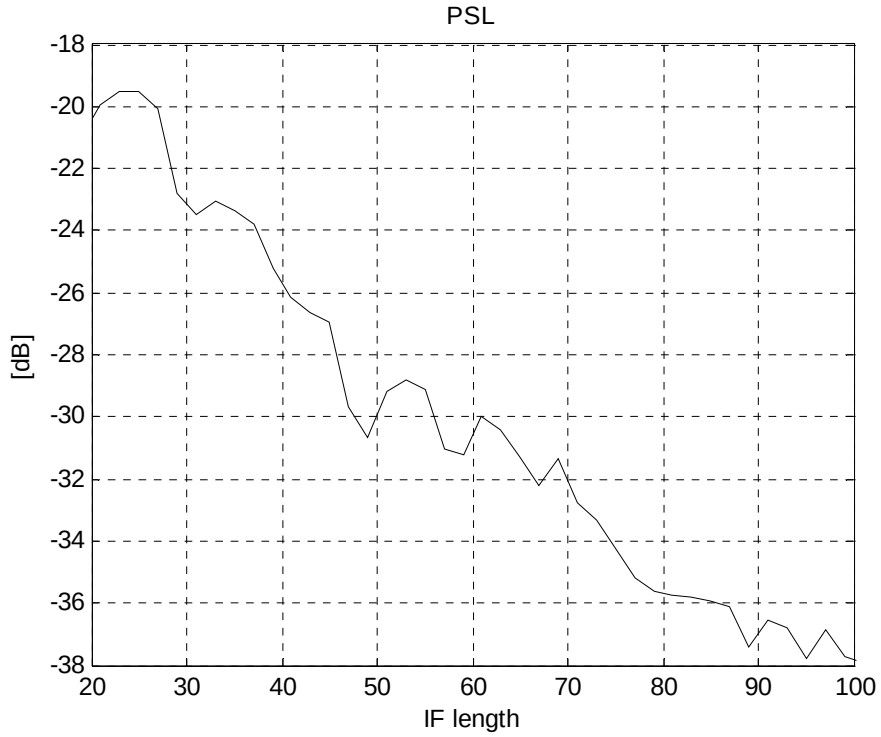

Figure 3.13 PSL versus IF filter length

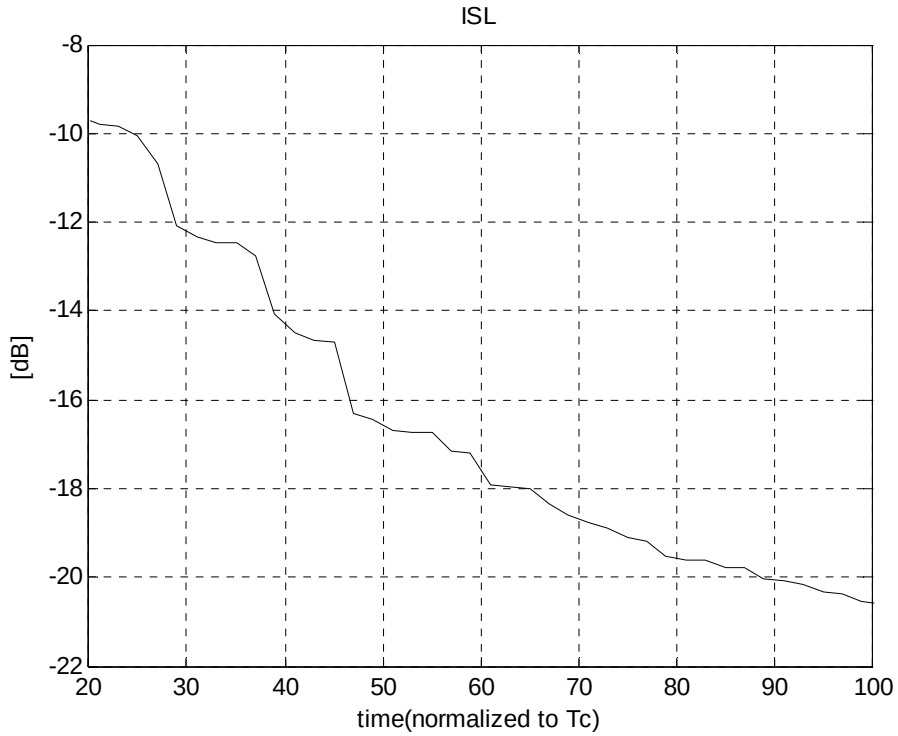

Figure 3.14 ISL versus IF length

ISL versus the filter length is given in Figure 3.14. Inverse filtering overcomes the problem of obtaining codes with low ISL. According to Figure 3.14, if the IF filter of length 100 is used, the ISL value of the inverse filter output is 14 dB lower than that of the matched filter output.

As stated before, in comparison to the matched filter case, the main lobe gets narrower when inverse filtering is applied. An increment of the filter length from 20 to 100 causes a decrement in the MLW from 1.11 chips to 1.01 chips.

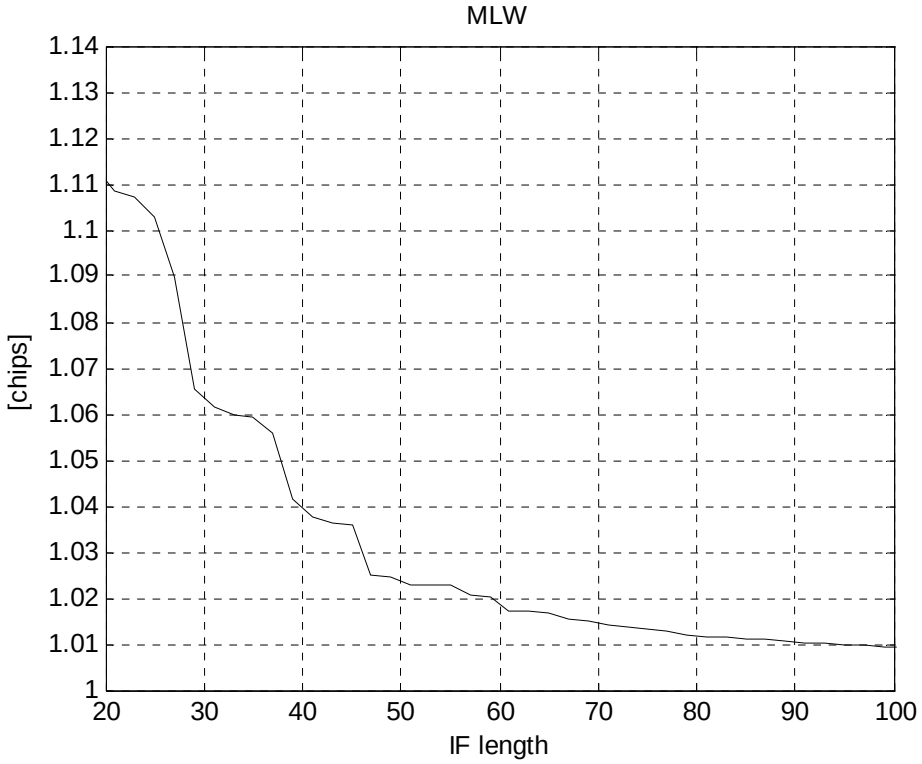

Figure 3.15 MLW versus IF length

Figure 3.16 shows the effect of the filter length on SNR loss. As the filter length increases, SNR loss also increases. The IF of length 20 has 0.4 dB of SNR loss. This value increases to 1.15 dB when the length of IF increases to 100.

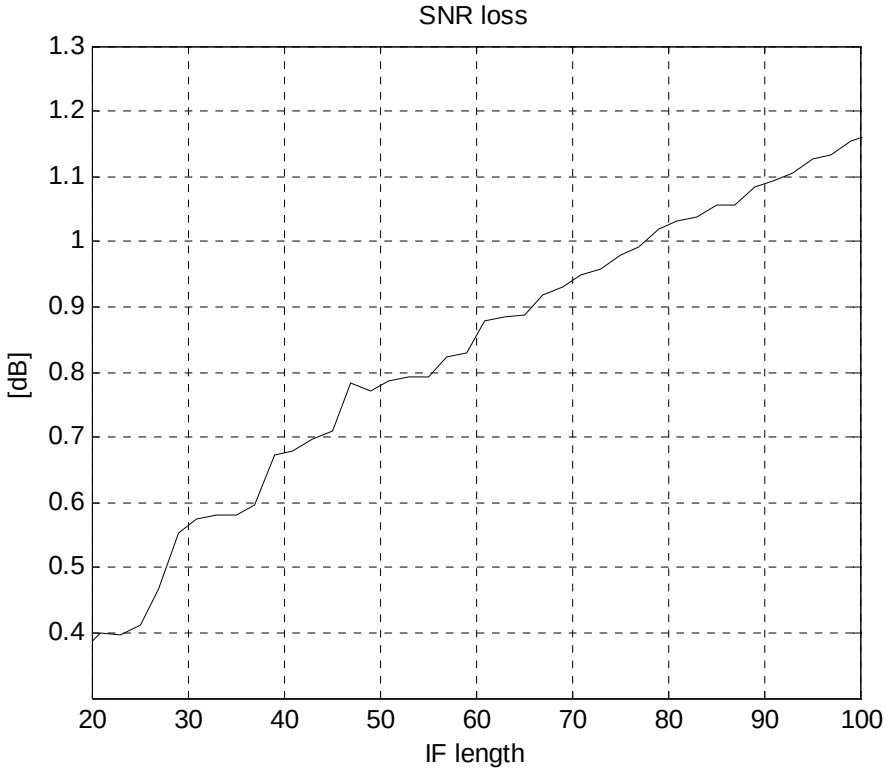

Figure 3.16 SNR loss versus IF length

The results show that, one can choose the filter length depending on requirements and priorities. Assume that a QPSK code of length 20 is used in a radar system. This radar system contains an optimum filter which has a PSL value on the order of -30 dB, an ISL value on the order of -19 dB, an SNR loss not greater than 1 dB and a minimum main lobe width. In this case, the length of IF should be selected within the interval [70, 80].

3.5. Optimum Continuous Phase Memoryless Waveforms

3.5.1. Phase Shaping Pulse

In the previous sections, each chip in a pulse is assumed to have a discrete phase value. In continuous time, it can be thought that the phase of each chip is shaped by a rectangular pulse. This case causes high level sidelobes in the spectrum. For the time being, in order to form the phase of each chip, a new phase shaping pulse is demonstrated in Figure 3.17 is used.

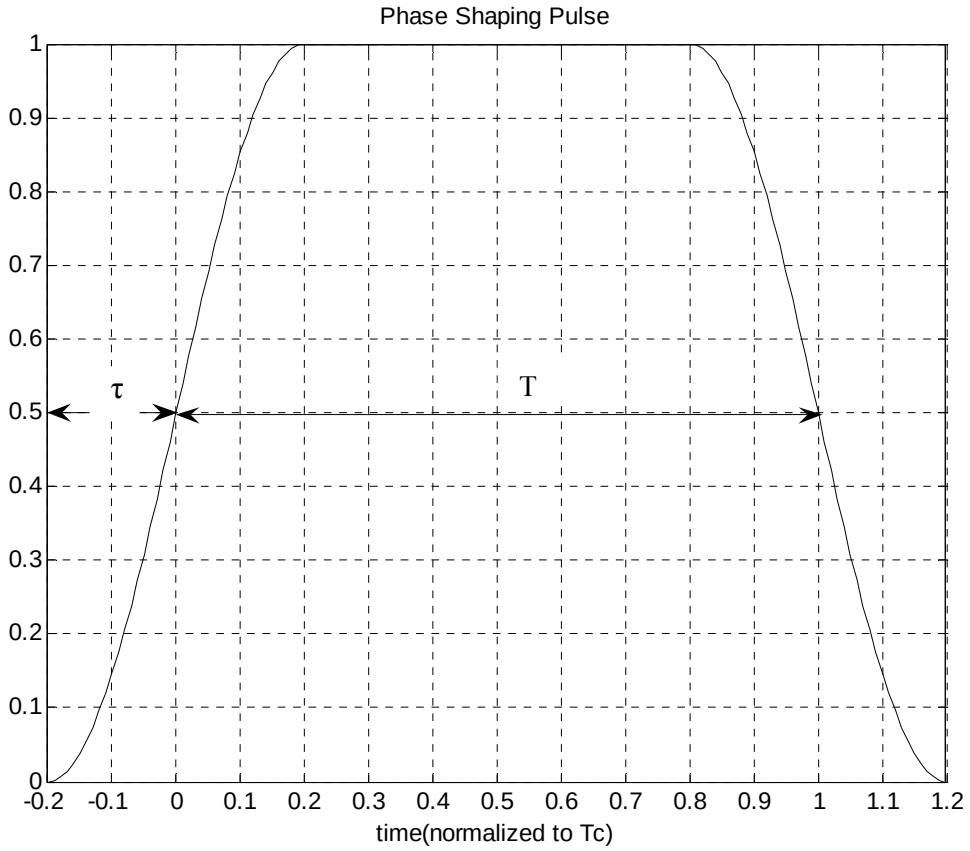

Figure 3.17 Phase Shaping Pulse for $\tau = T/5$, T=100

In the pulse, each of the transition regions has a half-cosine shape. It is assumed that the total duration of the transition in each chips phase is never greater than T/2 where T is equal to the chip width, T_c.

3.6. Continuous Phase Waveforms

3.6.1. Continuous Phase BPSK Waveforms

If the phase shaping pulse given in the previous section is used to form the phase of the BPSK pulse with N=20, the phase variation becomes as in Figure 3.18. The initial phase is assumed to be equal to the constant phase of the first chip. And also the tail of the last chip phase is not allowed and it is equalized to the constant phase of last chip.

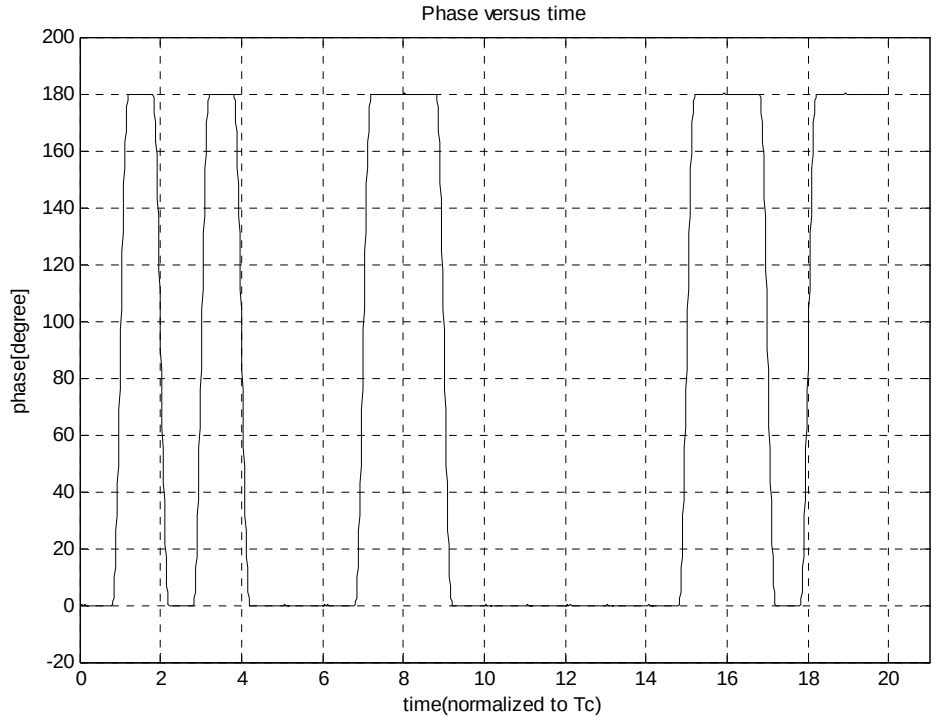

Figure 3.18 Phase variation of the continuous phase 20-length BPSK signal, $\tau = T/5$

In Figure 3.18, the continuous ACF of the continuous phase BPSK waveform formed by the code of length 20 is given where the duration of the transition is taken as T/5. The PSL value is higher compared to the discrete case.

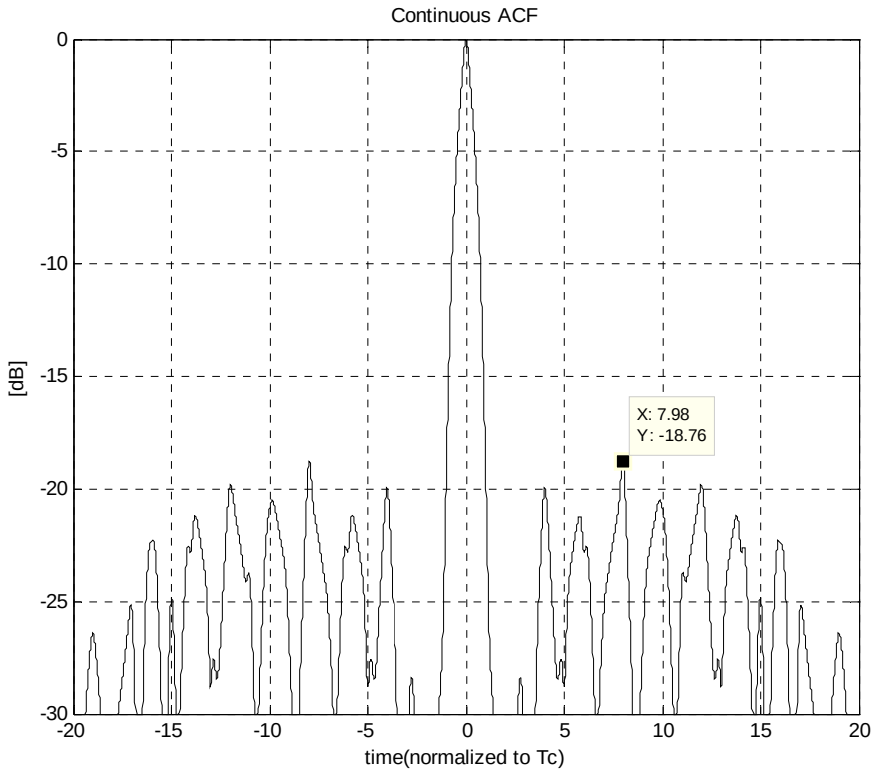

Figure 3.19 Aperiodic ACF of BPSK pulse, N = 20, $\tau = T/5$

The PSL value of the continuous phase systems matched filter output is -18.76 dB which is 1.24 dB higher than the discrete phase case. Table 3.5 gives the variation of PSL and ISL values with respect to duration of transition in the phase shaping pulse. The case, $\tau = 0$ refers to the discrete phase case. In this case, the PSL value of the MF output is -20 dB. The output of the matched filter in the continuous phase case with $\tau = T/4$, has 1.56 dB higher PSL than the discrete phase case. As the duration of the transition increases, the PSL and the ISL values get higher. In contrary to the discrete case, all of the ISL values are lower in the continuous phase case. This may be due to the definition of the main lobe and the characteristic of the code. The worst case where $\tau = T/4$ has -7.72 dB of ISL which is 0.23 dB lower than the discrete phase case.

Table 3.5 PSL and ISL of the continuous phase BPSK pulse, N = 20, τ = T/5

Duration of Transition	PSL(dB)	ISL(dB)
0	-20.000	-7.490
T/50	-19.9255	-8.1327
T/25	-19.8024	-8.1239
2T/25	-19,5397	-8.0892
4T/25	-19.0213	-7.9557
T/5	-18.7587	-7.8604
T/4	-18.4352	-7.7193

Continuous ACFs of the other lengths of codes are given in Figures 3.20 through Figure 3.22.

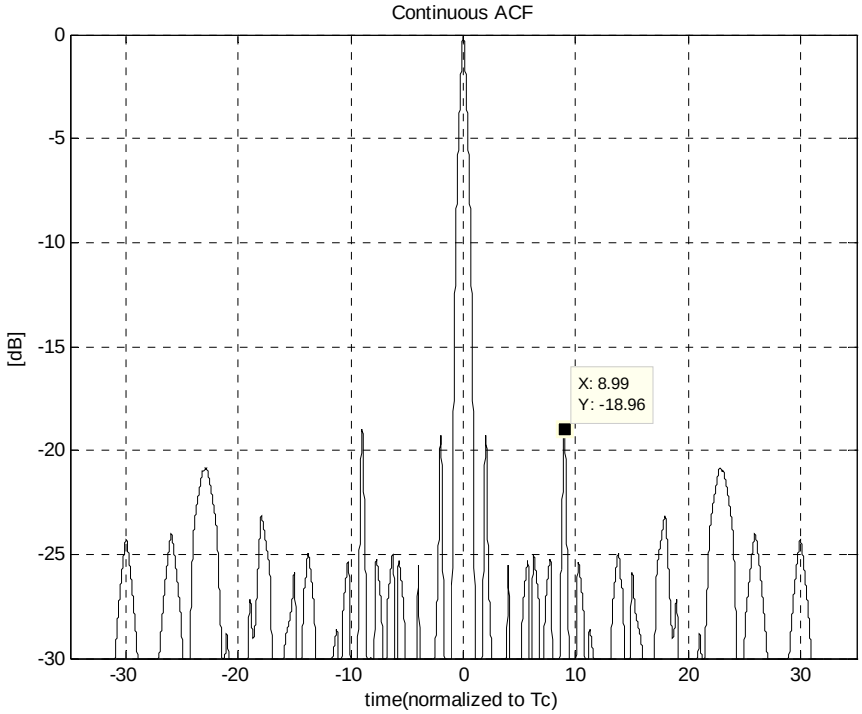

Figure 3.20 Aperiodic ACF of the BPSK pulse, N = 32, τ = T/5

The matched filter output of the continuous phase system has a PSL value of -18.96 dB which is 1.6 dB higher than the discrete case.

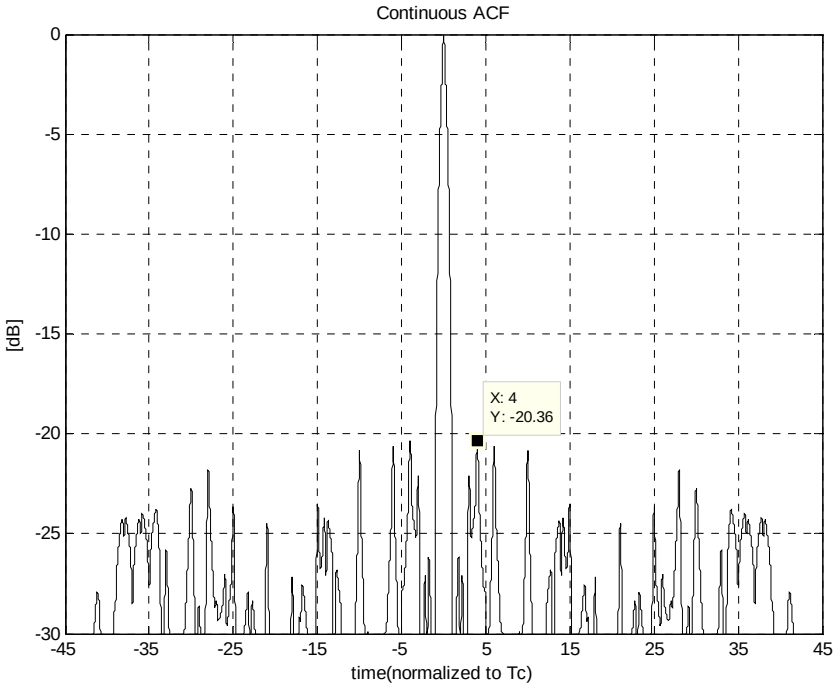

Figure 3.21 Aperiodic ACF of the BPSK pulse, N = 45, τ = T/5

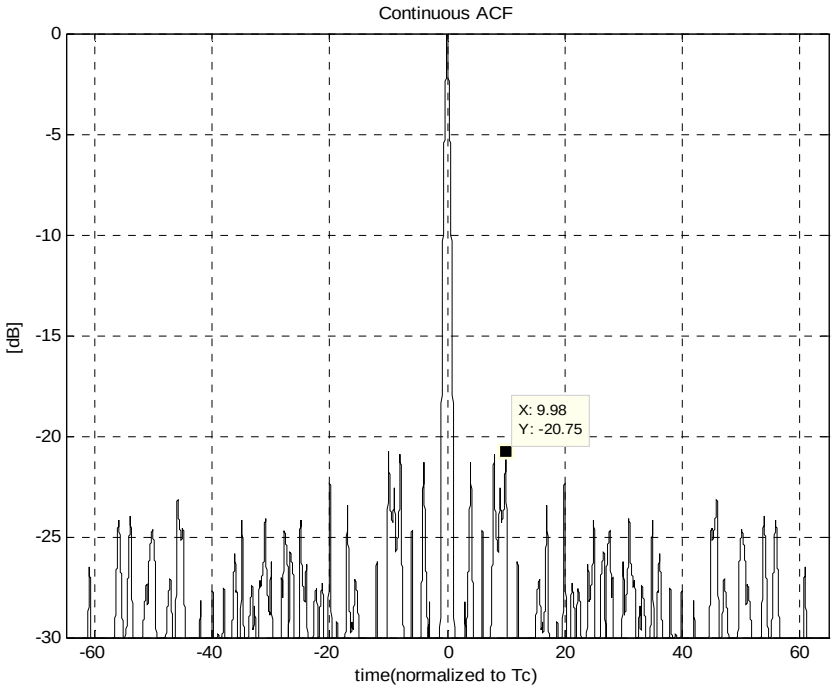

Figure 3.22 Aperiodic ACF of the BPSK pulse, N = 64, τ = T/5

Figure 3.21 and 3.22 show the continuous ACFs of the BPSK codes of lengths 45 and 64. The PSL values are again higher than the PSL values of the discrete phase MF outputs. Table 3.6 shows the variation of the PSL and the ISL of the BPSK codes of length 32, 45, 64 with respect to the duration of transition.

Table 3.6 PSL and ISL of the BPSK pulse with N = 32, 45, 64

Duration of Transition	PSL(dB)			ISL(dB)		
	N = 32	N = 45	N = 64	N = 32	N = 45	N = 64
0	-20.56	-23.5	-24.08	-8.95	-8.62	-7.41
T/50	-20.4001	-23.1988	-23.7235	-8.3732	-8.3160	-7.5926
T/25	-20.2304	-22.8728	-23.3693	-8.3652	-8.2781	-7.5662
2T/25	-19.8959	-22.2206	-22.6661	-8.3292	-8.1266	-7.4566
4T/25	-19.2562	-20.9565	-21.3605	-8.1585	-7.5526	-7.0111
T/5	-18.9505	-20.3559	-20.7536	-8.0172	-7.1611	-6.6870
T/4	-18.5809	-19.6391	-20.0376	-7.7878	-6.6105	-6.2093

The results demonstrate that as the duration increases, PSL and ISL of the matched filter output get higher. The PSL value of the MF output for the BPSK waveform with N = 64, τ = T/50 is -23.72 dB, occurs to be 3.7 dB lower than the case where the duration of transition is T/4.

3.6.2. Continuous Phase QPSK Waveforms

If the phase of each chip in the 20-length QPSK code is shaped with the phase shaping pulse in Figure 3.17, the phase variation of the pulse with respect to time becomes as in Figure 3.23. N refers to the number of chips in a pulse.

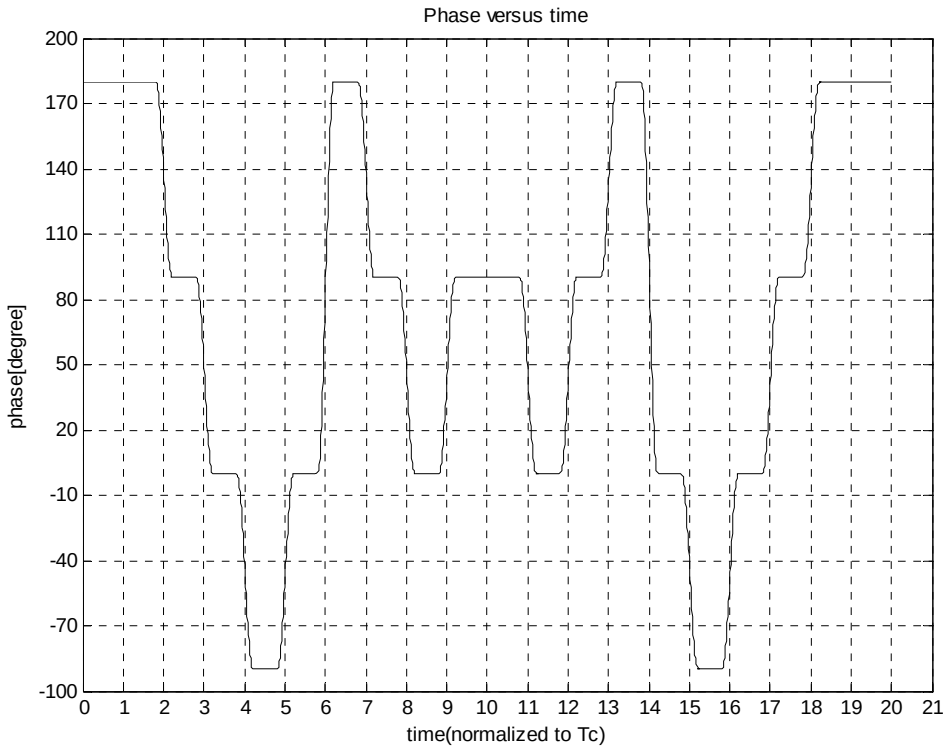

Figure 3.23 Phase variation of the continuous phase QPSK pulse, N=20, τ = T/5

The QPSK code of length 20 is a phase symmetric code and this symmetry is observable in Figure 3.23. In Figure 3.24, aperiodic ACF of the QPSK pulse with N = 20 is shown for the transition duration of T/5.

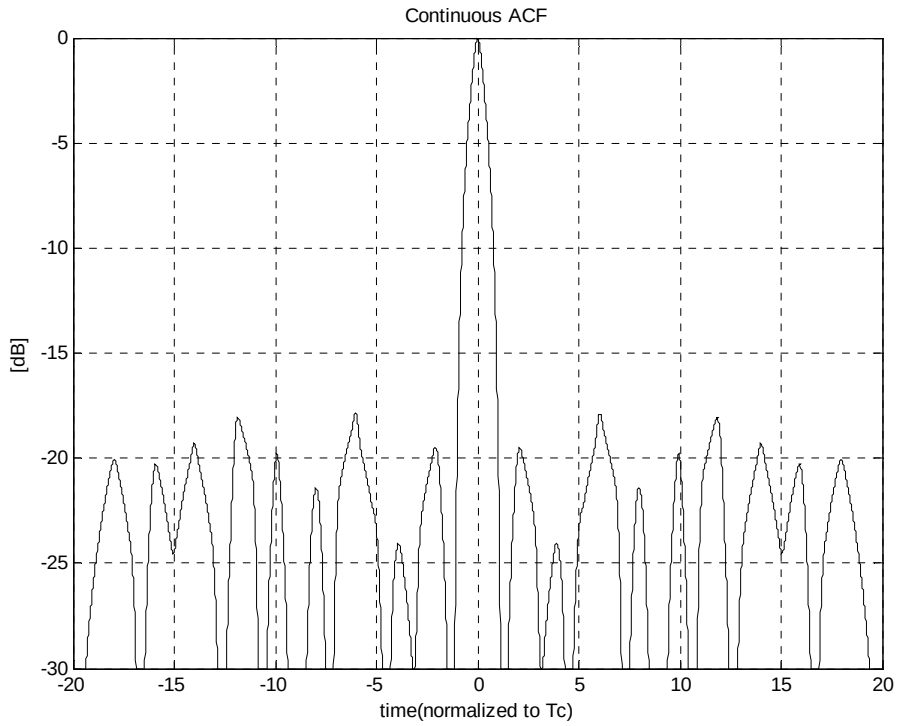

Figure 3.24 Aperiodic ACF of the QPSK pulse, N = 20, $\tau = T/5$

The PSL value of the continuous phase system is -17.84 dB, which is 2.16 dB higher than the discrete case. The decrement in PSL values of this pulse is more dramatic than the BPSK pulse of the same length. In Figure 3.25, the aperiodic ACFs of the QPSK pulse are drawn for different values of τ. The sidelobes close to the main lobe become higher than the sidelobes which are distant from the main lobe.

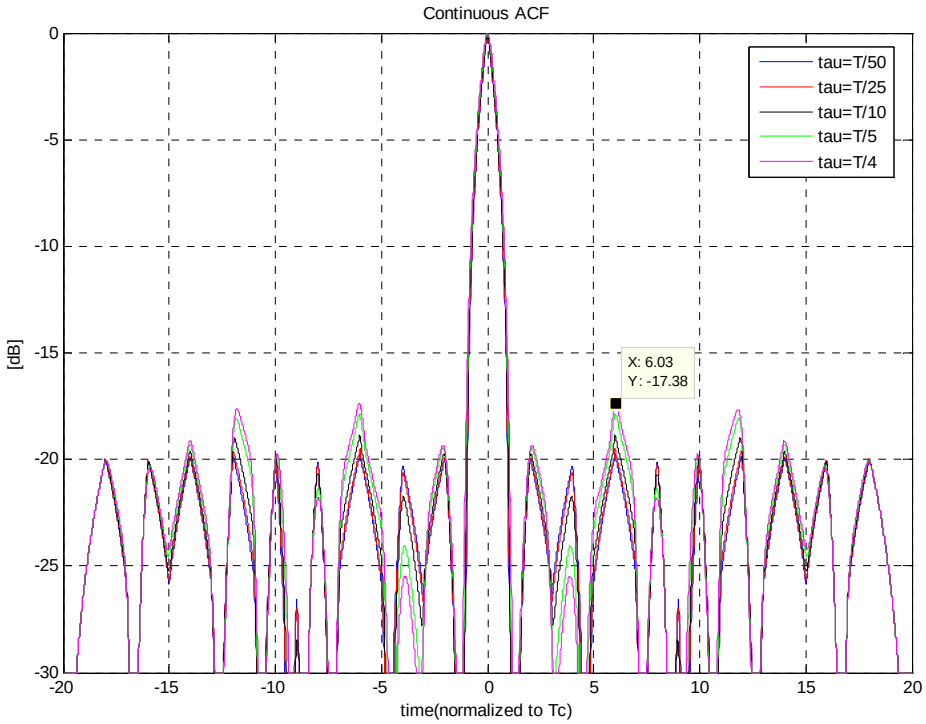

Figure 3.25 Aperiodic ACFs of the QPSK pulse, N=20

If a continuous phase pulse is to be used in a radar system, Table 3.7 may help any designer to decide on τ values. The variations of PSL and ISL with respect to the duration of transition are put into a table for the QPSK pulse with N = 20. The results again prove that the PSL and the ISL values depend on the value of τ. The PSL of the matched filter output in the continuous phase scheme with τ = T/50 is -19.75 dB which is 2.4 dB lower than the scheme with τ = T/4.

Table 3.7 Effect of Duration on PSL and ISL

Duration of Transition	PSL(dB)	ISL(dB)
0	-20.0000	-7.1181
T/50	-19.7512	-7.0553
T/25	-19.5137	-7.0578
2T/25	-19.0668	-7.0502
4T/25	-18.2307	-6.9896
T/5	-17.8426	-6.9395
T/4	-17.3789	-6.8611

In order to see the effect of the phase shaping pulse, the aperiodic ACFs of the QPSK pulses with N= 20, 32, 45 and 64 for $\tau = T/5$ are given in Figure 3.26.

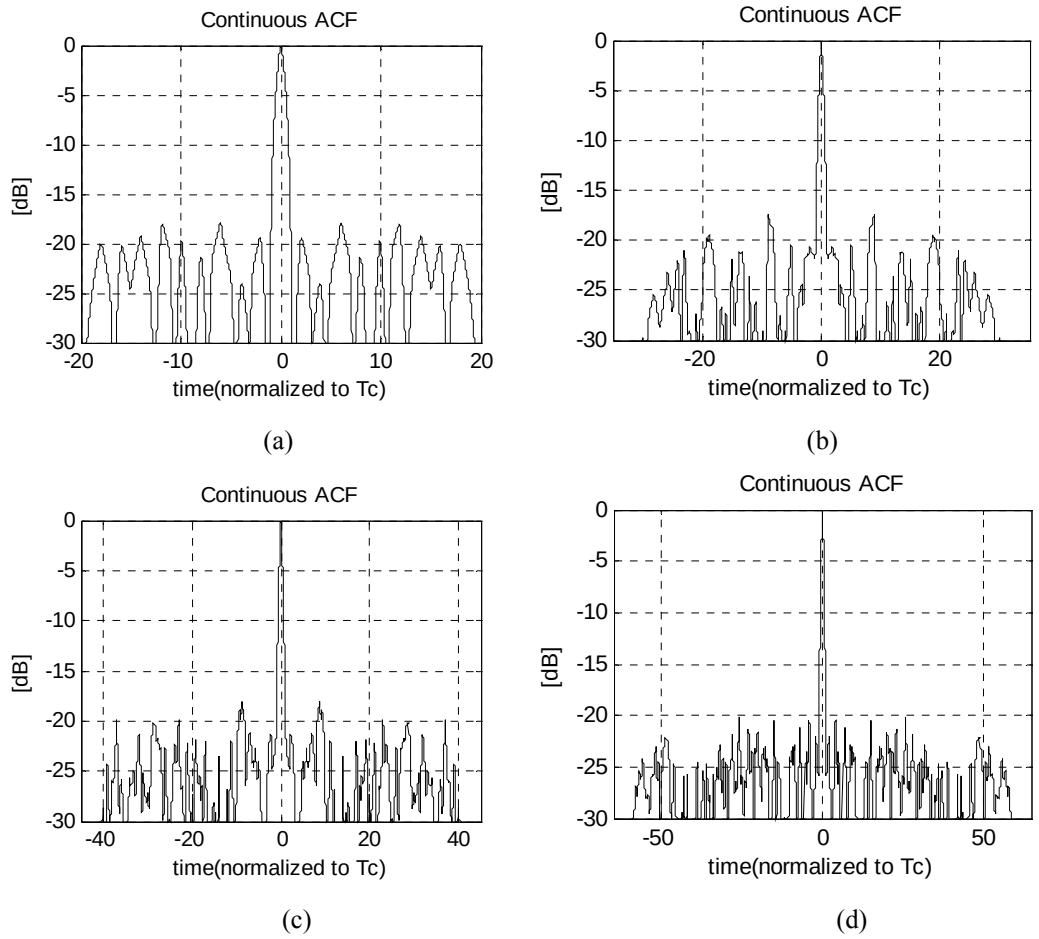

Figure 3.26 Aperiodic ACFs of QPSK pulses, N=20(a), 32(b), 45(c), 64(d)

In Table 3.8, the PSL and the ISL variations of the MF outputs of the QPSK pulses with N = 20, 32, 45, and 64 are summarized. The PSL of the matched filter output of the continuous phase scheme for the QPSK pulse with N = 32 and $\tau = T/50$ is -20.19 dB, which is 3.38 dB lower than that of the output of the scheme with the duration of T/4. The same comparison is made for the QPSK pulse with N = 45, and the difference is only 2.48 dB. For the QPSK pulse with N = 64, the difference becomes 1.1 dB. Consequently, as the code length increases, the effect of the duration on the PSL values decrease.

On the other hand and quite unexpectedly, for the QPSK pulse with N = 64, as the duration increases the ISL values of the MF outputs do not follow a pattern. The reason of this result may be the definition of the main lobe region and the specialty of the code.

Table 3.8 Effect of Duration on PSL and ISL

Duration of Transition	PSL(dB)			ISL(dB)		
	N = 32	N = 45	N = 64	N = 32	N = 45	N = 64
0	-20.10	-20.76	-21.50	-7.1213	-5.238	-4.2583
T/50	-20.1877	-20,5178	-20.7910	-6.9717	-5,3053	-3.9736
T/25	-19.8430	-20,2811	-20.7705	-6.9050	-5,3010	-3.9990
2T/25	-19.1747	-19,8188	-20.7246	-6.7158	-5,2776	-4.0416
4T/25	-17.9854	-18,9401	-20.4256	-6.1532	-5,1830	-4.0892
T/5	-17.4441	-18,5279	-20.0671	-5.8074	-5,1190	-4.0923
T/4	-16.8122	-18,0350	-19.6361	-5.3427	-5,0306	-4.0757

The previously defined LPT-QPSK codes are used to form the continuous phase pulses and aperiodic ACFs of the continuous phase pulses are computed.

The phase variation and the aperiodic ACF of the LPT-QPSK pulse (N = 20) with respect to time is given Figure 3.27 and in Figure 3.28 respectively.

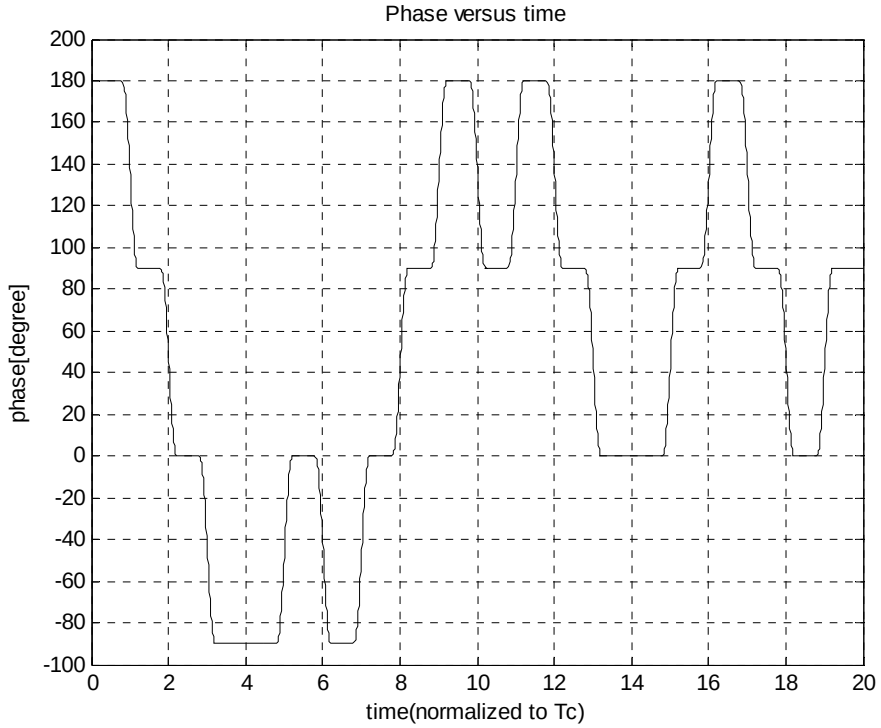

Figure 3.27 Phase variation of the LPT-QPSK pulse with N = 20, τ = T/5.

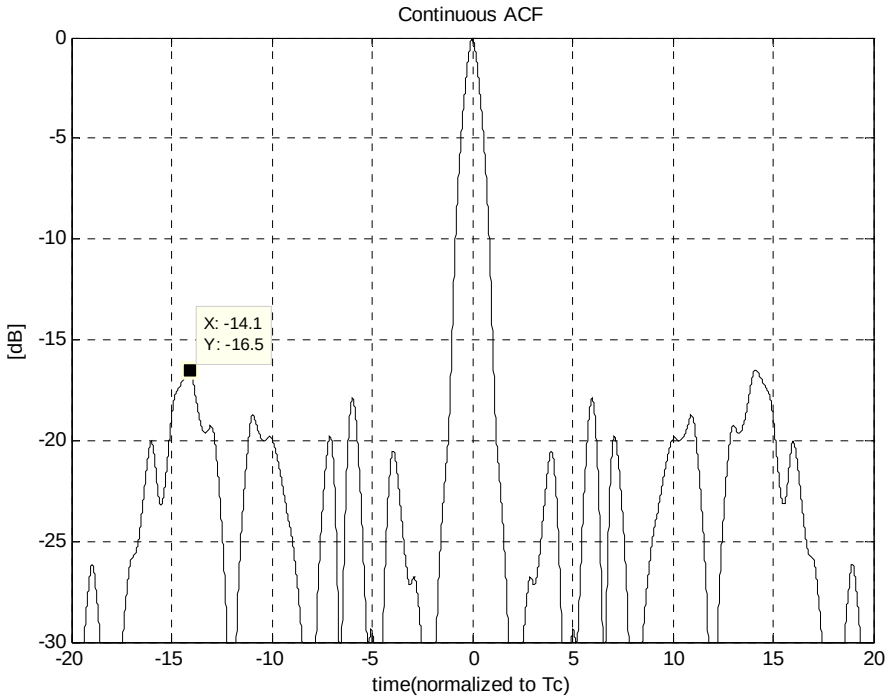

Figure 3.28 Aperiodic ACF of the LPT-QPSK pulse, N = 20, τ = T/5.

The PSL value of the continuous phase LPT-QPSK scheme with $\tau = T/5$ is -16.5 dB, which is 0.5 dB higher than that of the discrete case. In the previous section, the same decrement was calculated as 2.16 dB for the QPSK case. Table 3.9 summarizes the PSL and ISL variations of the MF output of the LPT-QPSK pulse with N = 20 with respect to the transition duration parameter (τ). The PSL of the matched filter output of the LPT- QPSK pulse with N = 20, $\tau = T/50$ is -16.93 dB, which is 0.55 dB lower than that of the output of the scheme with $\tau = T/4$. In general, any change in τ slightly affects the PSL and ISL values.

Table 3.9 Effect of Duration on PSL and ISL

Duration of Transition	PSL(dB)	ISL(dB)
0	-17.000	-5.3800
T/50	-16.9219	-6.3505
T/25	-16.8750	-6.3686
2T/25	-16.7792	-6.4065
4T/25	-16.5906	-6.4883
T/5	-16.4976	-6.5316
T/4	-16.3820	-6.5873

Aperiodic autocorrelations of codes of other lengths are given in Figure 3.29.

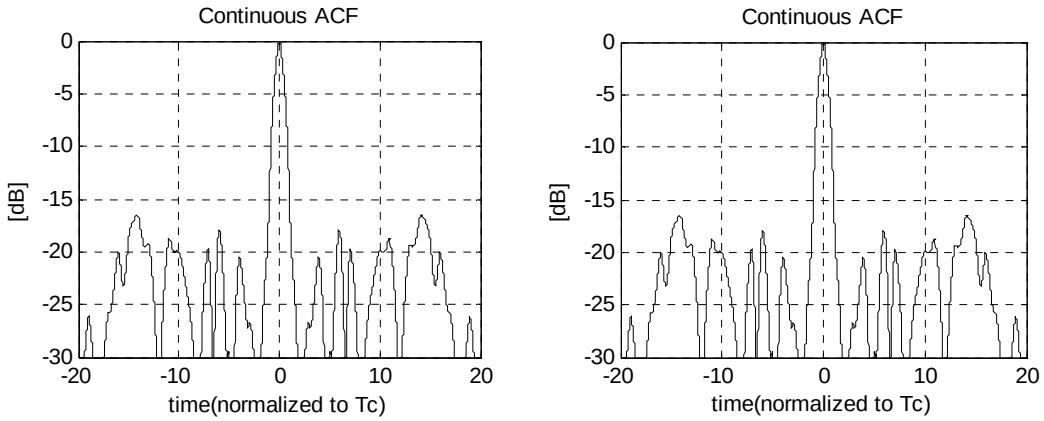

(a) (b)

Figure 3.29 Aperiodic ACFs of LPT-QPSK pulses, N = 20(a), 32(b)

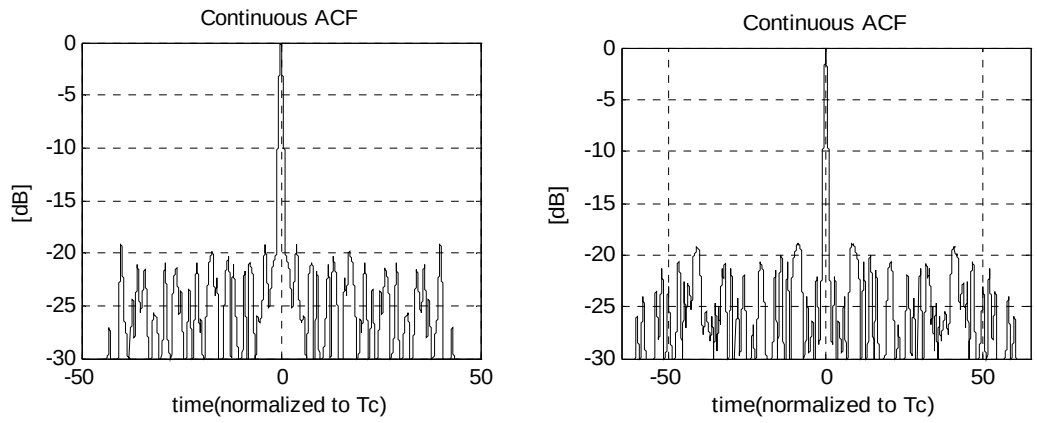

(c) (d)

Figure 3.29 (cont)Aperiodic ACFs of LPT-QPSK pulses, N = 45(c), 64(d).

Table 3.10 shows the variations of PSL, ISL and MLW values for different lengths of codes with respect to the duration of transition. The only considerable change occurs in the PSL value of the MF output of the LPT-QPSK pulse with N = 64. This pulse with the duration of T/50 has a PSL of –19.97dB, which is 1.4 dB lower than the PSL value for the same pulse with the duration of T/4. In general, all of the pulses with different lengths of codes are very resistant to the change of duration. This makes LPT-QPSK codes superior to other types of codes.

In the table below, the MLW values are also summarized for different values of the transition durations. The LPT-QPSK pulse with N=32, τ=T/50 has a main lobe width of 0.9377 chips, which is 0.17 chips wider than that of the LPT-QPSK pulse with N = 64. As the duration increases, the main lobe slightly widens. The LPT-QPSK pulse with N=32 has only a width of 1.24 chips when the duration reaches T/4.

Table 3.10 Effect of Duration on PSL and ISL

Duration of Transition	ISL(dB)			PSL(dB)			RESOLUTION(in chips)		
	N=64	N=45	N=32	N=64	N=45	N= 32	N=64	N=45	N=32
T/50	-3.5492	-5.0524	-6.3999	-19.974	-19.08	-19.021	1.1024	1.0091	0.9377
T/25	-3.549	-5.0647	-6.4007	-19.843	-19.084	-19.058	1.1257	1.0297	0.957
2T/25	-3.5481	-5.0905	-6.4023	-19.588	-19.093	-19.128	1.1719	1.0706	0.9953
4T/25	-3.5443	-5.1467	-6.4042	-19.098	-19.108	-19.25	1.2634	1.1509	1.0709
T/5	-3.5416	-5.1768	-6.4038	-18.863	-19.116	-19.301	1.3088	1.1905	1.1083
T/4	-3.5376	-5.2163	-6.4013	-18.578	-19.126	-19.226	1.3652	1.2396	1.1548

3.6.3. Spectral Improvement of Continuous Phase Modulation

The bandwidth that a signal occupies is an important aspect of its total performance. The radio frequency spectrum is a limited and valuable resource and its use is controlled by international standards. It is important to consume as little of it as possible.

In digital communication, in order to define bandwidth efficiency, the Nyquist Bandwidth, Null-to-Null Bandwidth or Percentage Bandwidths of a waveform are to be calculated. In the comparisons provided, percentage bandwidth is utilized because of the characteristics of waveform spectrums, i.e., null-to-null bandwidth no longer exists for continuous phase modulations. Commonly used percentage bandwidths are the 90% and 99% bandwidths. The 90% bandwidth is defined as the frequency band in which the 90% of the total power is occupied.

In fact, all the radar waveforms mentioned in this study are pulsed waveforms and they are periodic with PRI. However, instead of using these waveforms, it is preferable to choose one pulse consisting of chips. In addition, the Fourier Transform is performed on a finite length waveform not a continuous periodic waveform.

In order to compare the bandwidth efficiencies, the power spectral densities of the baseband waveforms are computed in MATLAB. Using these densities, 90% and 99% bandwidths are computed for all waveforms which are formed with the 20-length codes obtained in the previous sections.

In digital communication, many CPM schemes -especially MSK and GMSK- are widely used due to their spectral efficiencies. In order to observe this efficiency on the radar waveforms, firstly, the MSK waveform with 20-length CPM code, h=0.5, M=2 and 1REC is selected and the 90% and the 99% bandwidths are calculated as 4.27 MHz and 10 MHz respectively.

Then M is increased to 4 and the bandwidths become 8.85 MHz and 14 MHZ respectively. In the case of M = 8, the bandwidths are 15.87 MHz and 22.9 MHz. In conclusion, in CPM waveforms, the 90% and the 99% bandwidths widen as M increases. The percentage bandwidths of the BPSK, the QPSK and the LPT-QPSK waveforms are also computed and given in Tables 3.11, Table 3.12, and Table 3.13.

Table 3.11 $B_{90\%}$ and $B_{99\%}$ of the QPSK waveform, N=20

T	$B_{90\%}$ (MHz)	$B_{99\%}$ (MHz)
T/100	7.94	74.77
T/50	7.94	63.78
T/25	7.62	47.91
2T/25	7.02	34.79
4T/25	6.41	23.80
T/5	6.10	21.97
T/4	6.10	16.79

The effect of phase continuity is observable in Table 3.11, showing the percentage bandwidths of the QPSK waveform with different values of τ. The 90% bandwidth is 7.94 MHz for the QPSK waveform with the transition duration of T/100, which is 1.84 MHz wider than that of the same waveform with τ = T/4. A 1.84 MHz increment of the 90% bandwidth occurs. However, the 99% bandwidth narrows by 58 MHz. This means only 1% of the total power is carried in the spectral sidelobes outside the band of 16.8 MHz.

If a waveform is to be filtered through a bandpass filter with a narrower bandwidth than that of the waveform, a narrow bandwidth becomes a significant advantage. This filter cuts the tails of the waveform frequency response causing an amplitude variation on the filtered output. In order to observe these amplitude variations, a simulation setup is prepared in Advanced Design System (ADS) software. The regarding waveforms are generated at intermediate frequency of 70 MHz. Subsequently, these waveforms are filtered by a band pass filter centered at 70MHz with 20MHz bandwidth. Finally, the amplitude variations of continuous and discrete phase waveforms, which have occurred on the output waveforms, are compared.

Table 3.12 $B_{90\%}$ and $B_{99\%}$ of BPSK waveform, N = 20

τ	$B_{90\%}$ **(MHz)**	$B_{99\%}$ **(MHz)**
T/100	8.39	96.44
T/50	8.39	87.59
T/25	8.39	70.19
2T/25	8.24	48.83
4T/25	7.78	30.51
T/5	7.63	26.56
T/4	7.32	22.28

In Table 3.12, the 90% and 99% bandwidths for BPSK waveforms formed by the code of length 20 are summarized. The 90% bandwidth of the continuous phase BPSK waveform with the transition duration of T/100 is 8.39 MHz, which is 1.07 MHz higher than the scheme with the transition duration of T/4.

The 99% bandwidth of the continuous phase scheme with the duration of T/4 is 22.28 MHz, which is 5.49 MHz higher than that of the continuous phase QPSK scheme with the same duration In addition, the 99% bandwidth for the duration of T/100 is 96.44 MHz, which is 21.67 MHz higher than the continuous phase QPSK scheme with the same duration. As a conclusion, QPSK waveforms are spectrally more efficient in comparison to BPSK waveforms.

Table 3.13 $B_{90\%}$ and $B_{99\%}$ of the LPT-QPSK waveform, N = 20

τ	$B_{90\%}$ (MHz)	$B_{99\%}$ (MHz)
T/100	7.63	67.139
T/50	7.63	56.152
T/25	7.32	43.945
2T/25	6.71	31.738
4T/25	6.10	21.362
T/5	6.10	16.479
T/4	5.80	14.954

In fact, the LPT-QPSK pulses are discovered to be resistant to the duration changes in terms of PSL and ISL. The spectral superiority of these waveforms are observable in Table 3.13, which shows the $B_{90\%}$ and the $B_{99\%}$ of the LPT-QPSK pulse for different values of τ. Compared to the other MLESSM waveforms, LPT-QPSK waveforms have the lowest $B_{90\%}$ and $B_{99\%}$ for all transition durations.

In example, for the transition duration of T/4, the LPT-QPSK waveform has a 5.80 MHz %90 bandwidth, which is 0.3 MHz narrower than that of the QPSK waveform. It is also 1.52 MHz narrower than that of the BPSK waveform. To sum up, the results of the simulations demonstrate that spectrally the most efficient modulation among all the MLESSM waveforms is the LPT-QPSK waveform with τ = T/4. Table 3.14 arranges the bandwidths of all MLESSM waveforms.

Table 3.14 $B_{90\%}$ and $B_{99\%}$ of MLESSM waveforms, N = 20

τ	$B_{90\%}$ (MHz)			$B_{99\%}$ (MHz)		
	BPSK	**QPSK**	**LPT-QPSK**	**BPSK**	**QPSK**	**LPT-QPSK**
T/100	8.39	7.94	7.63	96.44	74.77	67.139
T/50	8.39	7.94	7.63	87.59	63.78	56.152
T/25	8.39	7.62	7.32	70.19	47.91	43.945
2T/25	8.24	7.02	6.71	48.83	34.79	31.738
4T/25	7.78	6.41	6.10	30.51	23.80	21.362
T/5	7.63	6.10	6.10	26.56	21.97	16.479
T/4	7.32	6.10	5.80	22.28	16.79	14.954

In the table above, the bandwidths of the CPM waveforms are not included but it should be remembered that the MSK waveform has a 4.27 MHz $B_{90\%}$ and a 10 MHz $B99_{\%,}$ being the narrowest among all modulation types. Adding this result to the results given in the table above, one can agree that among MWM modulation techniques spectrally the most efficient modulation is MSK and the LPT-QPSK with τ = T/4 is the most efficient technique among all continuous phase MLESSM modulation techniques. To sum up, MSK is the most efficient modulation technique in all modulations with a 4.27 MHz $B_{90\%}$.

3.6.4. Continuous Phase Modulations and System Imperfections

The main concern in this study is to find the optimum waveform which when filtered has the lowest possible amplitude variation. In order to compare waveform optimality, a simulation setup is prepared using ADS software. Figure 3.30 shows how this simulation is realized. The simulation sampling rate is hundred times the inverse of the chipwidth. In order to represent discrete phase waveforms, the waveform with the rectangular phase shaping pulse is used. The phase shaping pulse in Figure 3.17 is applied to shape the phase of each continuous phase waveform chip.

SETUP:

T_c = 100ns

F_c = 70MHz

Ts = 1ns

N = 20

M = 4 for CPM

h (t) = a bandpass filter centered at 70 MHz with 20MHz bandwidth

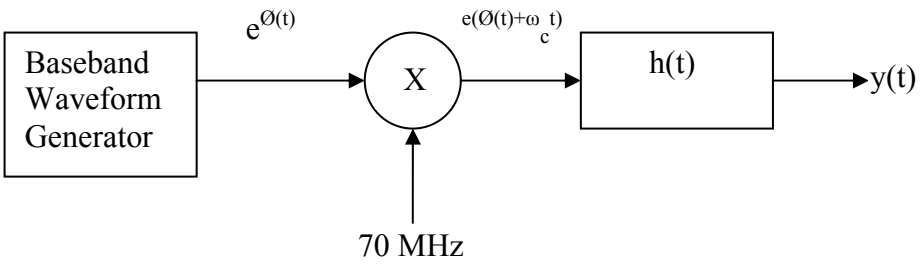

Figure 3.30 Simple Radar Transmitter

In the simulations, a band pass filter centered at 70MHz with a 20MHz bandwidth is used. This filter is designed on PC using GENESYS software and the result layout is printed on an FR-4 substrate. The filter characteristic is measured using HP8753ES Network Analyzer and it is plotted in Figure 3.31.

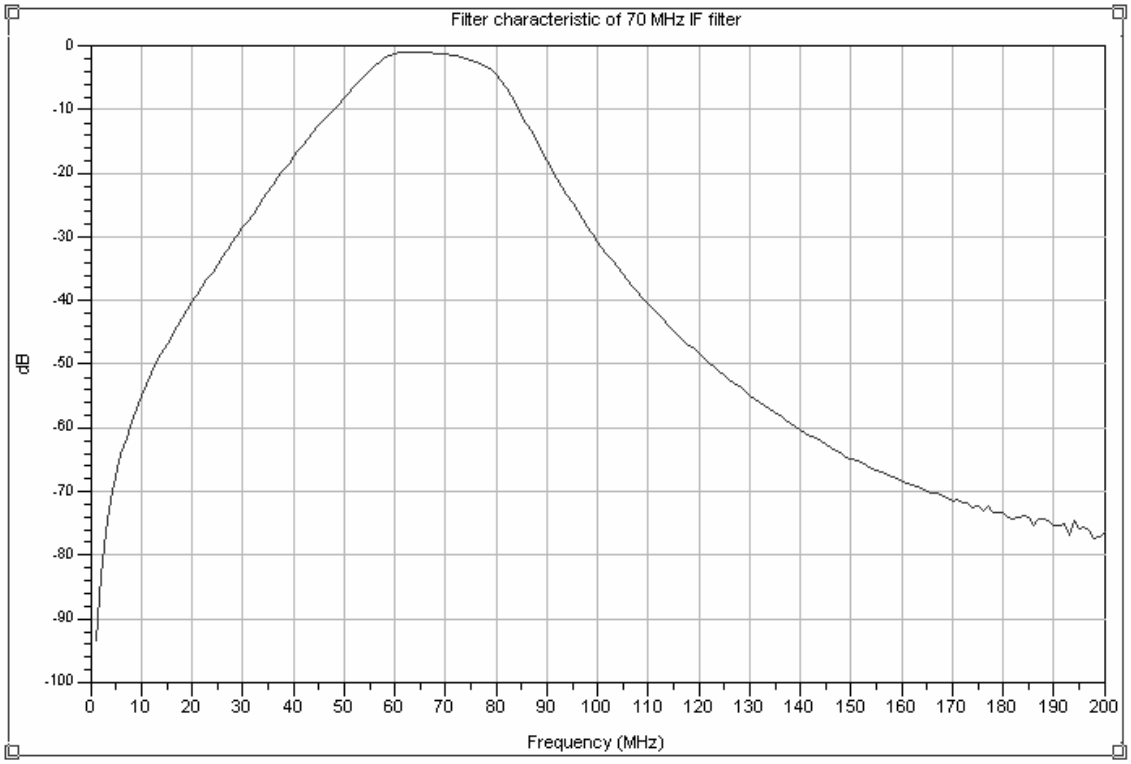

Figure 3.31 Bandpass filter

The QPSK waveforms before and after filtering through the bandpass filter are given in Figure 3.32 and Figure 3.33 respectively. In the previous section, the bandwidth efficiencies of MLESSM and MWM waveforms were compared. It is proved that among all modulated waveforms, the discrete phase QPSK waveform has the highest sidelobe levels and the widest 90% and 99% bandwidths in comparison to those of continuous phase and CPM waveforms. In the simulations, a discrete phase QPSK, a continuous phase QPSK and a CPM waveform are generated and the filtered outputs are observed. It is expected that the filtered discrete phase QPSK waveforms have the highest amplitude variation.

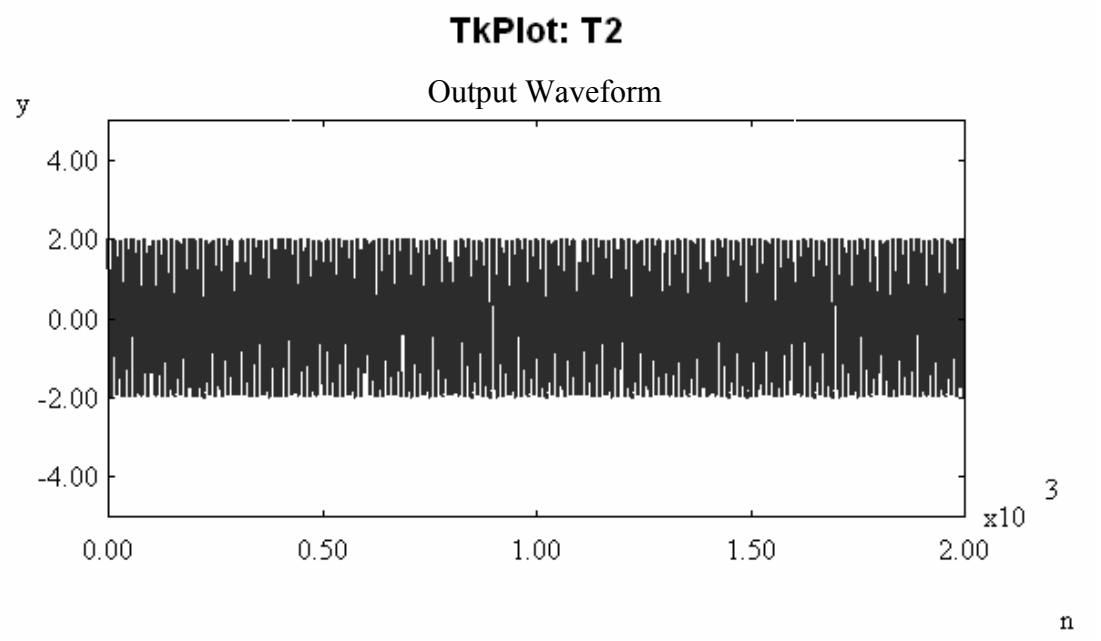

Figure 3.32 Discrete Phase QPSK Waveform before Filtering

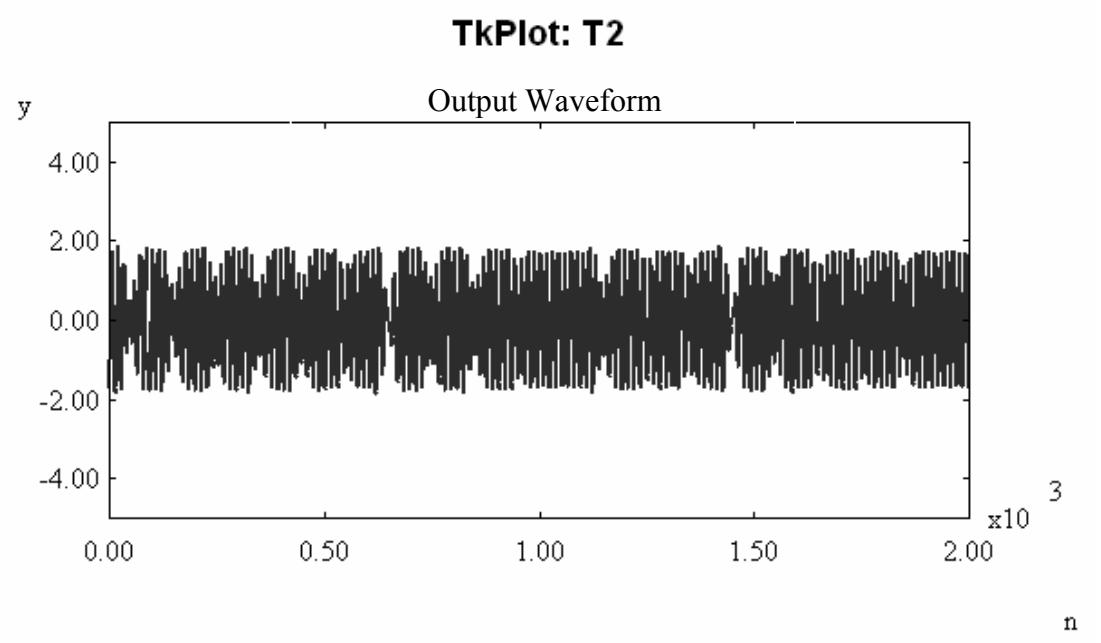

Figure 3.33 Discrete Phase QPSK Waveform after Filtering

A frequent amplitude variation occurs on the discrete phase QPSK waveform. The amplitude variation is higher especially on phase transition regions due to the sharp transitions.

When the new phase shaping pulse with $\tau = T/4$ is used to form the continuous phase waveform, the output waveform after filtering through the bandpass filter occurs to be as in Figure 3.34.

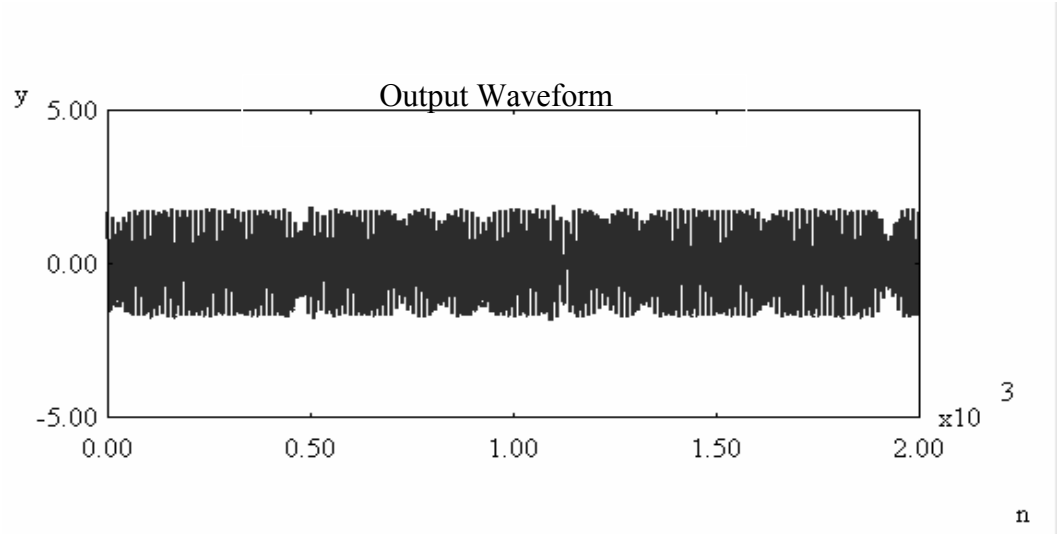

Figure 3.34 Continuous Phase QPSK Waveform after Filtering, $\tau = T/4$

Finally, in order to see the superiority of CPM waveforms, the same simulation setup is used to observe the filtered CPM waveform. The resulting waveform is shown in Figure 3.35.

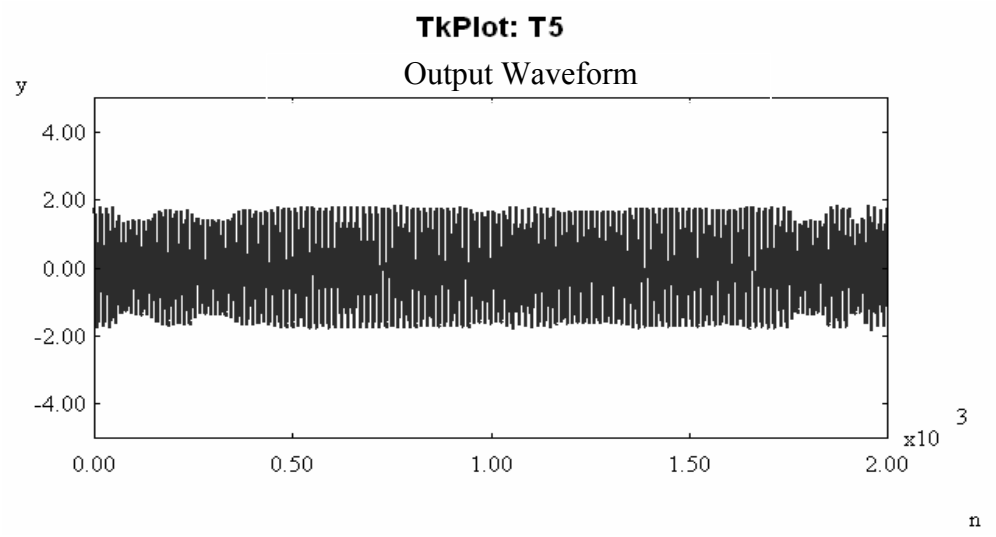

Figure 3.35 CPM Waveform after Filtering, M = 4, h = 0.5, 1REC

CHAPTER 4

SAMPLING MISMATCH IN RADAR WAVEFORMS

4.1. Introduction

The return signal from a target is received by the radar receiver and sampled in the A/D devices. In the following sections, effects of the system Nyquist rate sampling and half the system Nyquist rate sampling on PSL, ISL, peak SNR and MLW are assessed. Half Nyquist rate is the rate of one sample per chip and nyquist rate is 2 samples per chip since the chipwidth is 100ns. Throughout this analysis, the SNR loss corresponds to the decrease in the peak value of the receiver filter output. This decrement occurs in a mismatch condition. When correct samples are taken at constant phase points outside the transition regions of each chip, the sampling is considered to be ideal. If non-constant phase points are applied, the condition is defined as a sampling mismatch condition.

4.2. Half Nyquist Rate Sampling

4.2.1. Sampling Mismatch on QPSK Codes

In the previous chapter, the optimum discrete phase and the continuous phase waveforms were analyzed regarding the continuous aperiodic autocorrelation functions and the bandwidths of these waveforms. In the following studies, the QPSK waveform with N = 20 is provided as an example. Initially, the half Nyquist rate is used. In this case, the A/D device samples the waveform with the rate of 1 sample/chip. The matched filter coefficients are formed by the correct samples taken

at ideal constant phase points. The ideal case occurs when the A/D samples the chips at midpoints. This condition guaranties the highest peak value at the MF output. In any other case, a mismatch occurs between the obtained samples and the MF coefficients causing a mismatch loss at the MF output. In a mismatch case, not only SNR loss occurs but also PSL, ISL and MLW values decrease. For each and every sampling point, PSL, ISL and MLW values are computed and plotted with respect to the sampling time shift. Exactly the same sampling points are obtained for the shift of T/2. Due to this fact, the figures showing PSL, ISL and MLW variations for the code of length 20 are plotted for the mismatch time interval of [-T/2, T/2] where T is equal to the chip width, T_c. In addition, in order to see the periodicity of the variations, the figures for all waveforms are drawn for the interval of [-T, T].

The mismatch effects of half the Nyquist rate sampling on PSL, ISL, SNR loss and MLW are presented in the following figures. The maximum main lobe width for the worst case is never greater than $\pm 3T_c$. For that reason, the main lobe region is supposed to be $\pm 3T_c$ in the simulations. The letter, "S" represents the number samples in a chip

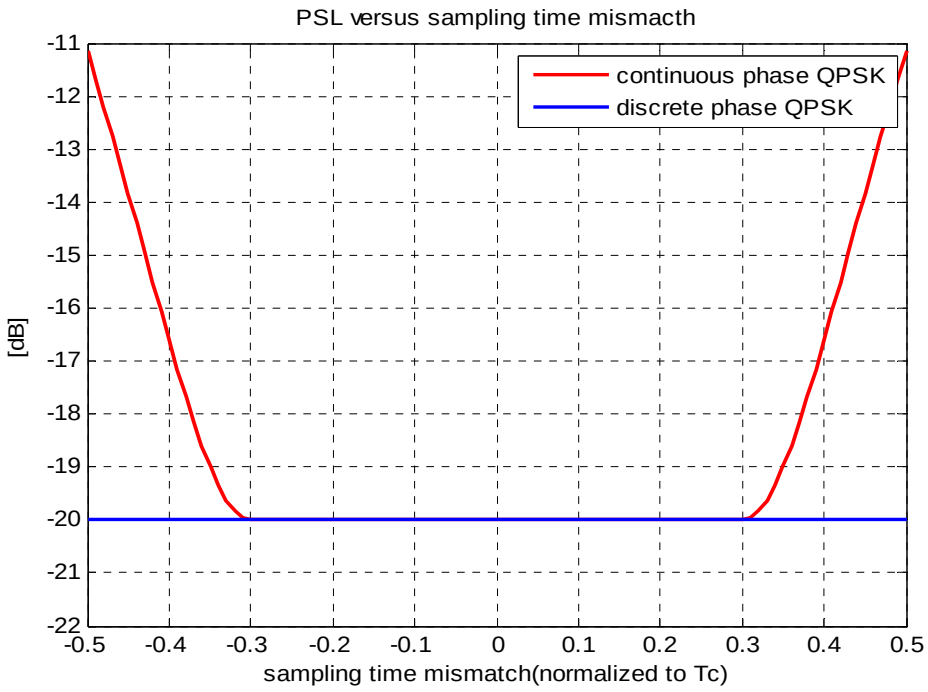

Figure 4.1 PSL versus sampling time shift for discrete and continuous phase QPSK waveforms, $\tau = T/5$, S = 1,

The PSL value of -11 dB, which is 9 dB higher than that of the discrete phase QPSK waveform, is obtained for the shift of T/2. In the interval of [-0.3T_c, 0.3T_c], which is out of the transition regions, the PSL value is the same with the discrete phase waveform.

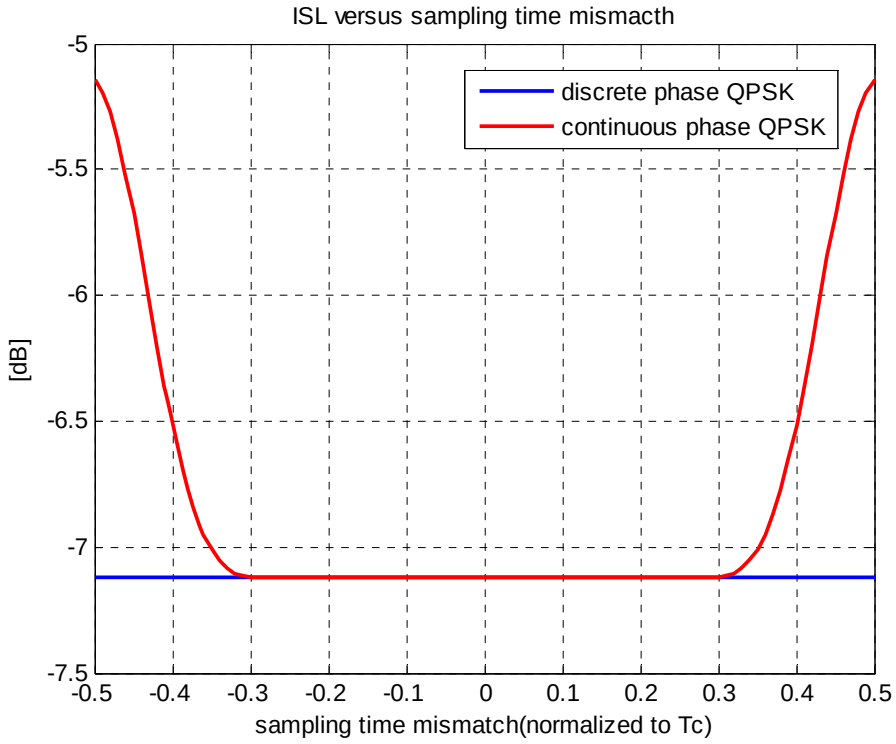

Figure 4.2 ISL versus sampling point shift for discrete and continuous phase QPSK waveforms, τ = T/5, S=1

In Figure 4.2, the ISL variation with respect to the sampling point shift is given. When the shift reaches T/2, the highest ISL occurs. This value is nearly 2.5 dB higher than the ISL for the discrete phase scheme.

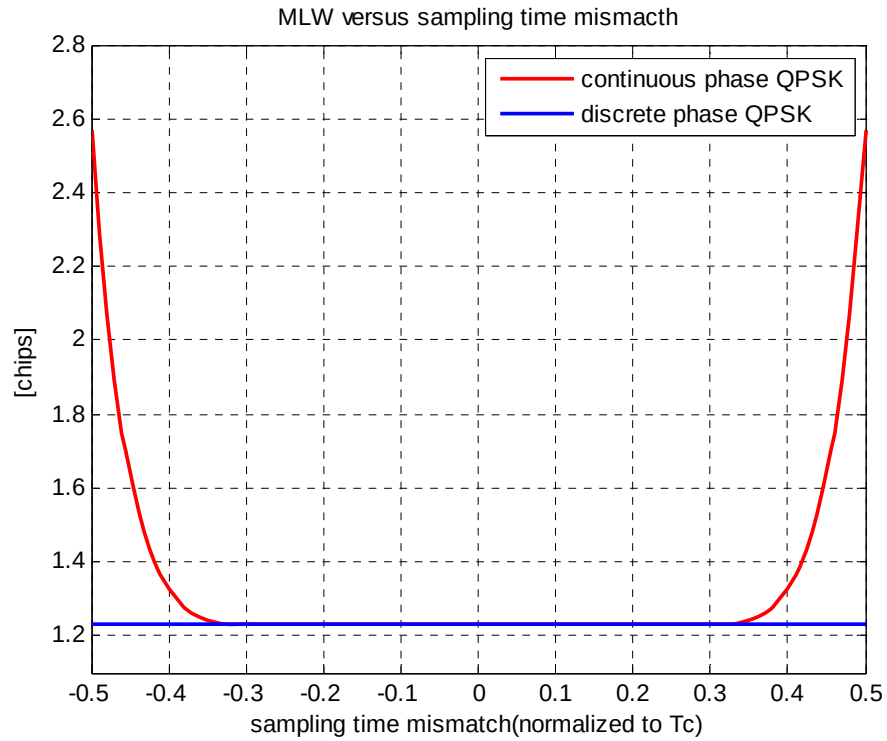

Figure 4.3 Main lobe width versus sampling point shift for discrete and continuous phase QPSK waveforms, $\tau = T/5$, $S = 1$.

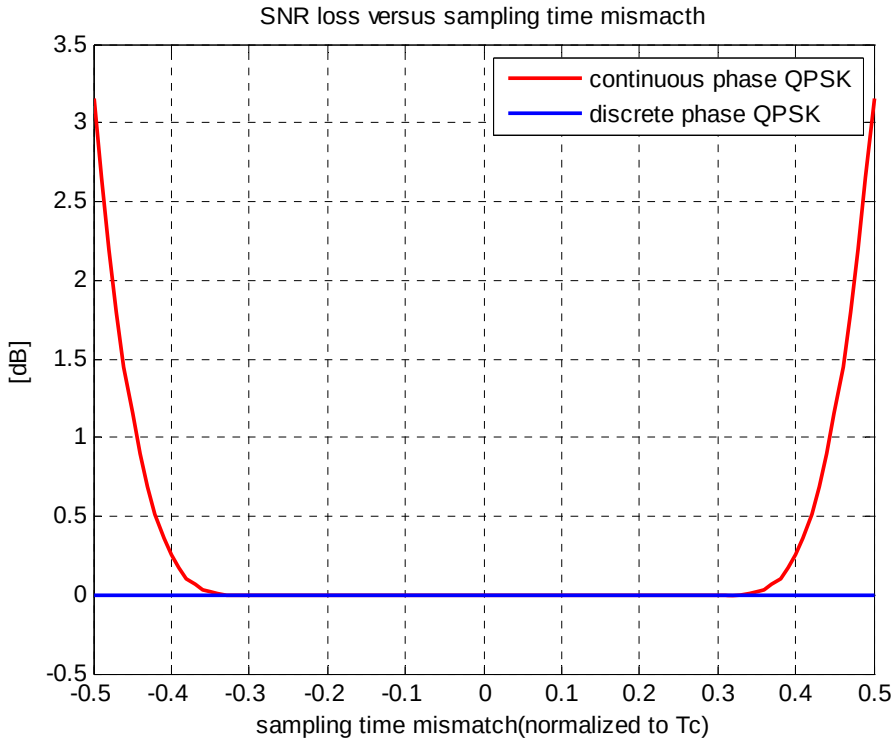

Figure 4.4 SNR loss versus sampling point shift for discrete and continuous phase QPSK waveforms, $\tau = T/5$, $S=1$.

These figures show that the SNR loss and MLW increase, the PSL and ISL get higher as the sampling point moves away from the ideal sampling point which is the midpoint at half the Nyquist rate. In addition, main lobe width is normalized to the main lobe width of ideal MF output.

When the same calculations are repeated for the QPSK waveforms with N = 32, 45 and 64, the results given through Figure 4.5 to 4.8 are accomplished. In Figure 4.5, the PSL variation is provided for different lengths of the codes. The waveforms with N = 32, 45, 64 have lower PSL values for the ideal sampling condition in comparison to the PSL value of the waveform with N = 20. However, these waveforms are observed to be very sensitive to the mismatch effect. Figure 4.6 shows the ISL variations of all waveforms. Unexpectedly, the obtained ISL values at maximum shift of T/2 are positive. In other words, the total power in the sidelobes is higher than the power in the main lobe. This situation is not acceptable for two-target or clutter dominant systems due to excessive power in the sidelobes.

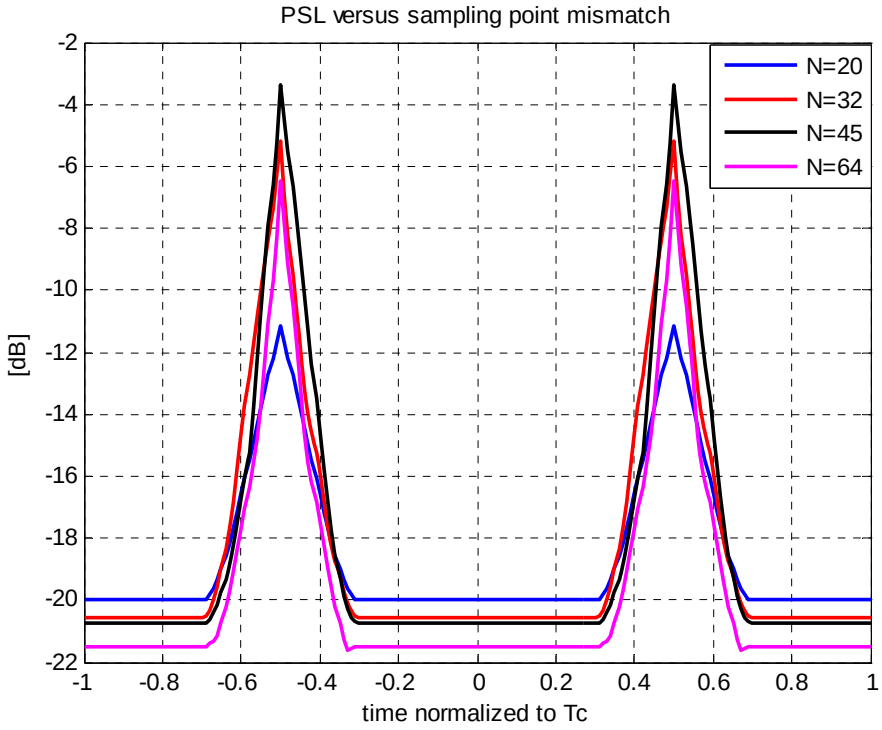

Figure 4.5 PSL versus sampling point shift for QPSK waveforms with N = 20, 32, 45 and 64, S = 1, τ = T/5.

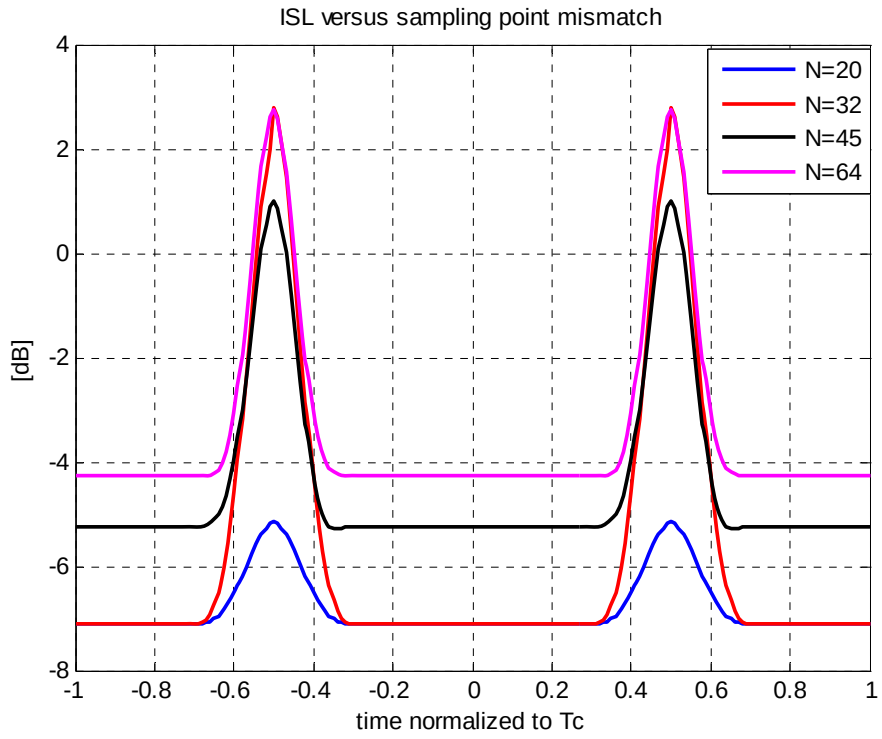

Figure 4.6 ISL versus sampling point shift for QPSK waveforms with N = 20, 32, 45 and 64, S = 1, τ = T/5.

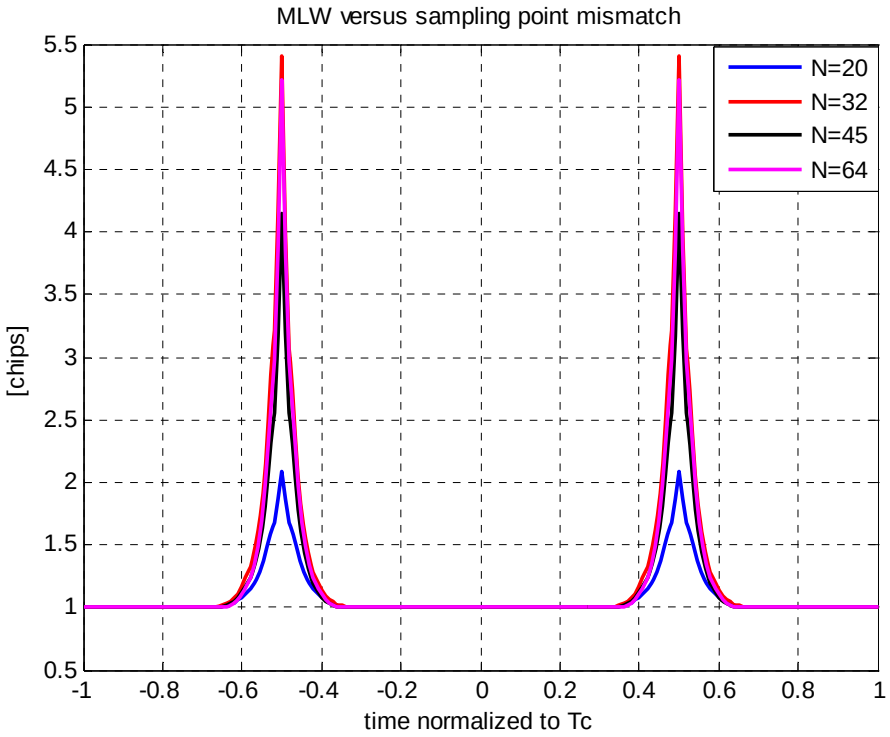

Figure 4.7 MLW versus sampling point shift for QPSK waveforms with N = 20, 32, 45, 64, S = 1, τ = T/5.

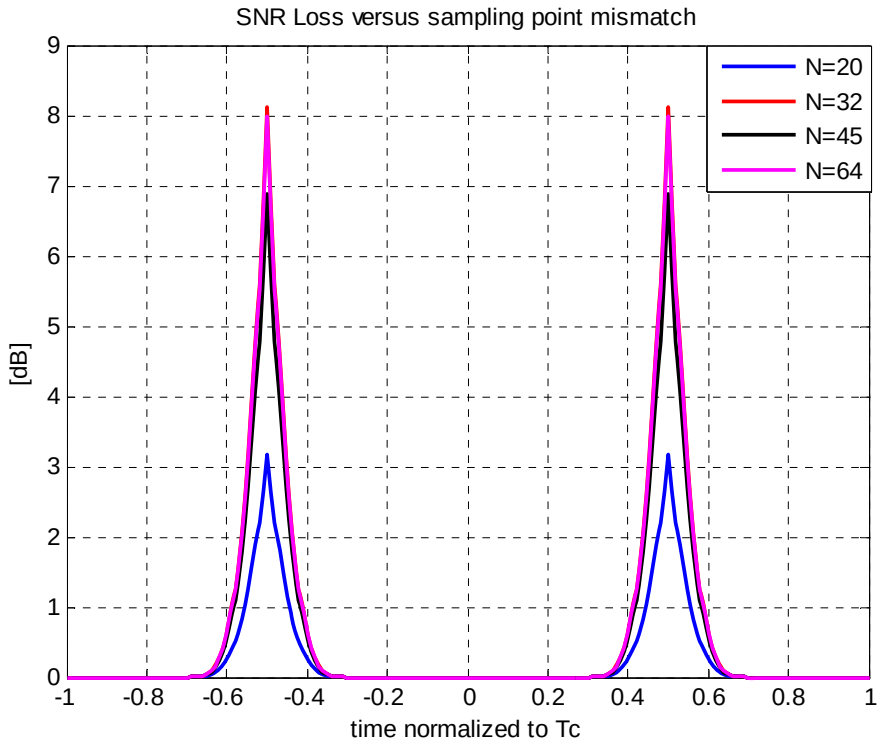

Figure 4.8 SNR loss versus sampling point shift for QPSK waveforms with N = 20, 32, 45 and 64, S = 1, τ = T/5.

MLW and SNR loss also increase as the shift from ideal sampling points and the length of the code increase. The worst case would be the shift of T/2 from the ideal sampling point. In this case, an 8 dB SNR loss occurs for the waveform with N = 64 where it is 6.89 dB for the waveform with N = 45.

The results provided in the figures above are summarized in Table 4.1. Minimum values are obtained at the ideal sampling condition and maximum values at the worst sampling condition. The MLW values are normalized to the MLW value of matched filter output in ideal case.

Table 4.1 Max and Min values of PSL and ISL under sampling mismatch, S = 1

Code Length	PSL(dB)		ISL(dB)	
	Min	Max	Min	Max
20	-20	-11.15	-7.12	-5.15
32	-20.56	-4.7763	-7.12	2.80
45	-20.76	-3.39	-5.29	1.02
64	-21.6	-6.47	-4.28	2.76

Table 4.2 Max and Min values of SNR Loss and MLW under sampling mismatch, S=1

Code Length	MLW(chips]		Loss(dB)	
	Min	Max	Min	Max
20	1.000	2.0879	0	3.16
32	1.000	5.6447	0	8.12
45	1.000	4.1422	0	6.89
64	1.000	5.2191	0	8.00

4.3. Nyquist Rate Sampling

4.3.1. Sampling Mismatch on QPSK Codes

In Nyquist rate sampling, two samples are taken during each chip interval. In addition, the MF coefficients are formed by using the ideal constant phase samples taken on the transmitted waveforms. In any sampling mismatch condition, due to the fact that the duration of transition is never greater than T/4, at least one ideal constant phase sample is obtained in the sampling process. As a result, PSL, ISL, MLW and

SNR loss values occur to be better than those of half the Nyquist rate sampling for the worst case. The variations of PSL, ISL, SNR loss and MLW with respect to the sampling point shift under nyquist rate sampling are given in Figure 4.9, Figure 4.10, Figure 4.11, and Figure 4.12. The SNR loss values are given with respect to the matched filter output of the ideal sampling case. The MLW values are normalized to the MLW value of ideal MF output.

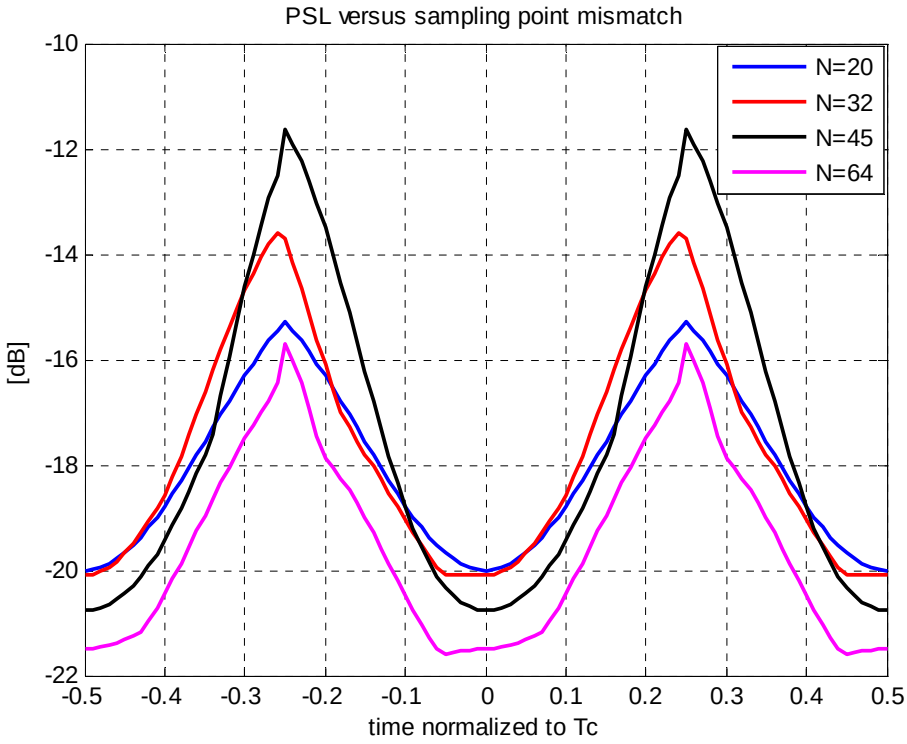

Figure 4.9 PSL versus sampling point shift for QPSK waveforms with N = 20, 32, 45, and 64, S = 2, τ = T/5

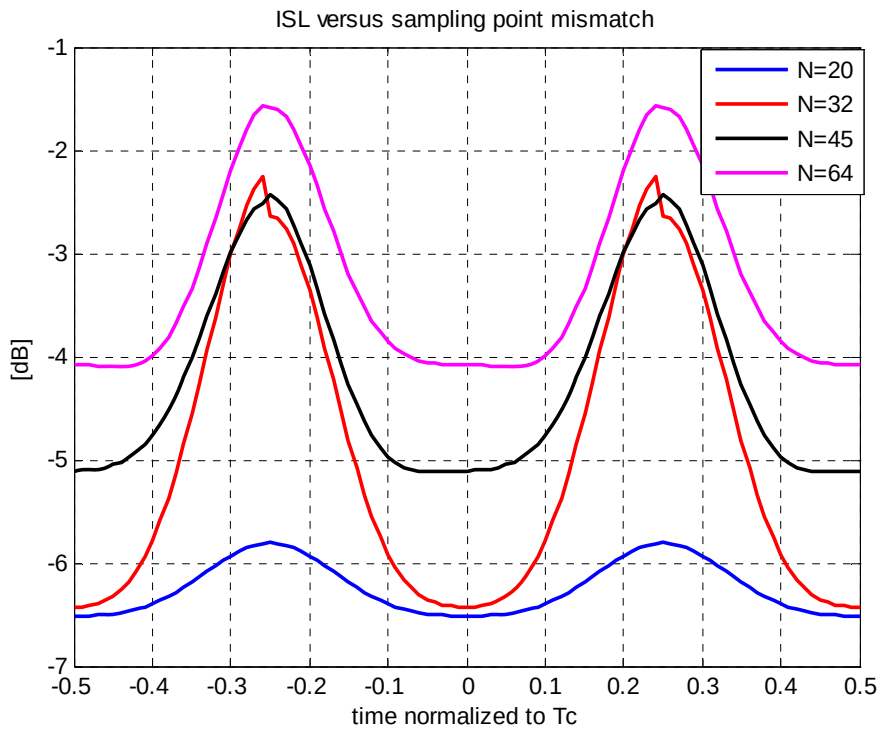

Figure 4.10 ISL versus sampling point shift for QPSK waveforms with N=20, 32, 45, 64, S = 2, τ = T/5

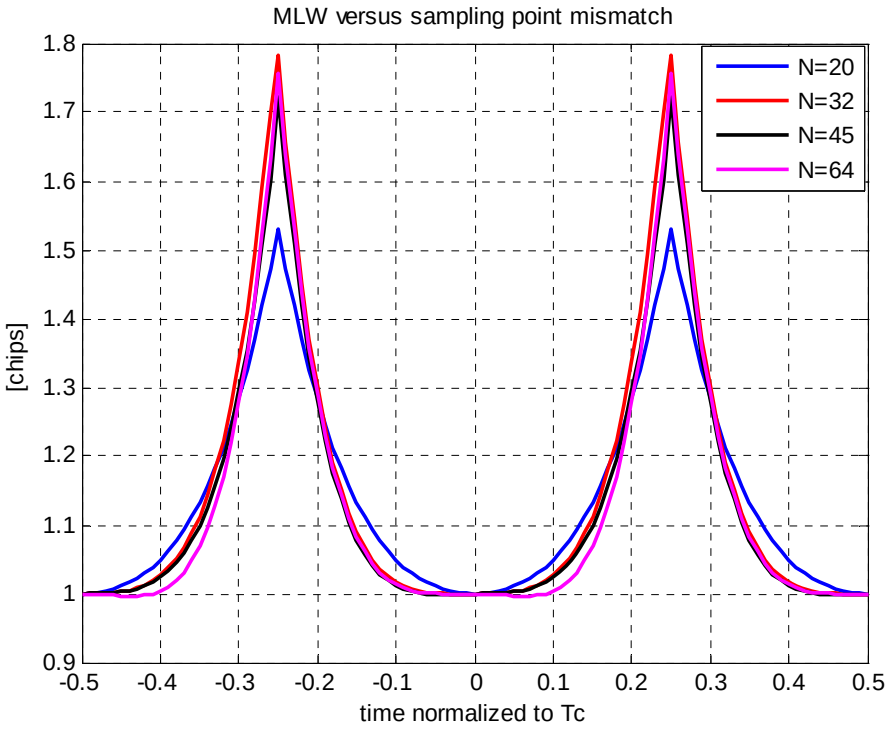

Figure 4.11 MLW versus sampling point mismatch for QPSK waveforms with N = 20, 32, 45 and 64, S = 2, τ = T/5

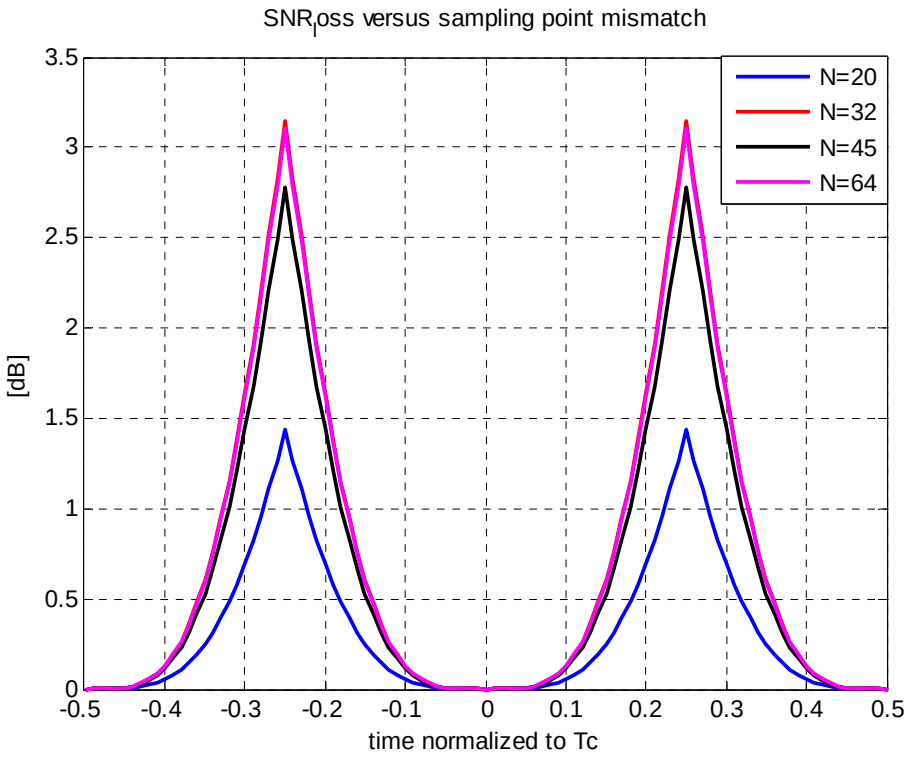

Figure 4.12 SNR Loss versus sampling point mismatch for QPSK waveforms with N = 20, 32, 45 and 64, S = 2, τ = T/5

These results are summarized in Table 4.3 and Table 4.4.

Table 4.3 Max and Min PSL and ISL values for QPSK waveforms under sampling mismatch, S = 2

Code Length	PSL(dB)		ISL(dB)	
	Min	Max	Min	Max
20	-20.00	-15.27	-6.52	-5.81
32	-20.10	-13.59	-6.43	-2.26
45	-20.76	-11.62	-5.12	-2.42
64	-21.58	-15.69	-4.10	-1.57

Table 4.4 Max and Min MLW and Loss values for QPSK waveforms under sampling mismatch, S = 2

Code Length	MLW[chips]		Loss[dB]	
	Min	Max	Min	Max
20	1.0000	1.5315	0	1.4373
32	1.0000	1.7800	0	3.1484
45	1.0000	1.7226	0	2.7800
64	1.0000	1.7574	0	3.1091

All of the results are observed to be better than those of half the Nyquist rate sampling. Minimum PSL value for QPSK waveforms with N=20 sampled at the Nyquist rate is 4.1 dB lower than that of the waveforms sampled at half the Nyquist rate. The corresponding differences in the PSL value for other waveforms with N = 32, 45 and 64 are 8.6 dB, 8.2 dB and 9.2 dB respectively. These differences show that the waveforms with longer codes improve more than those with short codes for Nyquist rate sampling. A similar result is obtained for the ISL values. While the ISL of the waveform with N = 20 increases 0.7 dB, the waveform with N = 32 improves 5.0 dB.

In comparison to the ideal sampling case, in general, ISL and PSL values get higher even at nyquist rate sampling under sampling mismatch due to the usage of the system Nyquist rate. The QPSK waveform with N = 20 has a 0.71 dB higher ISL for the worst case. The PSL value of the MF output for this waveform increases by 4.73 dB while the increment for the waveform with N = 32 and 9.1367 dB for the waveform with N = 45. 5.90 dB of PSL improvement is achieved for the waveform with N = 64. Maximum PSL difference at the worst case occurs for the waveform with N = 45.

It can be inferred from Table 4.2 and Table 4.4 that SNR Loss and MLW values also

improve in the Nyquist rate sampling case.

In the following parts, the effect of sampling point mismatch on MF output is studied for the spectrally efficient LPT-QPSK waveforms. PSL versus sampling point shift is demonstrated in Figure 4.13. In the calculations, the transition duration of T/5 and Nyquist rate sampling are used.

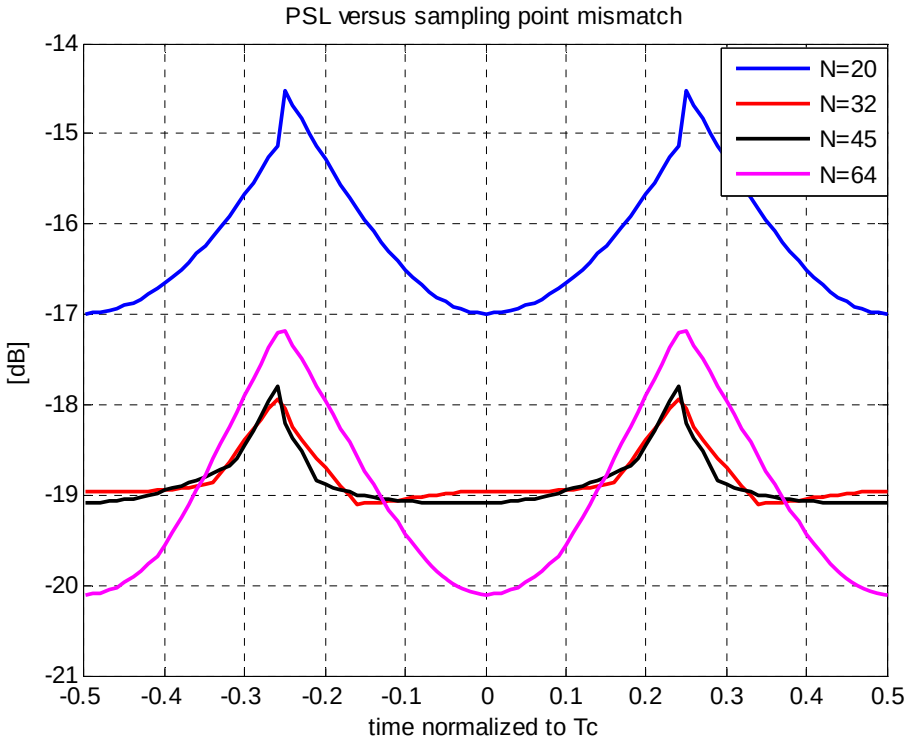

Figure 4.13 PSL versus sampling point mismatch for LPT-QPSK waveform with N = 32, 45, 64, S = 2, τ = T/5

The graphs of sampling point mismatch effect have nearly the same shape for all waveforms. Therefore, tables may be sufficient to describe the effect. In the following sections, minimum values in the tables are obtained for the ideal sampling points, and maximum values are obtained at the worst sampling points. In contrary to half the Nyquist rate sampling, the figures are drawn for the sampling point shift interval of [-T/2, T/2].

Maximum PSL decrement due to the sampling mismatch is only 2.46 dB for the

QPSK waveform with N = 20 while it is 1.254 dB for the waveform with N = 32. The maximum PSL decrement is 1.43 dB for the waveform with N = 45 and 3.0697 dB for the waveform with N = 64. On the other hand, the sampling mismatch has little effect on the ISL values for the worst case. Maximum ISL difference of 0.30 dB occurs for the waveform with N = 20. As stated before, LPT-QPSK waveforms have the narrowest bandwidths in all MLESSM waveforms.

Table 4.5 Min and Max values of PSL and ISL for LPT-QPSK waveforms under sampling mismatch, S = 2, τ = T/5

Code Length	PSL(dB)		ISL(dB)	
	Min	Max	Min	Max
20	-16.99	-14.53	-6.45	-6.15
32	-19.10	-17.94	-6.24	-6.16
45	-19.09	-17.81	-4.91	-4.70
64	-20.10	-17.19	-3.44	-3.35

Table 4.6 Min and Max of MLW and Loss values for LPT-QPSK waveforms under sampling mismatch, S = 2, τ = T/5

Code Length	MLW[chips]		Loss[dB]	
	Min	Max	Min	Max
20	1.0000	1.4588	0	1.1529
32	1.0000	1.4990	0	1.1911
45	1.0000	1.4953	0	1.2114
64	1.0000	1.5240	0	1.2137

It can be inferred from Table 4.5 and Table 4.6 that LPT-QPSK waveforms have less SNR loss values in comparison to QPSK waveforms. For the worst case, maximum SNR loss of 1.2137 dB occurs for LPT-QPSK waveform with N = 64 while this loss amounts to 3.11 dB for the QPSK waveform with the same length. The amount of loss is even smaller in other LPT-QPSK waveforms. In conclusion, LPT-QPSK waveforms are discovered to be more resistant to the sampling mismatch effect at the system Nyquist rate.

4.3.2. Sampling mismatch on BPSK codes

The same simulations are repeated for BPSK waveforms to examine the sampling mismatch effect. The results are summarized in Table 4.7 and Table 4.8.

Table 4.7 Min and Max values of PSL and ISL under sampling mismatch, S = 2, $\tau = T/5$

Code Length	PSL(dB)		ISL(dB)	
	Min	Max	Min	Max
20	-20.0000	-14.5170	-7.8165	-4.7550
32	-20.5606	-16.4648	-8.3372	-4.7712
45	-23.5218	-15.2830	-8.1524	-4.8396
64	-24.0824	-18.1219	-7.4916	-4.4353

Table 4.8 Min and Max values of MLW and SNR Loss under sampling mismatch, $S = 2$, $\tau = T/5$

Code Length	MLW[chips]		Loss[dB]	
	Min	Max	Min	Max
20	1.000	1.6357	0	2.2094
32	1.000	1.6996	0	2.4988
45	1.000	1.7193	0	2.4347
64	1.000	1.6934	0	2.3197

The simulation results show that there is not a certain relationship between the PSL decrement and the code length. For example, in the worst case, the BPSK waveform with N = 20 has a maximum PSL value of -14.52 dB which is 5.48 dB higher than that of the ideal sampling case. The PSL decrement at the MF output of the waveform with N = 32 is 4.1 dB and it is 8.46 dB for the waveform with N = 45.

PSL versus ISL values of the MLESSM waveforms for the worst sampling condition are arranged in Figure 4.14. This graph is a useful tool to decide on optimum waveforms under sampling mismatch. As the waveform get closer to the left-down corner of the graph, optimality under sampling mismatch increases. It is observable from the graph that the optimum waveform under sampling mismatch is 32-LPT-QPSK waveform.

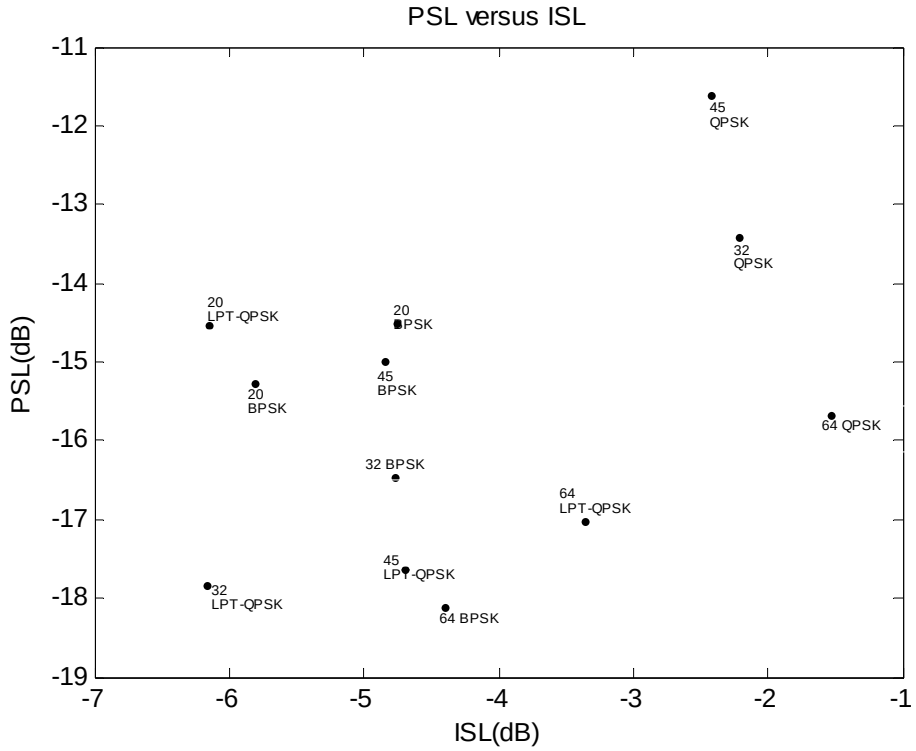

Figure 4.14 Maximum ISL versus maximum PSL under sampling mismatch

4.3.3. Sampling mismatch on CPM codes

For CPM waveforms, Table 4.9 and Table 4.10 summarize the results. In the simulations, the system Nyquist rate (2 samples per chip) is used.

Table 4.9 Min and Max values of PSL and ISL under sampling mismatch, M = 2, h= 0.5, 1REC

Code Length	PSL(dB)		ISL(dB)	
	Min	Max	Min	Max
20	-17.8394	-16.5371	-5.7749	-5.4653
32	-17.5503	-16.8747	-6.8932	-6.6631
45	-17.2510	-16.2295	-3.7337	-3.7241
64	-17.7848	-16.9330	-3.0038	-2.9028

The MF outputs of the CPM waveforms with M = 2, like those of the continuous phase LPT-QPSK waveforms, have higher PSL values compared to those of BPSK and QPSK waveforms. It is obvious in Table 4.9 that sampling mismatch has little effect on the CPM waveforms. The PSL difference between the ideal sampling condition and the worst sampling condition for the CPM waveform with N = 20, M = 2, is only 1.3 dB. This difference is 5.48 dB for the BPSK waveform with N = 20 and 4.73 dB for the QPSK waveform of the same length.

In addition, sampling mismatch has little effects on ISL values. The maximum ISL variation of 0.31 dB occurs for the CPM waveform with N = 20, M = 2. The ISL variations for the other CPM waveforms may be taken as negligible. These result are expected because of the narrowest bandwidth of the MSK waveform.

Table 4.10 Max MLW and SNR Loss values of CPM waveforms, M = 2, h = 0.5, 1REC

Code Length	MLW[chips]		Loss[dB]	
	Min	Max	Min	Max
20	1.000	1.1077	0	0.6877
32	1.000	1.1065	0	0.6877
45	1.000	1.0976	0	0.6873
64	1.000	1.1057	0	0.6877

The SNR losses of all waveforms are very close to each other and it is approximately 0.69 dB. In general, the MLW values for the worst case increase as the code length increases. But the highest one is even 1.11 chips for the CPM waveform with N = 64.

When M is increased to 4, the results in Table 4.11 and Table 4.12 are obtained. In general, the PSL variations for the waveform with M = 4 increase compared to the

waveform with M = 2. The PSL difference between the worst and the ideal case for CPM waveform with N = 20, M = 2 is 1.3 dB while it is 3dB for the waveform of the same length with M = 4. As a consequence, the PSL and ISL variations increase as M increases.

Table 4.11 Min and Max values of PSL and ISL under sampling mismatch, M = 4, h = 0.5, 1REC

Code Length	PSL(dB)		ISL(dB)	
	Min	Max	Min	Max
20	-16.9897	-13.9192	-5.0724	-4.0293
32	18.7997	-14.1360	-4.4591	-3.3259
45	-19.7399	-16.0038	-3.7651	-2.8779
64	-19.8383	-16.2165	-2.6747	-1.9702

Minimum MLW values are smaller than those of the waveforms with M = 2. On the other hand, SNR losses which are on the order of 3.5 dB are higher in these waveforms.

Table 4.12 Max and Min values of MLW and Loss under sampling mismatch, M=4 h = 0.5, 1REC

Code Length	MLW[chips]		Loss[dB]	
	Min	Max	Min	Max
20	1.000	1.7075	0	3.3056
32	1.000	1.6666	0	3.4769
45	1.000	1.7960	0	3.2844
64	1.000	1.8002	0	3.4558

When M is increased to 8, the PSL and ISL values get higher and MLW and SNR loss values increase. The PSL values even reach 0 dB which means that the main

lobe peak no longer exits. The ISL values also increase to a positive value. As stated before, the MSK waveforms have the narrowest bandwidths (4.27 MHz of 90% bandwidth and 10 MHz of 99% of bandwidth). Therefore, the system nyquist rate works on these waveforms successfully.

Table 4.13 Min and Max values of PSL and ISL under sampling mismatch, M = 8 h = 0.5, 1REC

Code Length	PSL(dB)		ISL(dB)	
	Min	Max	Min	Max
20	-12.1383	-0.3308	-1.9907	7.9399
32	-16.0132	-0.2572	-2.3507	8.7269
45	-14.0415	-0.0030	-1.0980	11.2166
64	-16.8039	-0.5448	-0.8388	10.1755

Table 4.14 Max and Min values of MLW and SNR Loss under sampling mismatch, M = 8 h = 0.5, 1REC

Code Length	MLW[chips]		Loss[dB]	
	Min	Max	Min	Max
20	1.000	7.8886	0	12.2612
32	1.000	9.6459	0	12.3766
45	1.000	17.4569	0	16.5845
64	1.000	19.4709	0	16.2854

The MLW and SNR loss values show that the MF output in this case can not be used in target detection. The SNR loss for the waveform with N = 64 is reaches up to 16.29 dB. In other words the target is lost. This loss is due to the sampling the signal

at lower rate than its own nyquist rate. The CPM waveform with M=8 has a 22.9 MHz $B_{99\%}$ and 15.87 MHz $B_{90\%}$.which is very high compared to other MLESSM and MWM waveforms. In the following section, higher sampling rates are used to observe MF outputs.

4.4. Higher Rate Sampling

As mentioned previously, CPM waveforms with M = 8 can not be used with the system Nyquist rate because of the SNR loss that occurs at the MF output. If the sampling frequency higher than the system Nyquist rate is used together with the increased size of matched filter there is an improvement in PSL values. The number of samples in a chip is altered and the PSL, ISL and SNR loss values are recorded. These results are presented in Table 4.15. In the previous section, it has been observed that the CPM waveform with N = 64, M = 8, provides the highest values. Therefore, this waveform is used in the following simulations.

Table 4.15 Effect of Number of Samples on CPM waveform with N = 64, M = 8

#of samples	PSL		ISL		MLW		SNR loss	
	Min	Max	Min	Max	Min	Max	Min	Max
2	-16.80	-0.55	-1.03	10.00	1.00	19.47	0	16.29
5	-20.50	-18.92	-1.84	-1.78	1.00	1.48	0	1.91
10	-20.72	-20.56	-1.85	-1.81	1.00	1.10	0	0.46

Results show that optimality increases when the sampling frequency is increased to a value which is five times the inverse of the chipwidth. In this case, the PSL value

increases to -18.92 dB while it is -0.55 dB in the case which two samples are used. The ISL value increased to -1.78 dB when five samples are used while it is 10 dB when two are used. The most important improvement occurs in the SNR value. If the number of samples in a chip is increased to 10, the minimum SNR loss decreases to 0.46 dB. These values prove an improvement of 15.8 dB in comparison to the case which 2 samples are used per chip.

With regard to the CPM waveform with N = 64 with M = 4, when the number of samples in a chip increase the results in Table 4.17 are obtained.

Table 4.16 Effect of Number of Samples on CPM waveform, N = 64 M = 4

#of samples	PSL		ISL		MLW		SNR loss	
	Min	Max	Min	Max	Min	Max	Min	Max
2	-17.79	-16.93	-3.24	-3.12	1.00	1.8	0	0.69
5	-17.81	-17.61	-3.31	-3.26	1.00	1.10	0	0.11
10	-17.82	-17.73	-3.29	-3.26	1.00	1.02	0	0.027

The results show that the waveforms which require much higher sampling rate than the system Nyquist rate can not be used in this radar system. In order to get optimum results, the system sampling rate should be increased or the waveforms with narrow bandwidths should be used.

CHAPTER 5

SUMMARY AND CONCLUSIONS

In this thesis, optimum waveforms for a pulse doppler radar with an X-band high power traveling tube amplifier in the transmitter were investigated. The waveform optimality was defined regarding the PSL and ISL values of the matched filter output and the bandwidth efficiency in the spectrum.

In this radar system, pulse compression was used to compress the waveform in the receiver. Phase coding, one of the most important pulse compression methods, was mainly focused on throughout this study.

In the first part of this study, different kinds of phase modulated waveforms were analyzed. As a starting point, the discrete phase MLESSM waveforms were studied. Genetic Algorithm is used to search minimum PSL codes. In order to decrease the sidelobe levels of the obtained codes, inverse filtering, a sidelobe reduction technique was applied on these codes. The improved sidelobe levels were reported and consequently it was observed that as the inverse filter length increase the sidelobe levels get lower.

Discrete phase jumps cause spectral high sidelobes in the spectrum. This problem is overcome with continuous phase modulated waveforms. When the discrete phase codes were obtained successfully by means of applying genetic algorithm, a new phase shaping pulse with a parameter of the duration of transition was defined. This pulse was applied on these codes to form continuous phase waveforms. The effect of

this shaping pulse on ACF was investigated for all waveforms modulated with different codes of different lengths. The PSL, ISL and MLW values of the continuous and discrete phase MF outputs were compared.

Following these comparisons, the spectrally efficient MWM modulation, the CPM was focused on. Optimum data sequences were searched using genetic algorithm. ACFs of the CPM waveforms were calculated for codes of different lengths and the PSL and ISL values of the waveforms were compared with each other.

In order to observe the spectral efficiency of the continuous phase waveforms, the bandwidths of the MLESSM and MWM waveforms were computed in MATLAB. It was discovered that as the transition duration increases the bandwidths of MLESSM waveforms get narrower. MSK with its narrowest bandwidth was concluded to be the spectrally most efficient method among MWM techniques while the LPT-QPSK with $\tau = T/4$ occurred to be the most efficient MLESSM technique. However, MSK waveforms were observed to provide the narrowest bandwidths among all modulation methods.

The last part of this thesis dealt with the sampling time mismatch effect on the matched filter outputs of each and every continuous phase system. It was concluded that the CPM schemes with $M = 2$ in MWM waveforms and LPT-QPSK in MLESSM waveforms are the most resistant to the sampling mismatch effect under the system Nyquist rate due to their narrowest bandwidths.

In this thesis, a specific pulse doppler radar with specified code lengths has been considered. Results may be expanded for general pulsed doppler radars as a future work. In addition, CPM waveforms with parameters other than those used in this study can be investigated with a particular focus on lowest sidelobe levels and bandwidth efficiency and optimum phase shaping pulses other than that defined in Section 3.5.1 can be searched.

REFERENCES

[1] Merill I.Skolnik, ***Introduction to Radar Systems*****,** McGraw-HILL, 1981

[2] G.Morris, Linda Harkness**,** ***Airborne Pulsed Doppler Radar***, Artech House, 1996**.**

[3] N.Levanon, E. Mozesoni, ***Radar Signals,*** John Wiley and Sons, 2004

[4] George W. Skolnik, ***Introductio*****n** ***to Airborne Radar,*** SCITECH, 1998

[5] John G.Proakis**,** ***Digital Communications*****,** McGraw-HILL, 1995

[6] Simon Haykin**,** ***Communication Systems*****,** John Wiley and Sons, 1994

[7] John B. Anderson, Tor Aulin, Carl-Erik Sundberg**,** ***Digital Phase Modulation*****,** Plenum Press, 1986

[8] Fred E., Nathanson, ***Radar Design Principles***, McGraw-HILL, 1991

[9] A.Özgür Yılmaz, ***Oversampling and Decimating Pulse Compression,*** Aselsan Technical Report, 2004

[10] A.Özgür Yılmaz, ***Phase Coding For Radar Pulse Compression,*** Aselsan Technical Report, 2004

[11] J.M. Baden and M.N. Cohen, ***Optimal Peak Sidelobe Filters for Biphase Pulse Compression***, IEEE National Radar Conference, pp. 249–252, 1990.

[12] Fuqin Xiong, ***Digital Modulation Techniques*****,** Artech House, 2000

[13] Frank F. Kretschmer, LAurance R.Welch, ***Sidelobe Reduction Techniques for Polyphase Pulse Compression Codes,*** IEEE International Radar Conference, pp. 416-421, 2000

[14] Karl R. Griep, James A.Ritcey, John J. Burlingame, ***Design of Mismatch Filters for Pulse Compression in a Multiple User Sonar Ranging System,*** IEEE International Radar Conference, 1993, pp.1111-1115

[15] Jeffrey M. Ashe, Robert L. Nevin, David J. Murrow, Harry Urkowitz, Nicholas J. Bucci, Jerald D. Nespor, ***Range Sidelobe Suppression of Expanded/ Compressed Pulses with Droop,*** IEEE International Radar Conference, 1994, pp.116-122.

[16] Reiji Sato, Masanori Shinriki***, Simple Mismatch Filter for Binary Pulse Compression Code with Small PSL and Small S/N Loss ,*** IEEE Transactions on Aerospace and Electronic Systems, vol. 39, No.2, pp.711-718, APRIL 2003

[17] Rohling Herman, ***Mismatch Filter Design for Pulse Compression,*** IEEE International Radar Conference, 1990, pp.253-257

[18] Anand K. Ojha, Daniel B. Kech, ***Effects of Processing Errors in the Quadrature Sampling of Complementary Coded Radar Signals,*** IEEE International Radar Conference, 1992, pp. 528-532

[19] Bassem R. Mahafza, ***Radar Systems Analysis and Design Using MATLAB,*** Chapman & Hall/CRC, 2002.

APPENDIX A

MODULATING PULSE SHAPES FOR CPM

LREC is a rectangular pulse with a length of L. LRECs g(t) (frequency shaping pulse) is defined by

$$g(t)=\begin{cases}\dfrac{1}{2LT}, & 0\le t\le LT\\ 0 & \text{otherwise}\end{cases} \tag{A.1}$$

phase shaping pulse q(t) is given by the formula,

$$q(t)=\int_{-\infty}^{\infty}\frac{1}{2T}dt=\begin{cases}\displaystyle\int_0^t\frac{1}{2T}dt, & 0<t<T\\ \displaystyle\int_0^T\frac{1}{2T}dt & t>T\end{cases}=\begin{cases}\dfrac{t}{2T}, & 0<t<T\\ \dfrac{1}{2}, & t>T\end{cases}$$

LRC is a raised cosine with a length of L. g(t) in LRC is defined in Formula A.2.

$$g(t)=\begin{cases}\dfrac{1}{2LT}\left[1-\cos\left(\dfrac{2\pi t}{LT}\right)\right], & 0\le t\le LT\\ 0 & \text{otherwise}\end{cases} \tag{A.2}$$

LSRC is the spectrally raised cosine pulse with length L. LSRC's frequency shaping pulse is

$$g(t) = \frac{1}{LT} \frac{\sin(\frac{2\pi t}{LT})}{\frac{2\pi t}{LT}} \frac{\cos(\beta \frac{2\pi t}{LT})}{1 - \left(\frac{4\beta t}{LT}\right)^2}, \qquad 0 \le \beta \le 1 \tag{A.3}$$

Frequency shaping pulse g(t) in tamed frequency modulation (TMF) is defined as

$$g(t) = \frac{1}{8}\left[a g_0(t - T) + b g_0(t) + a g_0(t + T)\right], \quad a = 1, b = 2$$

$$g_0(t) \approx \sin(\frac{\pi t}{T}) \left[\frac{1}{\pi t} - \frac{2 - \frac{2\pi t}{T} \cot\left(\frac{\pi t}{T}\right) - \left(\frac{\pi t}{T}\right)^2}{\frac{24\pi t^3}{T^2}} \right] \tag{A.4}$$

Finally, GMSK is the Gaussian minimum shift keying and g(t) for GMSK is given by

$$g(t) = \frac{1}{2T} \left[Q\left(2\pi B_b \frac{t - \frac{T}{2}}{\sqrt{\ln 2}} \right) - Q\left(2\pi B_b \frac{t + \frac{T}{2}}{\sqrt{\ln 2}} \right) \right], \quad 0 \le B_b T \le 1 \tag{A.5}$$

$$Q(t) = \int_t^\infty \frac{1}{\sqrt{2\pi}} \exp(-\frac{\tau^2}{2}) d\tau$$